



2  
2007

This is to certify that the  
thesis entitled

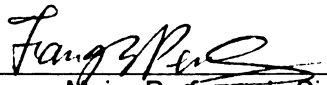
Z-SOURCE INVERTER DESIGN, ANALYSIS, AND ITS  
APPLICATION IN FUEL CELL VEHICLES

presented by

MIAOSEN SHEN

has been accepted towards fulfillment  
of the requirements for the

Ph.D degree in Electrical Engineering



Major Professor's Signature

12/11/2006

Date



**PLACE IN RETURN BOX** to remove this checkout from your record.  
**TO AVOID FINES** return on or before date due.  
**MAY BE RECALLED** with earlier due date if requested.

<b>DATE DUE</b>	<b>DATE DUE</b>	<b>DATE DUE</b>

**Z-SOURCE INVERTER DESIGN, ANALYSIS, AND ITS APPLICATION  
IN FUEL CELL VEHICLES**

**By**

**Miaosen Shen**

**A DISSERTATION**

**Submitted to  
Michigan State University  
in partial fulfillment of the requirements  
for the degree of**

**DOCTOR OF PHILOSOPHY**

**Department of Electrical and Computer Engineering**

**2006**



## **ABSTRACT**

# **Z-Source Inverter Design, Analysis, and Its Application in Fuel Cell Vehicles**

**By**

**Miaosen Shen**

With its unique structure, the *Z*-source inverter can utilize the shoot through states to boost the output voltage, which improves the inverter reliability greatly, and provides an attractive single stage dc-ac conversion that is able to buck and boost the voltage. For applications with a variable input voltage, this inverter is a very competitive topology.

This work starts with the PWM methods for the *Z*-source inverter. Three PWM methods are proposed with different boost ratios. In order to reduce the switching loss, a modified PWM scheme is proposed. A comparative study of the modified PWM method and a commonly used PWM method is conducted.

To facilitate closed loop controller design, a small signal model for the *Z*-source inverter is developed using the state space averaging and verified with simulation results. Based on this model, a closed loop controller is designed using gain scheduling method. The controller is verified with simulation and experimental results.

In order to show the strengths and weaknesses of the *Z*-source inverter, a comprehensive comparison of the *Z*-source inverter and traditional inverters for fuel cell vehicle traction

drives is conducted. The switching device power, passive components requirement, constant power speed ratio, reliability, and inverter efficiency are used as bench marks for the comparison. The comparison shows that the Z-source inverter is very suitable for applications with a moderate boost ratio needed, which most fuel cell/photovoltaic sources reside in. A detailed design process of the Z-source inverter is also provided.

Besides the two basic operation modes of the Z-source inverter, new operation modes have been found when the load power factor, modulation index, and the inductance of the inductors are low. The critical conditions, voltage gain, and the consequence of these operation modes are analyzed in detail.

Three configurations of Z-source inverter for fuel cell-battery hybrid vehicle traction drives are presented with the basic control methods. With a battery in the system, the effect of the undesirable operation modes is minimized. Also, control methods to totally eliminate the undesirable operation modes are proposed. A simple comparison of the three configurations is conducted.

## ACKNOWLEDGEMENTS

I would like to thank my advisor, Dr. Fang Z. Peng, for his guidance, encouragement, and support during my graduate studies. His incredible knowledge and insightful view of power electronics inspired me throughout my research. He has always been a model for me to follow.

I am grateful to my committee members, Dr. Robert Schlueter, Dr. Elias Strangas, and Dr. Rajan Mukherjee, for their inspiring classes, valuable discussion and suggestion, and for their serving on my committee.

I would also like to thank Dr. Zhaoming Qian, my first mentor in power electronics. His guidance and encouragement are always so valuable in the past and in the future.

It has been a great pleasure being a member of power electronics and motor drive laboratory at Michigan State University. I would like to thank all members of the lab, in particular, I would like to thank Dr. Jin Wang, Dr. Zhiguo Pan, Dr. Fan Zhang, Dr. Haiping Xu, Mr. Lihua Chen, Mr. Alan Joseph, Mr. Honnyong Cha for delightful discussions.

I would like to thank Mr. Qingsong Tang for his help in the DSP programming and experiments and Mr. Kent Holland for checking my thesis.

Finally and most importantly, I would like to thank my parents Bingshan and Qinxian for their care and unconditional support. There is no word can express my appreciation to them.

# TABLE OF CONTENTS

LIST OF TABLES .....	ix
LIST OF FIGURES .....	x
CHAPTER 1 Introduction.....	1
1.1 Traditional Inverters .....	1
1.1.1 Voltage Source Inverter.....	1
1.1.2 Current Source Inverter.....	4
1.2 The Z-Source Inverter .....	7
1.3 Previous Works on the Z-Source Inverter .....	10
1.3.1 PWM Methods.....	10
1.3.2 Modeling and Control of the Z-Source Inverter .....	12
1.3.3 Topology Derivation .....	13
1.3.4 Application of the Z-Source Inverter .....	16
1.4 Scope of the thesis.....	16
CHAPTER 2 PWM Schemes for the Z-Source Inverter.....	18
2.1 Simple Control.....	18
2.2 Maximum Boost Control.....	21
2.2.1 Description of the Control Method.....	21
2.2.2 Simulation and Experimental Verifications .....	27
2.2.3 Current Ripple.....	30
2.3 Maximum Constant Boost Control.....	32
2.3.1 Description of the Control Method.....	32
2.3.2 Simulation and Experimental Verifications .....	37
2.3.3 Voltage Stress Comparison.....	40
2.4 Modified PWM Scheme.....	42
2.5 Comparison of Different PWM Schemes.....	46
2.5.1 Switching Loss.....	46
2.5.2 Inductor Size .....	48
2.5.3 Capacitor Size .....	50
2.6. Summary .....	51
CHAPTER 3 Modeling and Control of the Z-Source Inverter with RL Load.....	52
3.1 Modeling of the Z-source Inverter .....	52
3.1.1 Model Simplification .....	52
3.1.2 Modeling by State Space Averaging .....	53
3.1.3 Model Verification .....	56
3.2 Controller Design .....	59
3.2.1 Gain Scheduling Controller .....	59
3.2.2 Controller Design.....	60
3.3 Simulation Results.....	64
3.4 Experimental Verification.....	66

3.5 Discussion .....	69
3.6 Summary .....	70
<b>CHAPTER 4 Z-Source Inverter for Fuel Cell Vehicles—Design and Comparison with Traditional Inverters.....</b>	<b>71</b>
4.1 Introduction .....	71
4.2 System Configurations for Fuel Cell Vehicle.....	72
4.3. Comparison Items, Conditions, Equations, and Results .....	74
4.3.1. Total Switching Device Power Comparison .....	75
4.3.2. Requirement of Passive Components Comparison.....	78
4.3.3. CPSR Comparison .....	87
4.3.4. Reliability Comparison .....	89
4.4 Comparison Example .....	89
4.5. Summary .....	96
<b>CHAPTER 5 Operation Modes and Characteristics of the Z-Source Inverter with Small Inductance or Low Power Factor.....</b>	<b>98</b>
5.1. Introduction .....	98
5.2. Operating Principle and Operation Modes Analysis .....	100
5.3. Circuit Analysis and Characteristics.....	104
5.3.1. Traditional SVPWM Control .....	104
5.3.2. Maximum Constant Boost Control with Third Harmonic Injection .....	107
5.4. Analysis Example.....	110
5.4.1. Voltage Gain.....	110
5.4.2. Relationship of Voltage Gain Versus Voltage Stress .....	111
5.4.3. Design Guidelines .....	112
5.5. Simulation and Experimental Verifications.....	113
5.6. Method to Eliminate the Unwanted Operation Modes.....	114
5.7. Summary .....	117
<b>CHAPTER 6 Application and Control of Z-Source Inverter for Traction Drive of Fuel Cell – Battery Hybrid Electric Vehicles.....</b>	<b>118</b>
6.1. Introduction .....	118
6.1.1 Fuel Cell-Battery Hybrid Vehicles .....	118
6.1.2. Fuel Cell and Battery Characteristics.....	121
6.1.3 Traditional power conditioner configurations.....	122
6.2. Configurations and Control of Z-source Inverter for FCHEVs .....	124
6.2.1 Configurations.....	124
6.2.2 Control of the Inverter.....	126
6.2.3. Simulation and experimental verification .....	130
6.3. Undesirable Operation Modes and Control to Eliminate Them.....	139
6.3.1 Undesirable Operation Modes Without Control .....	139
6.3.2 Control Method to Eliminate the Undesirable Operation Modes .....	141
6.3.3 Experimental Verification of the Control Method .....	143
6.4. Comparison of the Three Configurations.....	147
6.4.1 Configuration 1 .....	147

6.4.2 Configuration 2 .....	148
6.4.3 Configuration 3 .....	149
6.4.4 Comparison Summary.....	150
6.5 Summary .....	150
CHAPTER 7 Conclusions and Recommendations .....	152
7.1 Contributions.....	152
7.2 Recommendations for future works .....	153
APPENDIX 1 Switching Device Power Derivation.....	154
APPENDIX 2 Passive Components Requirement.....	160
APPENDIX 3 Critical Condition of New Modes Under SVPWM .....	162
APPENDIX 4 Critical Condition of New Modes Under Maximum Constant Boost Control with Third Harmonic Injection .....	164
APPENDIX 5 Characteristic Analysis of the Circuit Under CCM Condition.....	166
References.....	168

## LIST OF TABLES

Table 1.1 Possible Shoot Through States.....	11
Table 2.1 Theoretical voltage stress and output voltage under different conditions.....	28
Table 2.2 Theoretical voltage stress and output voltage under different conditions.....	38
Table 4.1 Switching device power comparison example.....	89
Table 4.2 Required passive components.....	90
Table 4.3 Operation conditions at different power.....	90
Table.6.1 Comparison of different configurations.....	150



## LIST OF FIGURES

Figure 1.1 Voltage source inverter. ....	3
Figure 1.2 Sketch map of PWM control of voltage source inverter. ....	3
Figure 1.3 Current source inverter.....	5
Figure 1.4 Waveforms of three-phase PWM current inverter.....	6
Figure 1.5 Z-source inverter .....	7
Figure 1.6 PWM control of the Z-source inverter .....	7
Figure 1.7 Experimental results of Z-source inverter. ....	9
Figure 1.8 Modulation method using six shoot through states .....	11
Figure 1.9 Examples of the existing controllers .....	13
Figure 1.10 Derived topologies.....	15
Figure 1.11 Configuration for Z-source inverter for photovoltaic systems .....	16
Figure 2.1 Simple boost control.....	20
Figure 2.2 Voltage gain of the simple boost control .....	21
Figure 2.3 Switches voltage stress versus voltage gain .....	21
Figure 2.4 Sketch map of maximum boost control.....	22
Figure 2.5 $V_{ac}/0.5V_0$ versus $M$ .....	22
Figure 2.6 Voltage stress versus voltage gain .....	24
Figure 2.7 Sketch map of third harmonic injection control .....	26
Figure 2.8 $V_{ac}/0.5V_0$ versus $M$ .....	26
Figure 2.9 Voltage stress of switches versus voltage gain of proposed control method...	27
Figure 2.10 Simulation results with $M=0.88$ and input voltage 170 V DC .....	29
Figure 2.11 Simulation results with $M=1$ and input voltage 220 V DC .....	29
Figure 2.12 Simulation results with $M=1.1$ with third harmonic injection and input voltage 250 V DC .....	29
Figure 2.13 Experimental result at $M=0.88$ and input voltage 170 V DC .....	30
Figure 2.14 Experimental result at $M=1$ and input voltage 220 V DC .....	30
Figure 2.15 Experimental result at $M=1.1$ with third harmonic injection and input voltage 250 V DC .....	30

Figure 2.16 Maximum boost control sketch map .....	31
Figure 2.17 Model of the circuit .....	32
Figure 2.18 Sketch map of constant boost control.....	33
Figure 2.19 $V_{ac}/0.5V_0$ versus $M$ .....	34
Figure 2.20 Sketch map of constant boost control with third harmonic injection.....	36
Figure 2.21 $V_{ac}/0.5V_0$ versus $M$ .....	37
Figure 2.22 Simulation results with $M = 0.8$ .....	38
Figure 2.23 Simulation results with $M = 1$ .....	38
Figure 2.24 Simulation results with $M = 1.1$ .....	39
Figure 2.25 Experimental results with $V_o = 145V$ and $M = 0.812$ .....	39
Figure 2.26 Experimental results with $V_o = 250V$ and $M = 1$ .....	39
Figure 2.27 Experimental results with $V_o = 250V$ and $M = 1.1$ .....	40
Figure 2.28 Voltage stress comparison of different control methods.....	41
Figure 2.29 Switching states sequence of traditional PWM control.....	42
Figure 2.30 Modified PWM scheme.....	43
Figure 2.31 Overall switching current comparison of different PWM .....	48
Figure 2.32 Six shoot through PWM when $v_a=v_c$ .....	49
Figure 2.33 Capacitor voltage ripple comparison for different power factor .....	51
Figure 3.1 Z-source inverter .....	53
Figure 3.2 dc equivalent circuit .....	53
Figure 3.3 Calculated bode diagram of $V_c/D$ .....	57
Figure 3.4 Calculated bode diagram of $V_c/M$ .....	57
Figure 3.5 Simulated bode diagram of $V_c/D$ .....	58
Figure 3.6 Simulated bode diagram of $V_c/M$ .....	59
Figure 3.7 Simulation result of closed loop performance.....	65
Figure 3.8 Circuit simulation results with parameter mismatch .....	66
Figure 3.9 Experimental results .....	68
Figure 4.1 Typical PEM fuel cell polarization curve .....	72
Figure 4.2 Three inverter system configurations for fuel cell vehicles. ....	73
Figure 4.3 Comparison of SDP of different inverters at different operation conditions...	77

Figure 4.4 Coupled inductors.....	80
Figure 4.5 Capacitor current ripple calculation .....	81
Figure 4.6 PWM scheme of different inverters at a certain interval.....	85
Figure 4.7 Capacitor current comparison of the inverters .....	86
Figure 4.8 Capacitor voltage ripple comparison of the inverters.....	87
Figure 4.9 Switching states sequence in one cycle .....	93
Figure 4.10 Calculated efficiency of inverters.....	94
Figure 4.11 Inverter efficiency calculated using software .....	94
Figure 4.12 Efficiency testing and results.....	96
Figure 5.1 The Z-Source inverter.....	100
Figure 5.2 Possible operation modes of Z source inverter.....	102
Figure 5.3 Inductor current waveforms for different operation conditions .....	105
Figure 5.4 Z-source inductor current for different operation conditions .....	108
Figure 5.5 Simulation results when operating at CCM condition .....	115
Figure 5.6 Experimental results of CCM condition.....	116
Figure 5.7 Comparison of analyzed results and simulation results of capacitor voltage	116
Figure 5.8 Bi-directional Z-source inverter .....	117
Figure 6.1 Medium power operating mode 1.....	120
Figure 6.2 High power operating mode 2 .....	120
Figure 6.3 Low power operating mode 3.....	120
Figure 6.4 Regenerative braking operating mode 4.....	121
Figure 6.5 Typical fuel cell polarization curve .....	122
Figure 6.6 Typical lithium-ion battery voltage versus SOC .....	122
Figure 6.7 Traditional configurations of FCVs.....	123
Figure 6.8 Configurations of Z-source inverter for FCHEV.....	125
Figure 6.9 PWM scheme for the third configuration.....	126
Figure 6.10 Power control of fuel cell by controlling the voltage. ....	128
Figure 6.11 Model of the Z-source network considering parasitic parameters when the fuel cell is turned off.....	128
Figure 6.12 Simulation case 1.....	132

Figure 6.13 Simulation case 2.....	133
Figure 6.14 Simulation case 3.....	134
Figure 6.15 Experimental setup .....	135
Figure 6.16 Experimental results for case 1.....	136
Figure 6.17 Experimental results for case 2.....	137
Figure 6.18 Experimental results for case 3.....	137
Figure 6.19 Z-source inverter based fuel cell converter control system.....	138
Figure 6.20 Simulation results of configuration 3 with battery connected to the neutral point of the motor.....	141
Figure 6.21 Fuel cell V-I characteristics .....	143
Figure 6.22 Experimental setup .....	144
Figure 6.23 Experimental result of case 1 .....	145
Figure 6.24 Experimental results for case 2.....	146
Figure A.1 Inverter model during shoot through .....	158

# CHAPTER 1 Introduction

Power electronics has been widely used in various applications since it was born. The three-phase inverter, which converts dc voltage/current into three-phase ac voltage/current is one of its most important and popular converters. It has been widely used in motor drives [1, 2], ac uninterruptible power supplies (UPS) [3, 4], induction heating [5], ac power supplies [6, 7], active power filters [8, 9], and static VAR generators or compensators [10, 11], etc. There are two types of traditional inverters, namely voltage source (fed) inverters and current source (fed) inverters. However, both inverters have some conceptual barriers, which will be discussed in detail later. The newly presented Z-source inverter [12] has some unique features and it can overcome some of these limitations. The purpose of this work is to investigate the properties of the Z-source inverter and its applications.

## 1.1 Traditional Inverters

### 1.1.1 Voltage Source Inverter

#### 1.1.1.1 Topology

Figure 1.1 shows the topology of the voltage source inverter. The input to the inverter is a dc voltage source usually with a capacitor in parallel to absorb the high frequency current ripple. The inverter bridge consists of six switches with a freewheeling diode in parallel with each of them.

#### 1.1.1.2 Control Methods

Basically there are two kinds of control methods, one is six step control, which turns each

switch on and off only once per fundamental cycle creating a six step stair case waveform for the output phase voltage; the other one is pulse width modulation (PWM), which switches the devices at high frequency (hundreds of Hz to hundreds of kHz) to output a voltage with very little low frequency harmonics as well as to control the output voltage level.

For six-step control, the output line peak fundamental voltage [15] is

$$V_p = \frac{2\sqrt{3}V_{in}}{\pi}, \quad (1.1)$$

where  $V_{in}$  is the dc bus voltage. The six-step method has advantages such as simple, low switching loss, on the other hand, it has limitations for it is unable to eliminate the low frequency harmonics and unable to control the output voltage level.

The sketch map of the basic PWM control for voltage source inverter is shown in Figure1.2. From Figure1.2, the two switches on the same phase leg are turned on and off complementally. There are 8 switching states including 6 active states and two zero states when the upper three or lower three switches are gated on shorting the load terminals.

The output peak phase voltage can be expressed as

$$V_{opk} = \frac{MV_{in}}{2}, \quad (1.2)$$

where  $V_{in}$  is the input voltage, and  $M$  is the modulation index, which ranges from 0 to 1.15 with third harmonic injection or space vector PWM control.

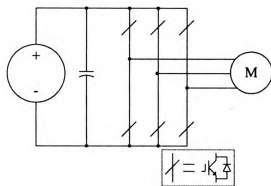


Figure 1.1. Voltage source inverter.

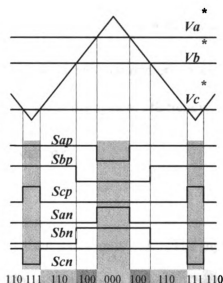


Figure 1.2. Sketch map of PWM control of voltage source inverter.

### 1.1.1.3 Limitations of Voltage Source Inverter

The voltage source inverter has several limitations as listed below.

From (1.2), the output voltage range is limited, the inverter cannot output a higher voltage than the dc bus voltage. For many applications, when the input dc voltage is not always constant, like a fuel cell, photovoltaic array, and during voltage sag, etc, a dc/dc boost converter is often needed to boost the dc voltage to meet the required output voltage. This increases the system complicity and the cost, and reduces the system

reliability.

The two switches on the same phase leg cannot be gated on at the same time, otherwise a short circuit will occur and destroy the inverter. The mistrigger caused by electromagnetic interference (EMI) is a major killer of the inverter. For safety reasons, there is always a dead time to make sure that the two switches will not be turned on simultaneously. However, the dead time can cause output voltage distortion and harmonic problems. The harmonic problem can be solved by implementing a current/voltage feedback control [13], however, this increases the system complexity.

A LC filter is needed for the load side compared to current source inverter, which increases the complexity and reduces the system efficiency.

## **1.1.2 Current Source Inverter**

### **1.1.2.1 Topology**

The current source inverter is shown in Figure 1.3. The input to the inverter is a current source or a voltage source with an inductor in series. The inverter bridge consists of six switches with a reverse blocking diode in series or switches with reverse blocking ability. Three capacitors are connected at the ac side of the inverter to provide a leading power factor load.

Because of the reverse blocking nature of the thyristor, it is often used in current source inverter. However, due to the fact that it is unable to be turned off by the gate signal, a leading power factor load is required to enable load commutation. This also limits the control to be six-step only, which will cause lots of low frequency harmonics in the output waveform.



Another group of current source inverters use self-commutated devices, such as GTO, IGBT, with reverse blocking diode in series. PWM control can be implemented in these inverters.

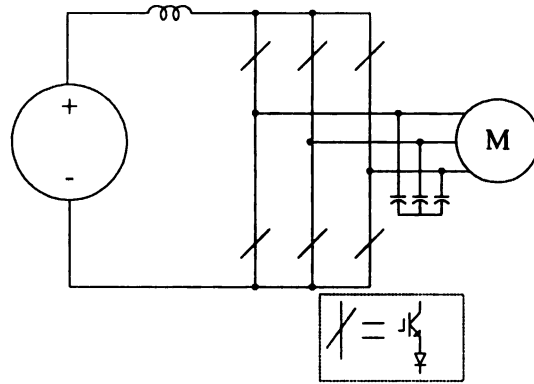


Figure 1.3. Current source inverter.

### 1.1.2.2 Control Methods

The current source inverter is a dual circuit of the voltage source inverter, therefore the dual of most of the PWM methods for voltage source inverter can be used to control the current source inverter. Generally the following rule has to be followed: there must be at least one device in the upper three devices and one in the lower three devices gated on at the same time to provide a current path. An example of the inverter current with PWM control is shown in Figure 1.4. The PWM waveform is the inverter current, the sinusoidal waveform is the current to the load after the capacitors.

### 1.1.2.3 Limitations of the Current Source Inverter

To keep the inductor average voltage zero, the maximum inverter dc side voltage, which is the peak line-to-line output voltage of the inverter has to be greater than the input dc voltage. Therefore, the inverter is basically a boost converter. For applications where a wide voltage range is required, extra circuitry has to be used to obtain the required

voltage. The commonly used methods include using a dc/dc converter or a controlled rectifier [14, 16]. However, these methods increase the circuit complexity and reduce the efficiency as well as the reliability.

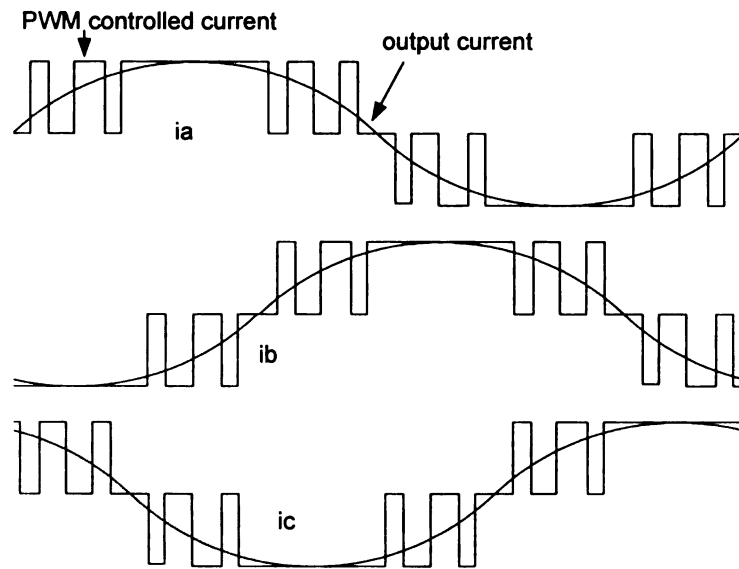


Figure 1.4. Waveforms of three-phase PWM current inverter.

At least one switch in the upper three devices and one in the lower three devices has to be turned on at the same time, or an open circuit will occur and destroy the inverter. Misttrigger caused by the EMI noise could significantly reduce the inverter reliability. To make sure that there will be no open circuit, overlap time is often needed, which will cause output waveform distortion and low frequency harmonic problem.

The main switches have to have the reverse blocking capability, which requires an extra diode in series with high-speed high-performance switches, such as an IGBT. This will reduce the system efficiency. With the emergence of the reverse blocking IGBT [24], this might not be a problem anymore.

## 1.2 The Z-Source Inverter

The newly proposed Z-source inverter [12] can overcome some of these limitations, it is shown in Figure 1.5.

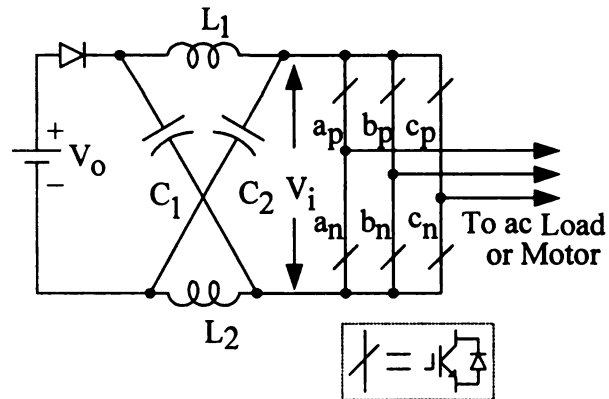


Figure 1.5. Z-source inverter.

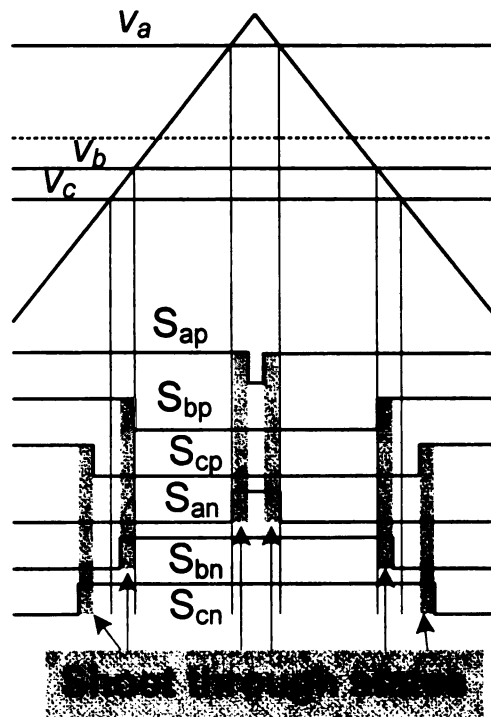


Figure 1.6. PWM control of the Z-source inverter.

The Z-source inverter employs an X shape LC network between the input voltage and the inverter bridge. A simple PWM control scheme is shown in Figure 1.6. From Figure 1.6, there is one more switching state, the shoot through state, besides the eight switching states (six active states and two zero states) for the traditional voltage source inverter. With the unique LC network, we can intentionally add the shoot through state to boost the output voltage. By utilizing this switching state to boost the output voltage, we can output voltage higher or lower than the DC link voltage. Therefore, the inverter is a buck-boost type converter and can output whatever voltage desired, and overcome the voltage limitation of the voltage source inverter and current source inverter. With the ability to handle the shoot through state, the reliability of the Z-source inverter is greatly enhanced. Also, without the need of dead time, output waveform distortion can be avoided. The detailed operation principle has been discussed in [12], the resulted output peak phase voltage is

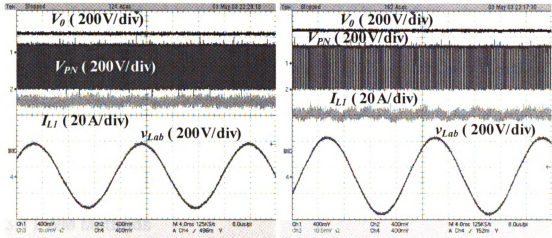
$$\hat{v}_{ac} = MB \frac{V_o}{2}, \quad (1.3)$$

where  $M$  is the modulation index and  $B$  is the boost factor, which can be express as

$$B = \frac{1}{1 - 2 \frac{T_0}{T}}, \quad (1.4)$$

where  $T_0$  is the shoot through time per cycle and  $T$  is the switching cycle.

To demonstrate the Z-source inverter properties, some experimental results are shown below.



(a)

(b)

$V_o$ : input dc voltage;  $V_{pn}$ : inverter PN voltage;  $I_{Li}$ : Z-source inductor current;  $V_{Lab}$ : output line voltage

Figure 1.7. Experimental results of Z-source inverter.

In Figure 1.7(a), the Z-source inverter produces 250 V ac when the dc voltage is only 145 V, while in (b), the inverter produces 300 V ac when the dc voltage is only 250 V. Whereas, with traditional voltage source inverter with modulation index of 1, the maximum output voltage obtainable for 145 V input is 89 V, and 153 V for 250 V dc input.

In summary, the Z-source inverter has several unique features:

1. The inverter can boost and buck the output voltage with a single stage structure;
2. The shoot through caused by EMI can no longer destroy the inverter, which increases the reliability of the inverter greatly.
3. Because of no dead time is required, perfect sinusoidal output waveform is obtainable.

## **1.3 Previous Works on the Z-Source Inverter**

Since the Z-source inverter was proposed in 2002 [12], lots of works have been done on this subject. Mainly the previous works include four major topics: PWM methods; modeling and control of the Z-source inverter; application of the Z-source inverter; and modification of the topology for other applications.

### **1.3.1 PWM Methods**

Different from traditional voltage source inverter, the Z-source inverter has an extra switching state, the shoot through state, which occurs when turning on both switches in the same phase leg. Theoretically there can be seven different shoot through states:

How to insert these switching states, and how much time the shoot through states should be used are very important to the circuit performance and even to the efficiency of the inverter.

Literatures [30, 50] presented several PWM methods based on different PWM methods for traditional voltage source inverters. In those works, the shoot through time is distributed between all traditional switching states, thus there are six shoot through states in one switching cycle.

Table 1.1 Possible shoot though states

Switches	$S_{ap}$	$S_{an}$	$S_{bp}$	$S_{bn}$	$S_{cp}$	$S_{cn}$
ST1	1	1	$B$	$\bar{B}$	$C$	$\bar{C}$
ST2	$A$	$\bar{A}$	1	1	$C$	$\bar{C}$
ST3	$A$	$\bar{A}$	$B$	$\bar{B}$	1	1
ST4	1	1	1	1	$C$	$\bar{C}$
ST5	1	1	$B$	$\bar{B}$	1	1
ST6	$A$	$\bar{A}$	1	1	1	1
ST7	1	1	1	1	1	1

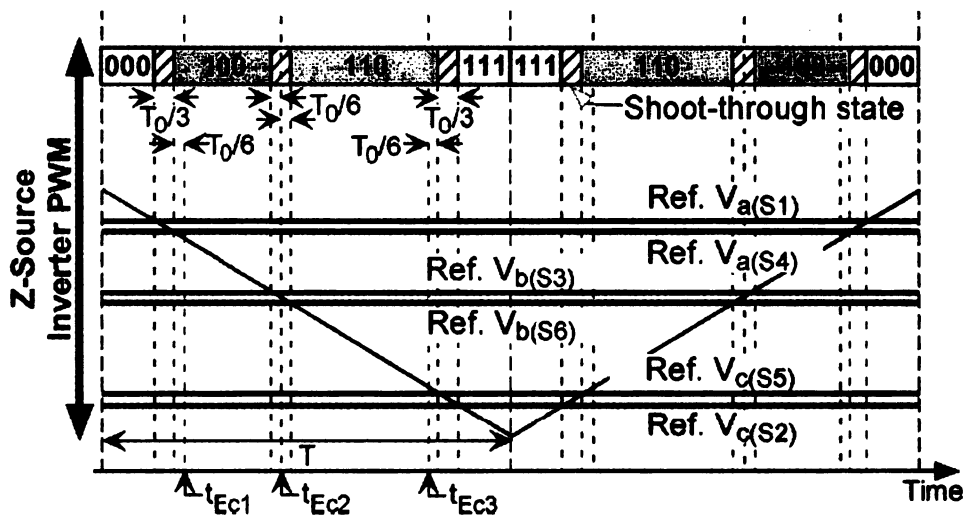


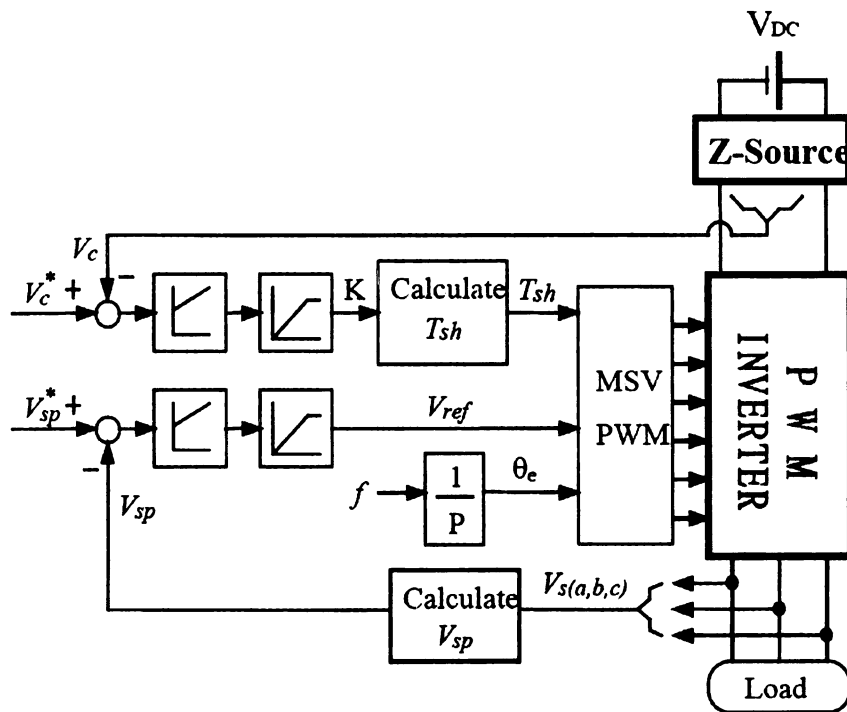
Figure 1.8. Modulation method using six shoot through states.

Also, there are some other PWM methods for other purposes, such as to reduce the common voltage by replacing the zero states with combination of active states [60]; and

PWM methods for multi-level Z-source inverters [52, 57, 73].

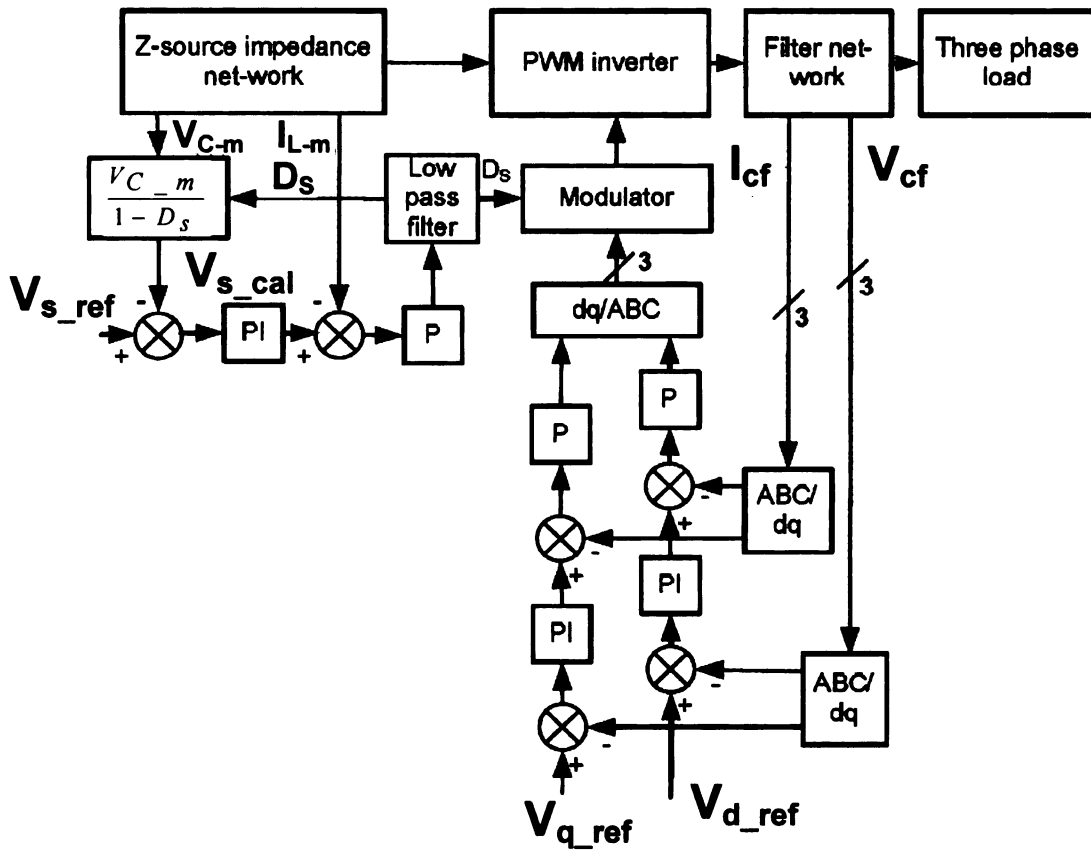
### 1.3.2 Modeling and Control of the Z-Source Inverter

Two small signal models have been developed for the Z-source inverter [40, 43, 51]. The models focus on the dc side of the inverter and only have one control variable, which is the shoot through duty ratio. Also, several control methods for the inverter have been developed [47, 59, 65], two examples of the controllers are shown in Figure 1.9. In these controllers, the capacitor voltage is controlled by the shoot through duty ratio and the output voltage is controlled by the modulation index. The two controllers are designed separately, thus the whole system stability is not guaranteed.



(a)



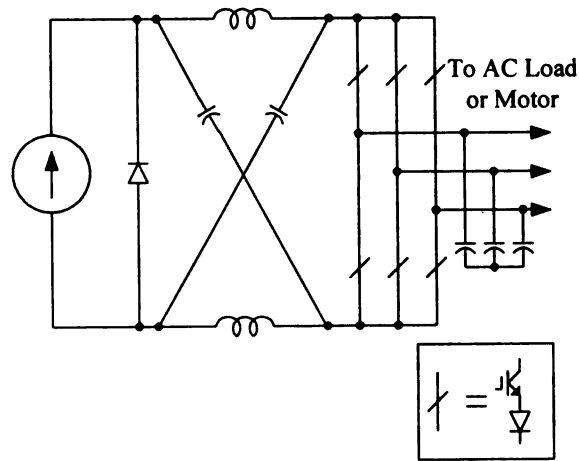


(b)

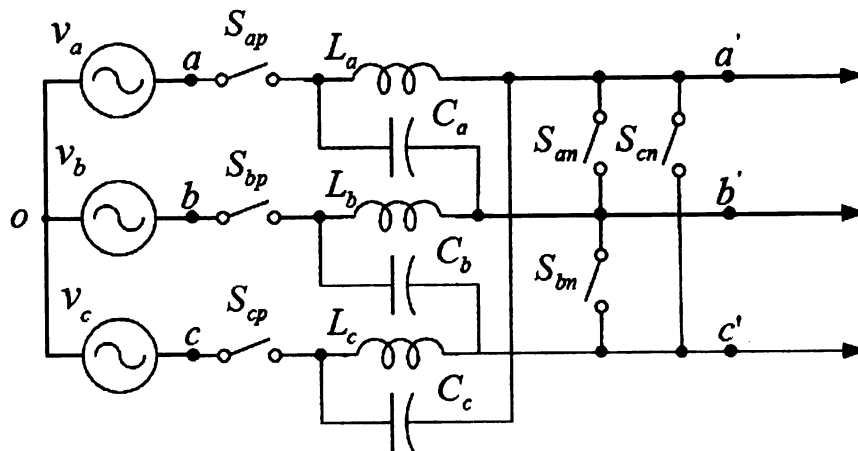
Figure 1.9 Examples of the existing controllers.

### 1.3.3 Topology Derivation

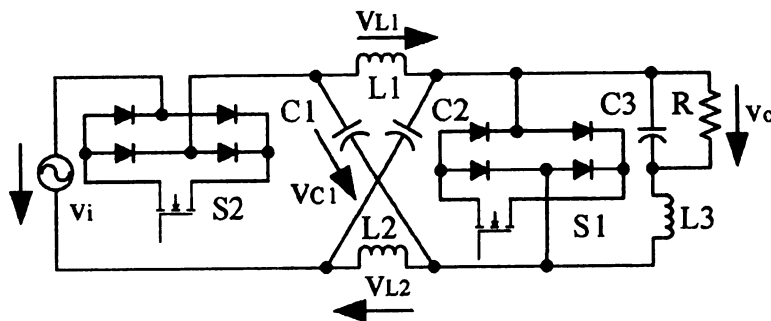
Since the first voltage fed Z-source inverter topology was proposed [12], a lot of topologies have been developed based on it. The derived topologies spread the whole spectrum of electric power conversion [23, 36, 41, 42, 46, 49, 54, 55, 62, 63, 72, 73], ie. AC/AC, AC/DC, DC/DC, DC/AC.



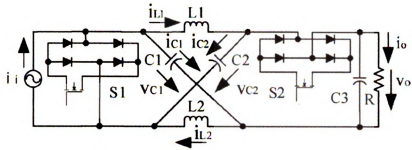
(a) Current fed Z-source inverter.



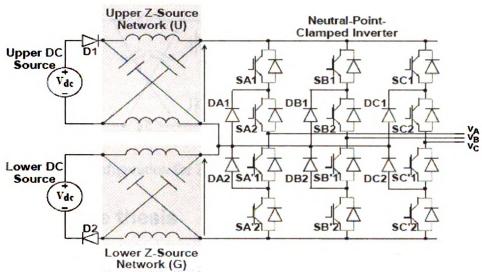
(b) Three phase ac/ac converter.



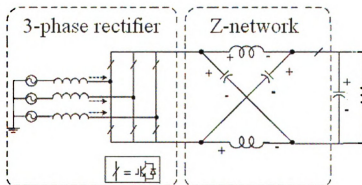
(c) Single phase voltage fed ac/ac converter.



(d) Single phase current fed ac/ac converter.



(e) Diode clamped multi-level Z-source inverter.



(f) Three-phase Z-source rectifier.

Figure 1.10. Derived topologies.

### 1.3.4 Application of the Z-Source Inverter

The application of the Z-source inverter also has been extensively examined. The most popular application of the inverter is for fuel cell and photovoltaic applications [22, 28, 34, 45, 58, 67]. Also applications for integrated starter alternator have been reported in [41, 46, 64], applications for general motor drives have been proposed in [25, 26, 72]. As an example, the configuration for photovoltaic system is shown in Figure 1.11.

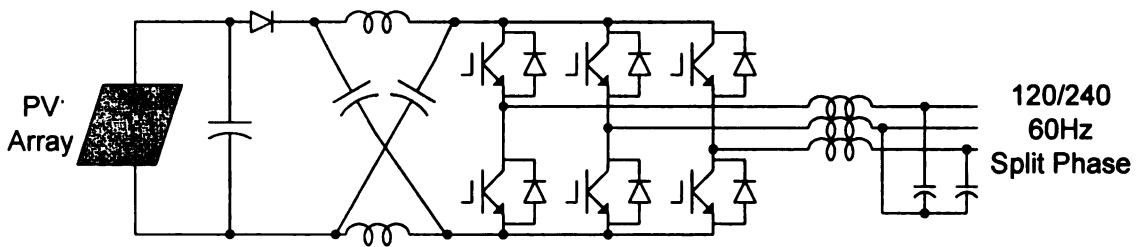


Figure 1.11. Configuration for Z-source inverter for photovoltaic systems.

## 1.4 Scope of the thesis

Based on the previous works of traditional inverter and Z-source inverter, this thesis focuses on the following subjects:

Chapter 2 discusses PWM methods for the Z-source inverter, and presents three PWM methods to achieve simple boost, maximum boost, and maximum constant boost of the Z-source inverter respectively. A modified method to achieve high efficiency is also presented and a brief comparison between the proposed methods and an existing method is conducted.

Chapter 3 presents a small signal model of the Z-source inverter for an inductive load, and constructs a nonlinear controller for the feed back control using gain scheduling method.

Chapter 4 conducts a comprehensive comparison of the Z-source inverter and traditional inverters for fuel cell vehicles. The design procedure of the Z-source inverter is also presented in detail.

Chapter 5 discusses possible operation modes of the Z-source inverter with small inductances, low power factor, and low modulation index. The circuit performance is also discussed under different conditions.

Chapter 6 focuses on the application of the Z-source inverter for fuel cell-battery hybrid vehicles. A control method to eliminate the undesirable operation modes is presented. Three configurations for fuel cell-battery hybrid vehicles are proposed and analyzed.

Chapter 7 discusses future work that needs to be done.

# CHAPTER 2 PWM Schemes for the Z-Source Inverter

Many PWM control methods have been developed and used for the traditional 3-phase Voltage-source (V-source) inverter. The traditional V-source inverter has six active vectors (or switching states), when the dc voltage is impressed across the load, and two zero vectors when the load terminals are shorted through either the lower or upper three devices. These total eight switching states and their combinations have spawned many PWM control schemes.

The Z source inverter has an additional zero vector, the shoot-through switching state, which is forbidden in the traditional V-source inverter. How to insert this shoot through state becomes the key point of the control methods. It is obvious that during the shoot through state, the output terminals of the inverter are shorted and the output voltage to the load is zero. The output voltage of the shoot through state is zero, which is the same as traditional zero states, therefore the duty ratio of the active states has to be maintained to output a sinusoidal voltage, which means shoot through only replaces some or all of the traditional zero states. Three different PWM methods will be presented in this chapter and be compared.

## 2.1 Simple Control

As described in [12], the voltage gain of the Z-source inverter can be expressed as:

$$\frac{\hat{V}_{ac}}{V_o/2} = MB, \quad (2.1)$$

where  $\hat{V}_{ac}$  is the output peak phase voltage,  $V_o$  is the input dc voltage,  $M$  is the modulation index, and  $B$  is the boost factor, which is determined by:

$$B = \frac{1}{1 - 2\frac{T_0}{T}}, \quad (2.2)$$

where  $T_0$  is the shoot-through time interval over a switching cycle  $T$ , or  $\frac{T_0}{T} = D_0$  is the shoot-through duty ratio.

Figure 2.1 illustrates the simple control method that employs a straight line equal to or greater than the peak value of the three phase references to control the shoot-through duty ratio in a traditional sinusoidal PWM. The Z-source inverter maintains the six active states unchanged as the traditional carrier based PWM control. For this simple boost control, the obtainable shoot-through duty ratio decreases with the increase of the modulation index,  $M$ . The maximum shoot-through duty ratio of the simple boost control is limited to  $(1-M)$ , thus reaching zero at a modulation index of one. The thick curve in Figure 2.2 shows the maximum obtainable voltage gain,  $M \cdot B$  versus  $M$ , which indicates no voltage boost and no voltage gain at  $M=1$ . The shaded area is the possible operation region under the simple control. In order to produce an output voltage that requires a high voltage gain, a small modulation index has to be used. However, small modulation indices result in greater voltage stress on the devices. Based on the (2.1) and (2.2), define the voltage gain  $G$  as

$$G = MB = \frac{\hat{V}_{ac}}{V_o/2} = \frac{M}{2M-1}. \quad (2.3)$$

For any desired voltage gain  $G$ , the maximum modulation index can be used is

$$M = \frac{G}{2G-1} \quad (2.4)$$

The voltage stress  $V_s$  across the switches is  $BV_o$ . The voltage stress under this voltage gain can be calculated

$$V_s = BV_o = (2G-1)V_o. \quad (2.5)$$

The voltage stress across switches versus the voltage gain is plotted in Figure 2.3. Using this control method, the voltage stress across the switches is quite high, which will restrict the obtainable voltage gain because of the limitation of device voltage rating.

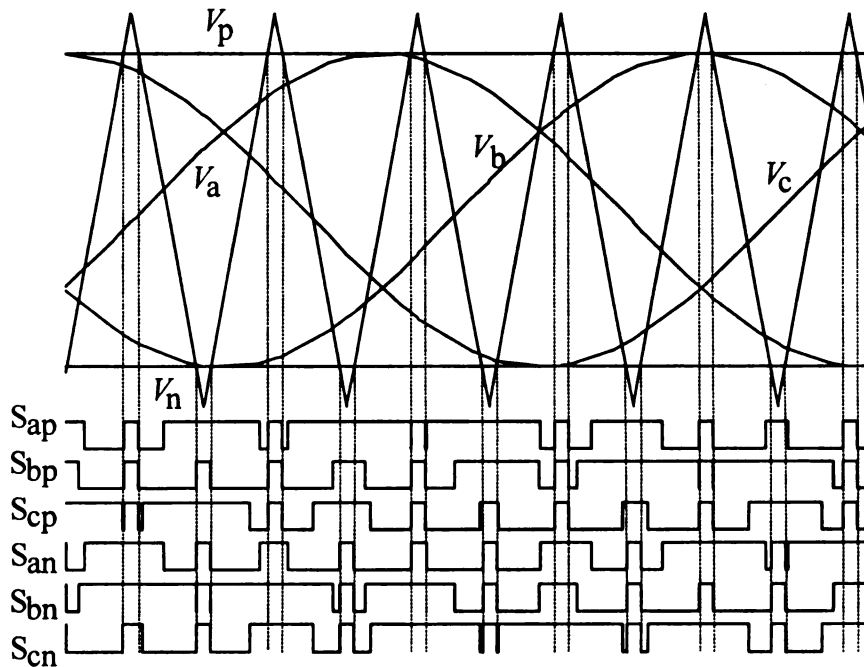


Figure 2.1. Simple boost control.



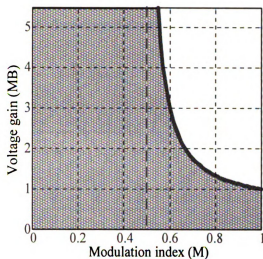


Figure 2.2. Voltage gain of the simple boost control.

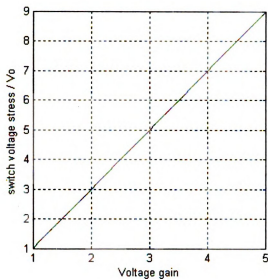


Figure 2.3. Switches voltage stress versus voltage gain.

## 2.2 Maximum Boost Control

### 2.2.1 Description of the Control Method

Reducing the voltage stress under a desired voltage gain now becomes important to the control of  $Z$  source inverter. As analyzed above, the voltage gain is defined as  $MB$ , and the voltage stress across the switches is  $BV_o$ , therefore, to minimize the voltage stress for any given voltage gain, we have to minimize  $B$  and maximize  $M$ , with the restriction of that their product is the desired value. On the other hand, we should maximize  $B$  for any given modulation index,  $M$ , to achieve the maximum voltage gain. Consequently, from (2.2), we have to make the shoot through duty ratio as large as possible.

Figure 2.4 shows the maximum boost control strategy. It is quite similar to the traditional carrier-based PWM control method. The point is: this control method maintains the six active states unchanged and turns all zero states into shoot-through zero

states. Thus maximum  $T_0$  and  $B$  are obtained for any given modulation index,  $M$ , without distorting the output waveform.

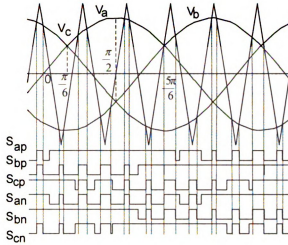


Figure 2.4. Sketch map of maximum boost control.

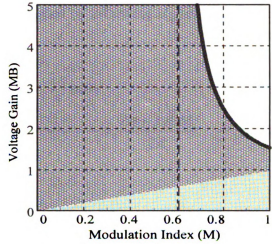


Figure 2.5.  $V_{ac}/0.5V_0$  versus  $M$ .

As can be seen from Figure 2.4, the circuit is in a shoot through state when the triangular carrier wave is either greater than the maximum of the references ( $V_a$ ,  $V_b$ ,  $V_c$ ) or smaller than the minimum of the references. The shoot through duty cycle varies each cycle. To calculate the voltage gain, what we are interested in is the average shoot through duty cycle.

The shoot through state repeats periodically every  $\frac{\pi}{3}$ . Assuming that the switching frequency is much higher than the fundamental frequency, the shoot-through duty ratio over one switching cycle in the interval  $(\frac{\pi}{6}, \frac{\pi}{2})$  can be expressed in the following equation

$$\frac{T_0(\theta)}{T} = \frac{2 - (M \sin \theta - M \sin(\theta - \frac{2\pi}{3}))}{2} \quad (2.6)$$

The average duty ratio of shoot-through can be calculated by following equation

$$\frac{\bar{T}_0}{T} = \frac{\int_{\frac{\pi}{6}}^{\frac{\pi}{2}} 2d\theta - (\int_{\frac{\pi}{6}}^{\frac{\pi}{2}} M \sin \theta d\theta - \int_{\frac{\pi}{6}}^{\frac{\pi}{2}} M \sin(\theta - \frac{2\pi}{3}) d\theta)}{\int_{\frac{\pi}{6}}^{\frac{\pi}{2}} 2d\theta} = \frac{2\pi - 3\sqrt{3}M}{2\pi} \quad (2.7)$$

The boost factor  $B$  is obtained:

$$B = \frac{1}{1 - 2\frac{\bar{T}_0}{T}} = \frac{\pi}{3\sqrt{3}M - \pi} \quad (2.8)$$

With this type of control method, the voltage gain can be determined by the modulation index  $M$ .

$$\frac{\hat{v}_{ac}}{V_0/2} = MB = \frac{\pi M}{3\sqrt{3}M - \pi} \quad (2.9)$$

The plot of  $\frac{\hat{v}_{ac}}{V_0/2}$  versus  $M$  is shown by the thick curve in Figure 2.5. The shaded area in the figure is the possible operation region. As can be seen from Figure 2.5, the output voltage increases when  $M$  decreases. As  $M$  approaches  $\frac{\pi}{3\sqrt{3}}$ , the output voltage increases to infinity.

Compared to Figure 2.2, the possible operation region of this control method is much

wider. On the other hand, for any given voltage gain, a higher modulation index can be used, which means lower voltage stress across the switches.

From equation (2.9) and voltage gain defined in (2.3), the maximum modulation index we can use for a given voltage gain  $G$  is

$$M = \frac{\pi G}{3\sqrt{3}G - \pi}. \quad (2.10)$$

Thus the voltage stress is

$$V_s = BV_o = \frac{\pi V_o}{3\sqrt{3}M - \pi} = \frac{3\sqrt{3}G - \pi}{\pi} V_o. \quad (2.11)$$

The voltage stress versus the voltage gain is shown in Figure 2.6.

Compared with the voltage stress in the simple control method, which is shown in Figure 2.3, the voltage stress in the maximum boost control method is much lower, which means that for given devices, the inverter can be operated to obtain a higher voltage gain.

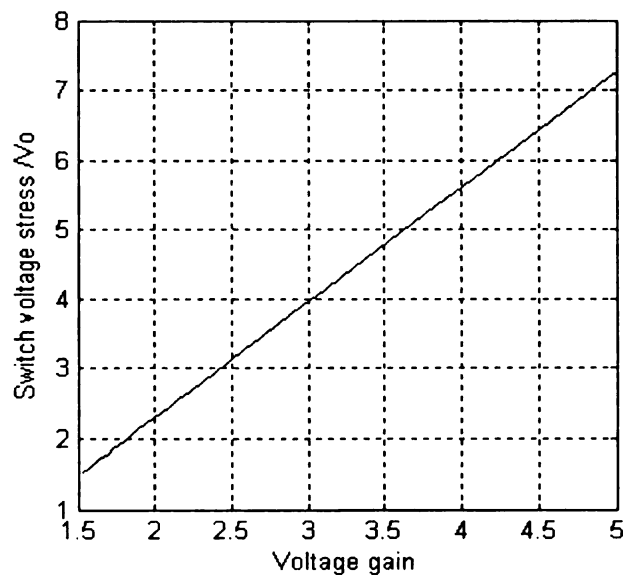


Figure 2.6. Voltage stress versus voltage gain.

Third harmonic injection is commonly used in three-phase inverter systems to increase the modulation index range. This can also be used here to increase the range of  $M$  so as to increase system voltage gain range. The sketch map is shown in Figure 2.7. The operating principle is identical to the above method, the only difference is that the reference waveforms are changed. In this control, the maximum modulation index

$$M = \frac{2}{\sqrt{3}} \text{ can be achieved at } \frac{1}{6} \text{ third harmonic injection [17].}$$

Similar to the previous case, the shoot through duty cycle repeats every  $\frac{\pi}{3}$ . We can also get the voltage gain through studying the behavior during  $(\frac{\pi}{6}, \frac{\pi}{2})$  under this control method. The shoot-through duty ratio in this period is described in the following equation.

$$\frac{T_0(\theta)}{T} = \frac{2 - (M \sin \theta + \frac{1}{6} M \sin 3\theta - (M \sin(\theta - \frac{2\pi}{3}) + \frac{1}{6} M \sin 3\theta))}{2} \quad (2.12)$$

From the above calculation, the average shoot-through duty ratio is:

$$\begin{aligned} \frac{\bar{T}_0}{T} &= \frac{\int_{\frac{\pi}{6}}^{\frac{\pi}{2}} 2d\theta - (\int_{\frac{\pi}{6}}^{\frac{\pi}{2}} (M \sin \theta + \frac{1}{6} M \sin 3\theta)d\theta - \int_{\frac{\pi}{6}}^{\frac{\pi}{2}} (M \sin(\theta - \frac{2\pi}{3}) + \frac{1}{6} M \sin 3\theta)d\theta)}{\int_{\frac{\pi}{6}}^{\frac{\pi}{2}} 2d\theta} \quad (2.13) \\ &= \frac{2\pi - 3\sqrt{3}M}{2\pi} \end{aligned}$$

Therefore:

$$B = \frac{1}{1 - 2\frac{\bar{T}_0}{T}} = \frac{\pi}{3\sqrt{3}M - \pi} \quad (2.14)$$

$$\frac{\hat{v}_{ac}}{V_0/2} = MB = \frac{\pi M}{3\sqrt{3}M - \pi} \quad (2.15)$$

The voltage gain is identical to the maximum boost control method for the same modulation index. The curve of voltage gain versus modulation index is shown in Figure 2.8, from which we can see that the possible operating region is extended with the increase of modulation index. From (2.9) and (2.15), the two control methods have identical voltage gain—modulation index relationship. Therefore they should share the same voltage stress for any given voltage gain except that the range of voltage gain is extended in the third harmonic injection method. The relationship of voltage stress versus voltage gain is shown in Figure 2.9.

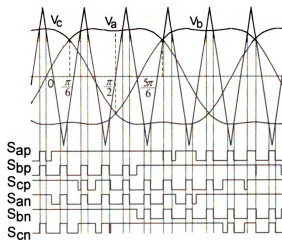


Figure 2.7. Sketch map of third harmonic injection control.

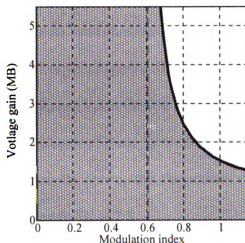


Figure 2.8.  $V_{ac}/0.5V_0$  versus  $M$ .

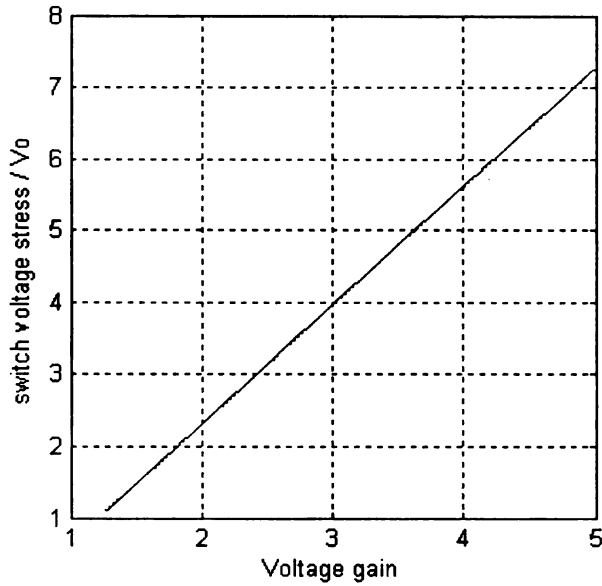


Figure 2.9. Voltage stress of switches versus voltage gain of proposed control method.

## 2.2.2 Simulation and Experimental Verifications

Simulation and experiments are conducted to verify the validity of the control strategies with the following parameters: Z-source network:  $L_1 = L_2 = 1\text{mH}$ ,  $C_1 = C_2 = 1.3\text{mF}$ , Switching frequency: 10 kHz. The simulation results with modulation index  $M=0.88$ ,  $M=1$ , and  $M=1.1$  with third harmonic injection are shown in Figure 2.10, Figure 2.11, and Figure 2.12 respectively, where  $V_o$  is the input voltage,  $V_{pn}$  is the DC bus voltage, and  $V_{Lab}$  is the output line to line voltage. The input voltages of these three cases are 170 V, 220V and 250 V respectively. Based on our analysis above, the theoretical voltage stress ( $V_{pn}$ ) and output line to line rms voltage is listed in Table.2.1.

Table 2.1 Theoretical voltage stress and output voltage under different conditions

Operation condition	Voltage stress (V)	Output voltage $V_{L-L}$ (V)
$M=0.88, V_o=170V$	373	200
$M=1, V_o=220 V$	336	206
$M=1.1, V_o=250 V$	305	205

The simulation results in Figure 2.10 through Figure 2.12 are quite consistent with the theoretical analysis, which verifies the above analysis and the control concept.

Experiments with the same operating conditions and system configuration as in the simulation were conducted. The results are shown in Figure 2.13, Figure 2.14, and Figure 2.15, where  $V_o$  is the input voltage,  $V_{PN}$  is the voltage stress,  $I_{Ll}$  is the current through the inductor in the Z-source network, and  $V_{Lab}$  is the output voltage after the filter. The figures show that the output voltage is kept nearly constant regardless of the wide varying range of the input voltage and the output voltage agrees with the analysis and simulation results very well. A lower input voltage requires a greater boost factor B, and smaller modulation index. Because the output voltage is nearly constant, the lower modulation index yields higher voltage stress,  $V_{PN}$ . This can also be observed from the experimental results. Based on these results, the validity of the control methods has been proven.



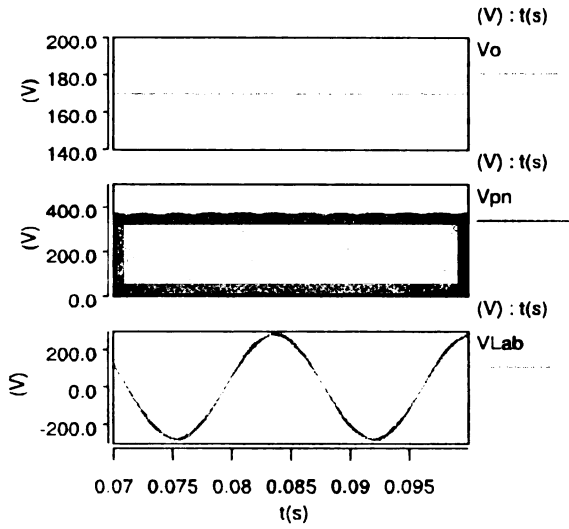


Figure 2.10. Simulation results with  $M=0.88$  and input voltage 170 V DC.

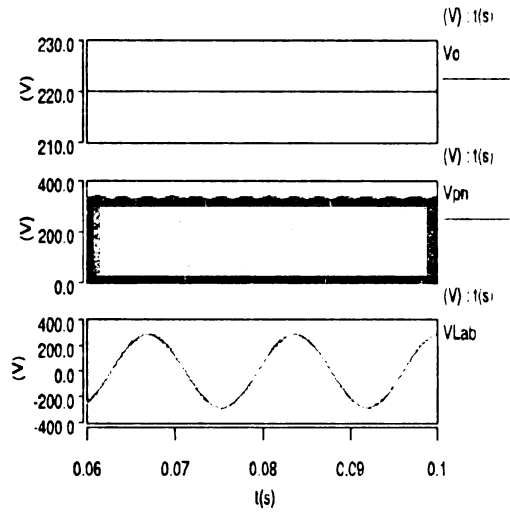


Figure 2.11. Simulation results with  $M=1$  and input voltage 220 V DC.

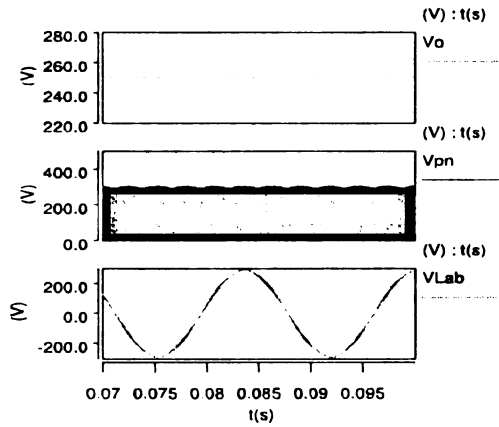


Figure 2.12. Simulation results with  $M=1.1$  with third harmonic injection and input voltage 250 V DC.

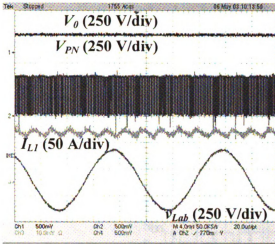


Figure 2.13. Experimental result at  $M=0.88$  and input voltage 170 V DC.

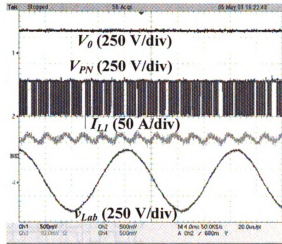


Figure 2.14. Experimental result at  $M=1$  and input voltage 220 V DC.

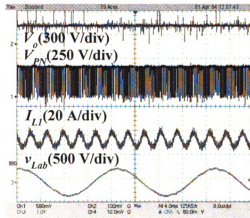


Figure 2.15. Experimental result at  $M=1.1$  with third harmonic injection and input voltage 250 V DC.

### 2.2.3 Current Ripple

This control method can achieve the minimal voltage stress across the switches for any desired voltage gain. However, from Figure 2.16, the shoot through duty cycle is not always a constant, and thus introduces current ripple through the inductors.

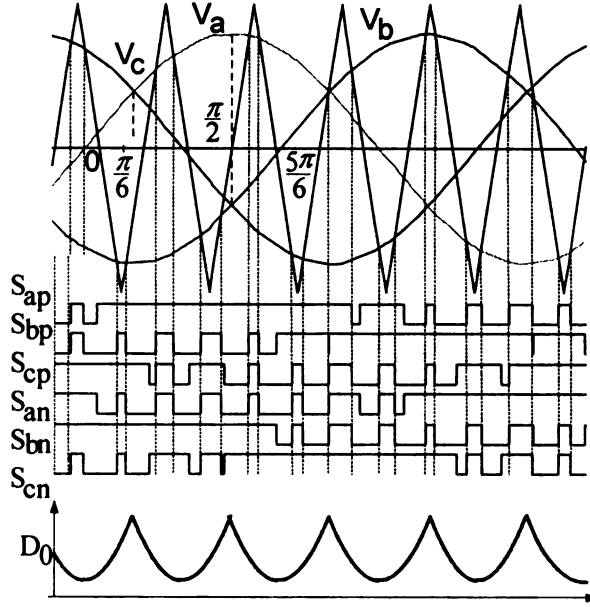


Figure 2.16. Maximum boost control sketch map.

To calculate the current ripple through the inductor, the circuit can be modeled as in Figure 2.17, where  $L$  is the inductor in the Z-source network,  $V_c$  is the voltage across the capacitor in the Z-source network, and  $V_i$  is the voltage fed to the inverter. Neglecting the switching frequency element, the average value of  $V_i$  can be described as

$$V_i = (1 - D_0) * BV_{dc} \quad (2.16)$$

From above analysis,

$$D_0(\theta) = \frac{2 - (M \sin \theta - M \sin(\theta - \frac{2}{3}\pi))}{2} = 1 - \frac{\sqrt{3}}{2} M \cos(\theta - \frac{1}{3}\pi) \quad (\frac{\pi}{6} < \theta < \frac{\pi}{2}) \quad (2.17)$$

and

$$B = \frac{\pi}{3\sqrt{3}M - \pi} \quad (2.18)$$

As can be seen from Eq. (2.17),  $D_0$  has minimum value when  $\theta = \frac{\pi}{3}$  and has

maximum value when  $\theta = \frac{\pi}{6}$  or  $\theta = \frac{\pi}{2}$ . If we assume the voltage across the capacitor is constant, the voltage ripple across the inductor can be approximated as a sinusoid with peak-to-peak value of

$$V_{pk2pk} = V_{i\max} - V_{i\min} = \left(\frac{\sqrt{3}}{2}M - \frac{\sqrt{3}}{2}M \cos\left(\frac{\pi}{6}\right)\right) * BV_{dc} = \frac{\left(\frac{\sqrt{3}}{2} - \frac{3}{4}\right)M\pi}{3\sqrt{3}M - \pi} V_{dc}. \quad (2.19)$$

If the output frequency is  $f$ , the current ripple through the inductor will be

$$\Delta I_L = \frac{V_{pk2pk}}{2 * \pi * 6f * L} = \frac{\left(\frac{\sqrt{3}}{2} - \frac{3}{4}\right)MV_{dc}}{12 * (3\sqrt{3}M - \pi)fL}. \quad (2.20)$$

As can be seen from Eq. (2.20), when the output frequency decreases, in order to maintain the current ripple in a certain range, the inductance has to be large.

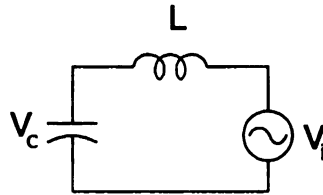


Figure 2.17. Model of the circuit.

## 2.3 Maximum Constant Boost Control

### 2.3.1 Description of the Control Method

In order to reduce the volume and cost, it is important to keep the shoot-through duty ratio always constant. At the same time, a greater voltage boost for any given modulation index is desired to reduce the voltage stress across the switches. Figure 2.18 shows the sketch map of the maximum constant boost control method, which achieves

the maximum voltage gain while always keeping the shoot-through duty ratio constant. There are five modulation curves in this control method: three reference signals,  $V_a$ ,  $V_b$ , and  $V_c$ , and two shoot-through envelope signals,  $V_p$  and  $V_n$ . When the carrier triangle wave is greater than the upper shoot-through envelope,  $V_p$ , or lower than the lower shoot-through envelope,  $V_n$ , the inverter is turned into shoot-through zero state. In between, the inverter switches in the same way as a traditional carrier-based PWM control.

Because the boost factor is determined by the shoot-through duty cycle, the shoot-through duty cycle must be kept the same in order to maintain a constant boost. The basic point is to get the maximum  $B$  while keeping it constant all the time. The upper and lower envelope curves are periodical and are three times the output frequency. There are two half-periods for both curves in a cycle.

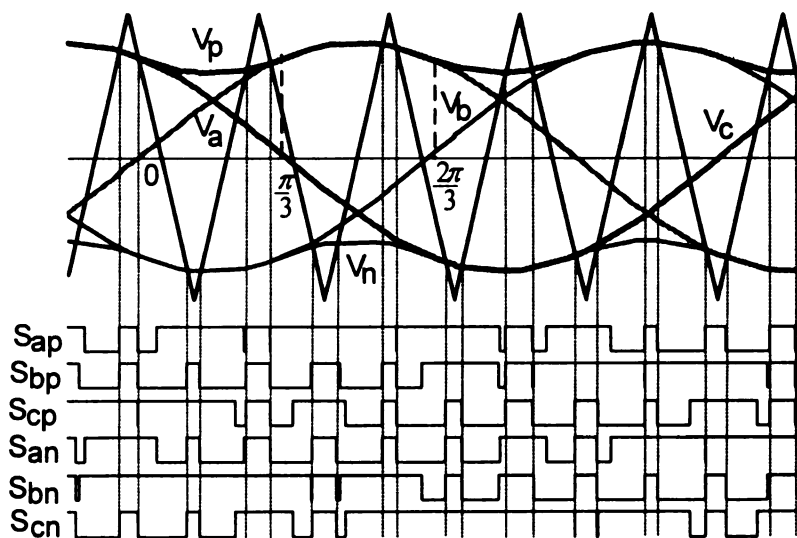


Figure 2.18. Sketch map of constant boost control.

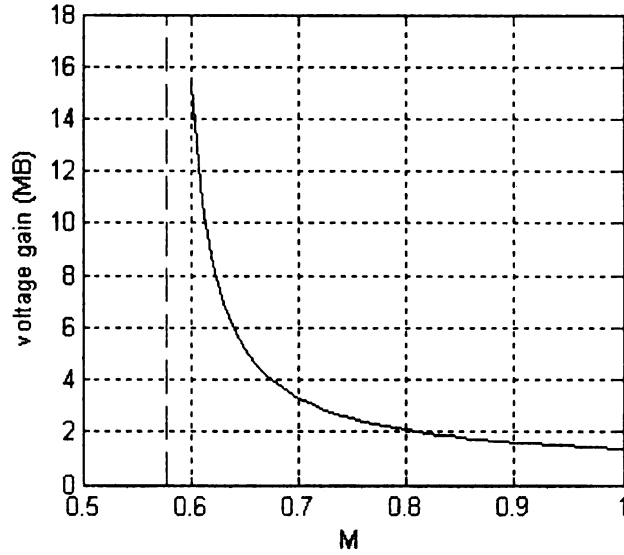


Figure 2.19.  $V_{ac}/0.5V_0$  versus  $M$ .

For the first half-period,  $(0, \pi/3)$  in Figure 2.18, the upper and lower envelope curves can be expressed by Eqs. (2.21) and (2.22), respectively.

$$V_{p1} = \sqrt{3}M + \sin\left(\theta - \frac{2\pi}{3}\right)M \quad 0 < \theta < \frac{\pi}{3} \quad (2.21)$$

$$V_{n1} = \sin\left(\theta - \frac{2\pi}{3}\right)M \quad 0 < \theta < \frac{\pi}{3} \quad (2.22)$$

For the second half-period  $(\pi/3, 2\pi/3)$ , the curves meet Eqs. (2.23) and (2.24) respectively.

$$V_{p2} = \sin(\theta)M \quad \frac{\pi}{3} < \theta < \frac{2\pi}{3} \quad (2.23)$$

$$V_{n2} = \sin(\theta)M - \sqrt{3}M \quad \frac{\pi}{3} < \theta < \frac{2\pi}{3} \quad (2.24)$$

Obviously, the distance between these two curves is always constant, that is,  $\sqrt{3}M$ .

Therefore the shoot-through duty ratio is constant and can be expressed as

$$\frac{T_0}{T} = \frac{2 - \sqrt{3}M}{2} = 1 - \frac{\sqrt{3}M}{2} . \quad (2.25)$$

The boost factor  $B$  and the voltage gain can be calculated:

$$B = \frac{1}{1 - 2\frac{T_0}{T}} = \frac{1}{\sqrt{3}M - 1} . \quad (2.26)$$

$$\frac{\hat{v}_o}{V_{dc}/2} = MB = \frac{M}{\sqrt{3}M - 1} . \quad (2.27)$$

The curve of voltage gain versus modulation index is shown in Figure 2.19. As can be seen in Figure 2.19, the voltage gain approaches infinity when  $M$  decreases to  $\frac{\sqrt{3}}{3}$ .

This maximum constant boost control can be implemented using third harmonic injection. A sketch map of the third harmonic injection control method, with 1/6 of the third harmonic, is shown in Figure 2.20. As can be seen from Figure 2.20,  $V_a$  reaches its peak value  $\frac{\sqrt{3}}{2}M$  while  $V_b$  is at its minimum value  $-\frac{\sqrt{3}}{2}M$ . Therefore, a unique feature can be obtained: only two straight lines,  $V_p$  and  $V_n$ , are needed to control the shoot-through time with 1/6 (16%) of the third harmonic injected.

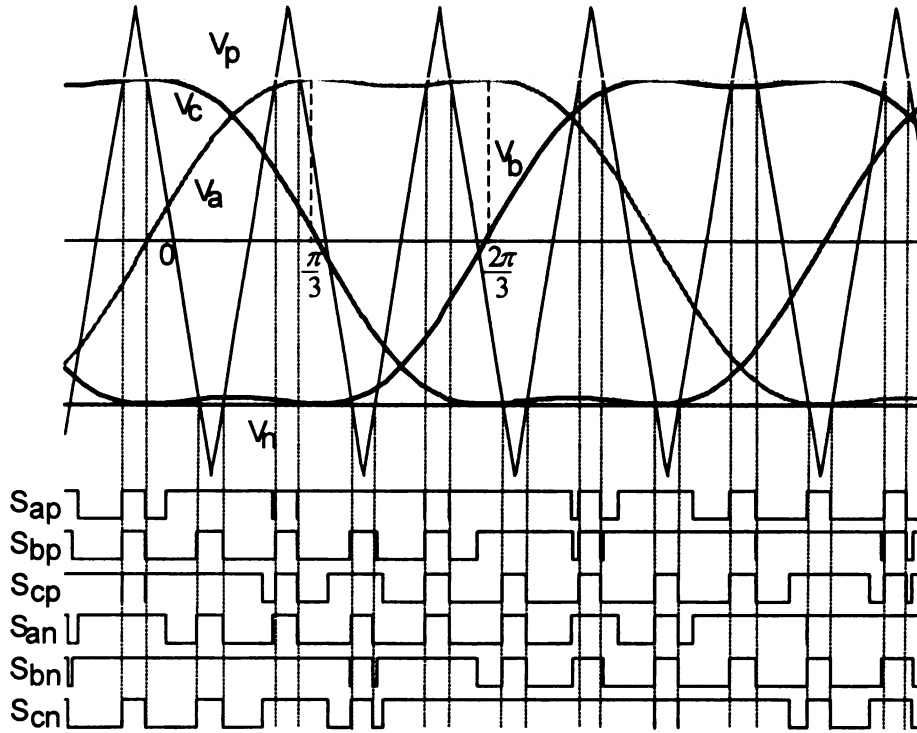


Figure 2.20. Sketch map of constant boost control with third harmonic injection.

The shoot-through duty ratio can be calculated by

$$\frac{T_0}{T} = \frac{2 - \sqrt{3}M}{2} = 1 - \frac{\sqrt{3}M}{2} \quad (2.28)$$

As we can see, it is identical to the previous maximum constant boost control method.

Therefore, the voltage gain can also be calculated by the same equation. The difference is

that in this control method, the range of  $M$  is increased to  $\frac{2}{3}\sqrt{3}$ . The voltage gain versus

$M$  is shown in Figure 2.21. The voltage gain can be varied from infinity to zero smoothly

by increasing  $M$  from  $\frac{\sqrt{3}}{3}$  to  $\frac{2}{\sqrt{3}}$  with shoot-through states (solid curve in Figure 2.21)

and then decreasing  $M$  to zero without shoot-through states (dotted curve in Figure 2.21).



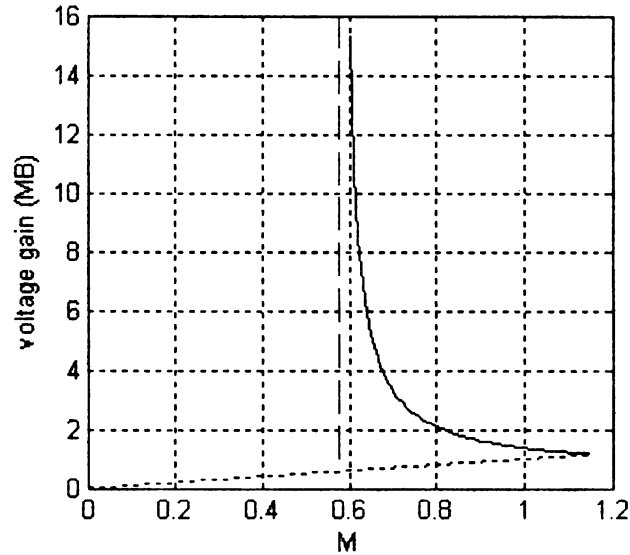


Figure 2.21.  $V_{ac}/0.5V_0$  versus  $M$ .

### 2.3.2 Simulation and Experimental Verifications

Simulation and experiments were conducted to verify the validity of the control strategies with the following parameters: Z-source network:  $L_1 = L_2 = 1$  mH (60 Hz inductor),  $C_1 = C_2 = 1,300$   $\mu$ F; switching frequency: 10 kHz; output power: 6 kW. The simulation results with the modulation index  $M = 0.812$ ,  $M = 1$  without third harmonic injection, and  $M = 1.1$  with third harmonic injection are shown in Figures 2.22 through 2.24, respectively, where the input voltages are 145, 250, and 250 V, respectively. Table 2.2 lists the theoretical voltage stress and output line-to-line rms voltage based on the previous analysis.

Table 2.2. Theoretical voltage stress and output voltage under different conditions

Operating condition	Voltage stress (V)	Output voltage $V_{L-L}$ (V)
$M = 0.812, V_{dc} = 145V$	357	177
$M = 1, V_{dc} = 250 V$	342	209
$M = 1.1, V_{dc} = 250 V$	276	186

The simulation results in Figures.2.22–2.24 are consistent with the theoretical analysis, which verifies the previous analysis and the control concept.

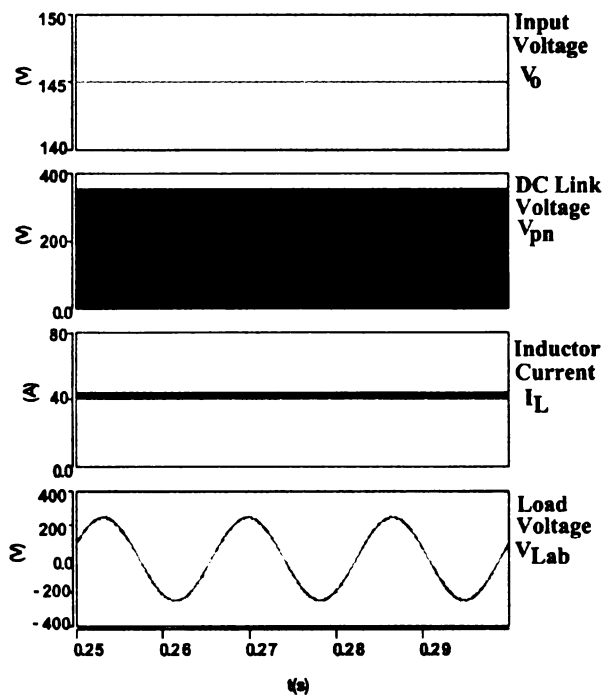


Figure 2.22. Simulation results with  $M = 0.8$ .

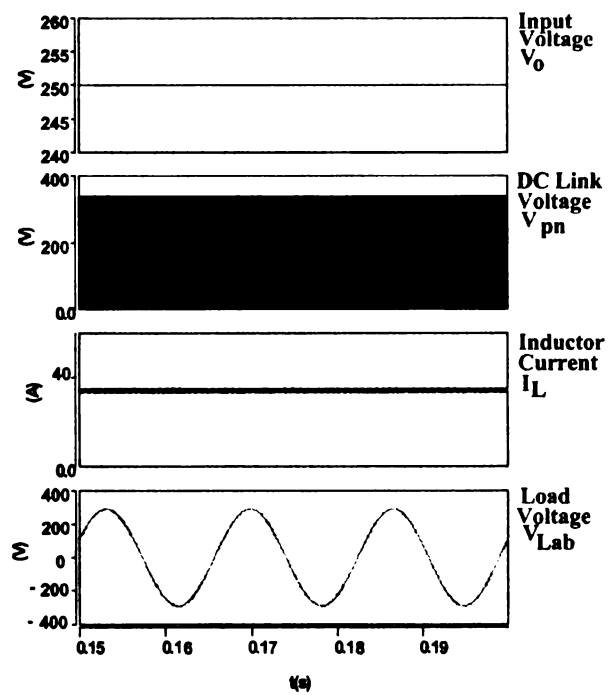


Figure 2.23. Simulation results with  $M = 1$ .

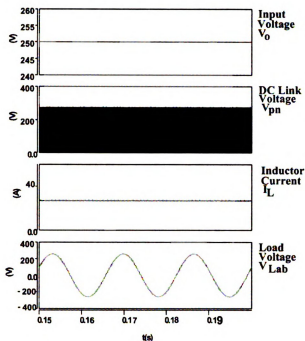


Figure 2.24. Simulation results with  $M = 1.1$ .

The experimental results with the same operating conditions are shown in Figures 2.26, 2.27, and 2.28, respectively.

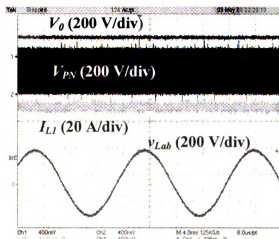


Figure 2.25. Experimental results with  $V_o = 145\text{V}$  and  $M = 0.812$ .

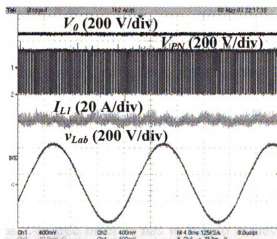


Figure 2.26. Experimental results with  $V_o = 250\text{V}$  and  $M = 1$ .

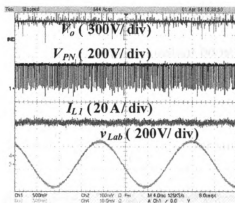


Figure 2.27. Experimental results with  $V_o = 250\text{V}$  and  $M = 1.1$ .

Based on these results, the experimental results agree with the analysis and simulation results very well. The validity of the control method and the analysis of the voltage gain and voltage stress are verified. Also from the simulation and experimental results, it is evident that there is no low-frequency ( $6\omega$ ) ripple in the inductor current. With the same input voltage, the output voltage is higher for the case with lower modulation index. With a lower input voltage, the voltage stress has to be higher to output a similar voltage.

### 2.3.3 Voltage Stress Comparison

To examine the voltage stress across the switching devices, an equivalent DC voltage is introduced. The equivalent DC voltage is defined as the minimum DC voltage needed for the traditional voltage-source inverter to produce an output voltage,  $\hat{V}_O$ . Obviously the equivalent DC voltage should be  $GV_{dc}$ . The ratio of the voltage stress to the equivalent DC voltage represents the cost that Z-source inverter has to pay to achieve voltage boost.

The voltage stress across the devices,  $V_S$  can be expressed as

$$V_S = BV_{dc}. \quad (2.29)$$

The ratios of the voltage stress to the equivalent DC voltage,  $V_S/(GV_{dc})$  for the simple control, maximum boost control, and maximum constant boost control are summarized as follows:

$$\frac{V_S}{GV_{dc}} = \frac{BV_{dc}}{GV_{dc}} = 2 - \frac{1}{G} \quad \text{for simple control} \quad (2.30)$$

$$\frac{V_S}{GV_{dc}} = \frac{BV_{dc}}{GV_{dc}} = \frac{3\sqrt{3}}{\pi} - \frac{1}{G} \quad \text{for maximum boost} \quad (2.31)$$

$$\frac{V_S}{GV_{dc}} = \frac{BV_{dc}}{GV_{dc}} = \sqrt{3} - \frac{1}{G} \quad \text{for maximum constant boost} \quad (2.32)$$

Figure 2.28 shows the voltage stress ratios. As can be seen from Figure 2.22, the maximum constant boost method has a much lower voltage stress across the devices than the simple control while having a slightly higher voltage stress than the maximum control method. The ideal voltage stress ratio is 1.

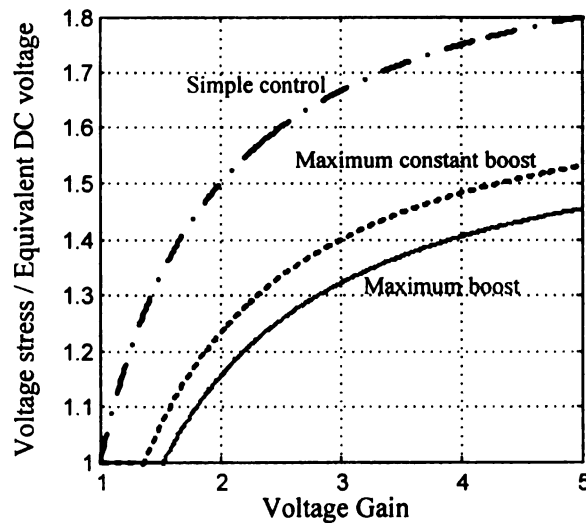


Figure 2.28. Voltage stress comparison of different control methods.

## 2.4 Modified PWM Scheme

The inverter with maximum constant boost control with third harmonic injection shoots through twice in one cycle (triangular waveform cycle), the equivalent frequency to the inductor is doubled, thus reducing the requirement to the inductors. However, it is obvious from Figure 2.20 that the real switching frequency of the device also doubled, which increases the switching loss.

In traditional PWM control, there is always a zero state after two active states as shown in Figure 2.29. There are two types of zero states, Zero 1 and Zero2, Zero 1 occurs when all upper three switches are turned on, and Zero 2 occurs when all lower three switches are turned on.

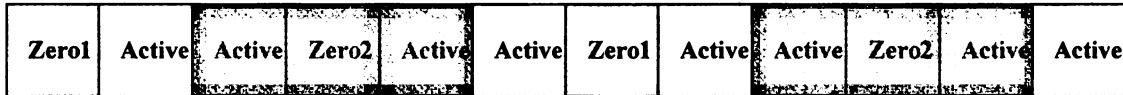


Figure 2.29. Switching states sequence of traditional PWM control.

The control of the Z-source inverter maintains the active states unchanged and shoots through some or all of the zero states. The key point of the modified PWM control is to turn half of the zero states (Zero1 or Zero 2) into shoot through state, and leave the active states unchanged. The duty ratio of that shoot through state equals to the shoot through duty ratio of maximum constant boost control, which is

$$D_0 = 1 - \frac{\sqrt{3}}{2} M. \quad (2.33)$$

Therefore, the shoot through period lasts  $(1 - \frac{\sqrt{3}}{2} M)T_s$  in each switching cycle  $T_s$ ,

which means that the zero state (Zero 1 or Zero 2) turned into shoot through state lasts

$(1 - \frac{\sqrt{3}}{2}M)T_s$ . To realize this function, there are two possible schemes shown in Figure

2.30 (a) and (b) respectively.

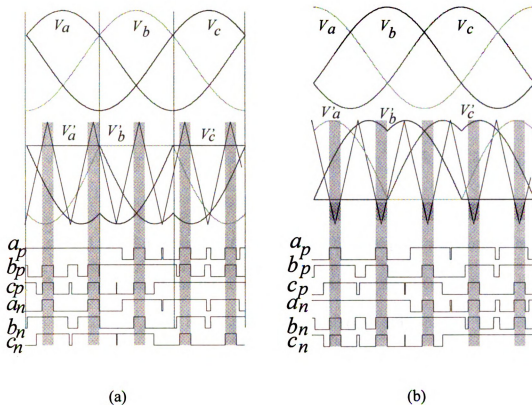


Figure 2.30. Modified PWM scheme.

For the case in (a), assume the reference signals in traditional SPWM are

$$\begin{aligned}
 v_a &= M \sin(\omega t) \\
 v_b &= M \sin(\omega t - \frac{2}{3}\pi). \\
 v_c &= M \sin(\omega t - \frac{4}{3}\pi)
 \end{aligned}
 \tag{2.34}$$

There are three different intervals in one line cycle in the modified PWM method, the reference signals in the three intervals are respectively

$$\begin{aligned}
v_a' &= \sqrt{3}M - 1 \\
v_b' &= \sqrt{3}M - 1 + v_b - v_a & 2k\pi + \frac{\pi}{6} \leq \omega t < 2k\pi + \frac{5}{6}\pi, \quad k = 0,1,2,\dots \quad (2.35) \\
v_c' &= \sqrt{3}M - 1 + v_c - v_a
\end{aligned}$$

$$\begin{aligned}
v_a' &= \sqrt{3}M - 1 + v_a - v_b \\
v_b' &= \sqrt{3}M - 1 & 2k\pi + \frac{5\pi}{6} \leq \omega t < 2k\pi + \frac{3}{2}\pi, \quad k = 0,1,2,\dots \quad (2.36) \\
v_c' &= \sqrt{3}M - 1 + v_c - v_b
\end{aligned}$$

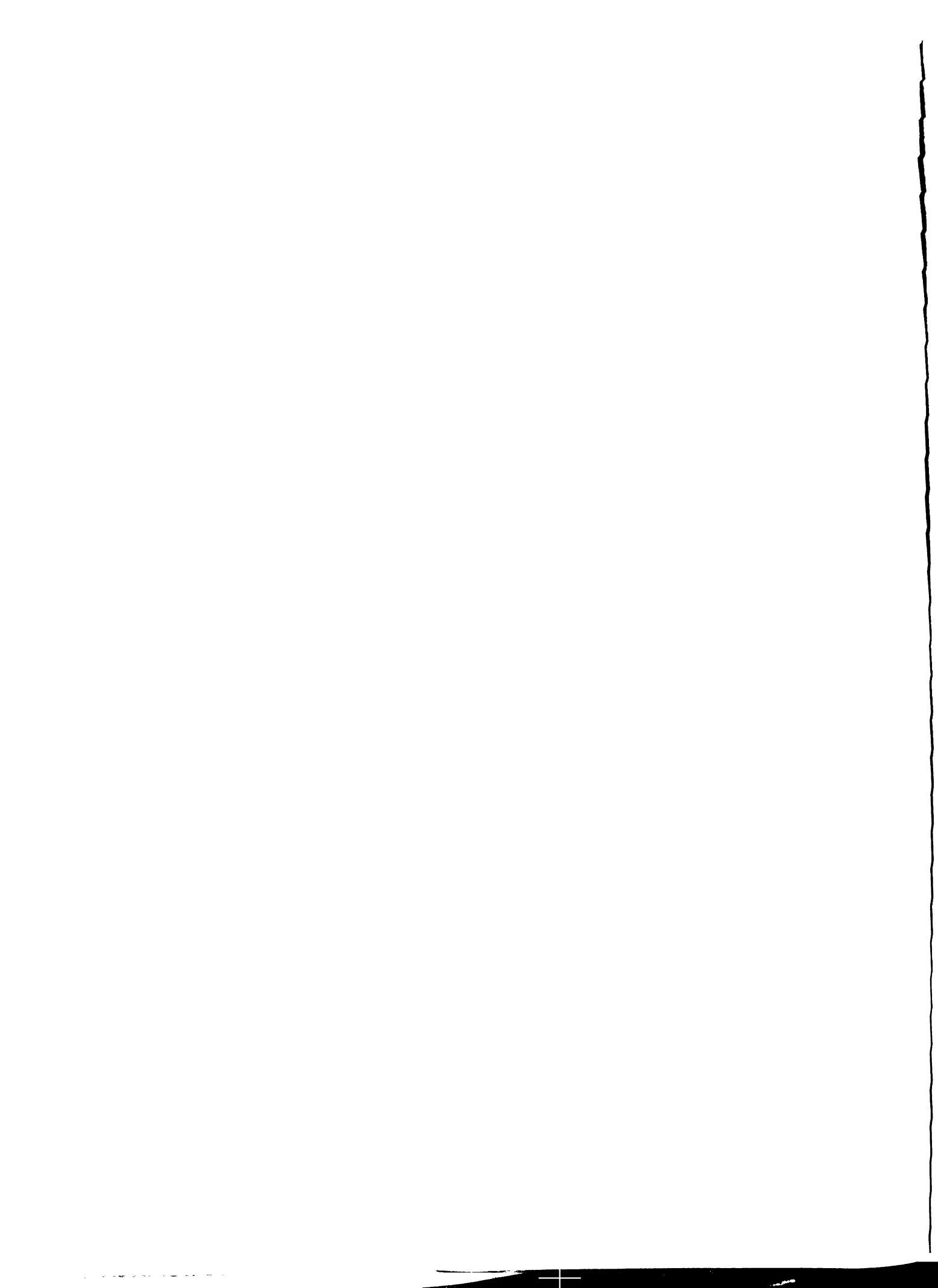
$$\begin{aligned}
v_a' &= \sqrt{3}M - 1 + v_a - v_c \\
v_b' &= \sqrt{3}M - 1 + v_b - v_c & 2k\pi + \frac{3\pi}{2} \leq \omega t < 2k\pi + \frac{13}{6}\pi, \quad k = 0,1,2,\dots \quad (2.37) \\
v_c' &= \sqrt{3}M - 1
\end{aligned}$$

where  $v_a$ ,  $v_b$ , and  $v_c$  are expressed in (2.34). When the triangular waveform is higher than the maximum value of the three, which is  $\sqrt{3}M - 1$ , the circuit is turned into a shoot through state by gating on all the switches, otherwise, it operates the same as traditional SPWM. It is obvious that the duration of each active state in a switching cycle is kept the same as in traditional SPWM by keeping the distance between the reference curves unchanged, therefore the fundamental element of the output voltage will still be kept sinusoidal.

The second case is shown in Figure 2.30 (b), also there are three different intervals in one line cycle for the modified PWM, the reference signals in the three intervals are respectively

$$\begin{aligned}
v_a' &= 1 - \sqrt{3}M \\
v_b' &= 1 - \sqrt{3}M + v_b - v_a & 2k\pi + \frac{7\pi}{6} \leq \omega t < 2k\pi + \frac{11}{6}\pi, \quad k = 0,1,2,\dots \quad (2.38) \\
v_c' &= 1 - \sqrt{3}M + v_c - v_a
\end{aligned}$$





$$\begin{aligned}
v_a' &= 1 - \sqrt{3}M + v_a - v_b \\
v_b' &= 1 - \sqrt{3}M \\
v_c' &= 1 - \sqrt{3}M + v_c - v_b
\end{aligned}
\quad 2k\pi + \frac{11\pi}{6} \leq \omega t < 2k\pi + \frac{5}{2}\pi, \quad k = 0, 1, 2, \dots \quad (2.39)$$

$$\begin{aligned}
v_a' &= 1 - \sqrt{3}M + v_a - v_c \\
v_b' &= 1 - \sqrt{3}M + v_b - v_c \\
v_c' &= 1 - \sqrt{3}M
\end{aligned}
\quad 2k\pi - \frac{\pi}{2} \leq \omega t < 2k\pi + \frac{1}{6}\pi, \quad k = 0, 1, 2, \dots \quad (2.40)$$

where  $v_a$ ,  $v_b$ , and  $v_c$  are expressed in (2.34). When the triangular waveform is lower than the minimum value of the three,  $1 - \sqrt{3}M$ , the inverter is turned into a shoot through state by gating on all the switches, otherwise, it operates the same as traditional SPWM. Also the duration of each active state in a switching cycle is kept the same as in traditional SPWM, therefore, the output waveform will still be kept sinusoidal.

From Figure 2.30, all six switches turn on and off 7 times in one cycle in total, which reduces the switching actions quite significantly. The equivalent frequencies to the inductors and to the load are both the triangular frequency.

The two different schemes achieve the same effect for the boost function of the inverter. But the switching actions and the on time of the upper and lower switches in a phase leg are different. From Figure 2.30.(a), all upper switches are turned on for 1/3 of the line cycle taking turns, and all the lower switches are turned on and off every switching cycle. It is the opposite for the case shown in (b). This results in unbalanced switching loss and conduction loss between each of the switches inside the IPM, which could increase the thermal stress of the switches. To minimize this unbalance, the two methods should be used alternatively every line cycle.

## 2.5 Comparison of Different PWM Schemes

In this section, a comparative study of two different PWM schemes will be examined using the switching loss, and passive components size as a benchmark. The two PWM schemes are the methods shown in Figure 1.8 and the modified PWM mentioned above. Basically, the first method shoots through six times in every switching cycle, and the latter one shoots through only once per switching cycle.

### 2.5.1 Switching Loss.

Assuming the inverter power is  $P$ , input voltage is  $V_{in}$ , load power factor is  $PF$ . There are two type of switching actions, one is the shoot through switching that is between shoot through state and traditional state, the other is traditional switching state, which is between traditional states.

#### a. *Six shoot through method*

For this method, every switching state is a shoot through switching state. Each switching state current is twice of the inductor current, whose average value is the average input current, thus the switching current is:

$$I_s = 2 \frac{P}{V_{in}} \quad (2.41)$$

#### b. *Modified PWM*

For this control method, there are two parts of switching losses: traditional switching (switching actions between traditional states) and shoot through switching (switching states between shoot through state and traditional states). The switching loss of traditional switching can be calculated by:

$$I_{swt} = I_{peak} \frac{1}{2\pi} \left( \int_0^\pi \sin x dx - \frac{1}{2} \int_{\frac{\pi}{6}-\alpha}^{\frac{5\pi}{6}-\alpha} |\sin x| dx \right)$$

$$= \begin{cases} I_{peak} \frac{1}{2\pi} \left( 2 + \frac{1}{2} \cos\left(\frac{5}{6}\pi - \alpha\right) - \frac{1}{2} \cos\left(\frac{\pi}{6} - \alpha\right) \right) & \alpha \leq \frac{\pi}{6} \\ I_{peak} \frac{1}{2\pi} \left( 1 + \frac{1}{2} \cos\left(\frac{5}{6}\pi - \alpha\right) + \frac{1}{2} \cos\left(\frac{\pi}{6} - \alpha\right) \right) & \alpha > \frac{\pi}{6} \end{cases}, \quad (2.42)$$

where  $I_{peak}$  is the peak load current,  $\alpha$  is the load phase angle. During shoot through state, the current from the dc side is  $2I_L$ , where  $I_L$  is the inductor current. Assuming that the current is evenly distributed in three phase legs, the average switching current of shoot through state is  $2I_L/3$ . In each cycle, there are 3 shoot through switching states, thus the shoot through switching loss of each IGBT is:

$$I_{sws} = \frac{P}{3V_{in}}, \quad (2.43)$$

For power factor of  $\cos\alpha$  and modulation index of  $M$ , the load peak current is

$$S = \frac{P}{\cos\alpha} = \frac{3}{2} I_{pk} \frac{MV_{dc}}{2(\sqrt{3}M - 1)} \quad (2.44)$$

Therefore,

$$I_{pk} = \frac{4(\sqrt{3}M - 1)P}{3 \cos\alpha MV_{dc}} \quad (2.45)$$

Putting all of this together, the overall switching current of the two different PWM methods for different power factors is shown in Figure 2.31. As can be seen from the figure, the switching current of the modified PWM is much smaller than in the six shoot through PWM method, which means higher efficiency.

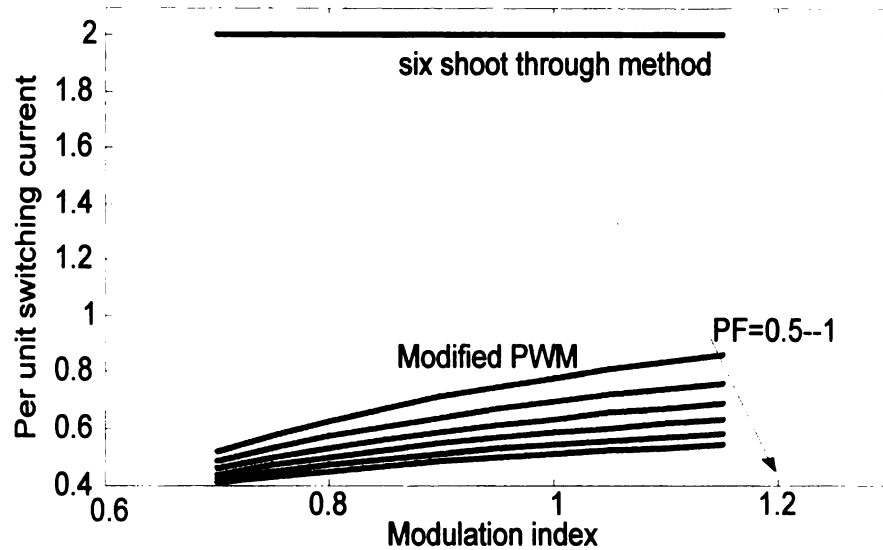


Figure 2.31. Overall switching current comparison of different PWM.

### 2.5.2 Inductor Size

The inductor size is based on the current and the inductance. The average currents through the inductors with different control methods are the same. The inductance is designed based on the same current ripple. The inductor current rises linearly during shoot through state and decreases linearly during other states.

*a. Modified maximum constant boost control*

The inductor current ripple is

$$\Delta I_L = \frac{V_c T_0}{L}, \quad (2.46)$$

where  $T_0$  is the total shoot through time in one switching cycle.

*b. Six shoot through method*

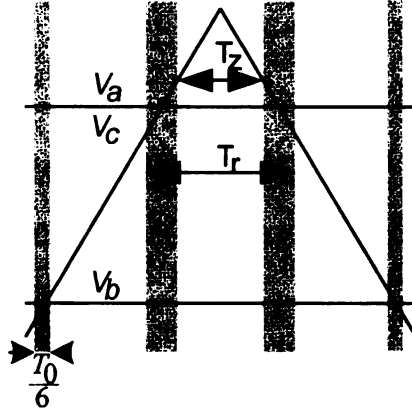


Figure 2.32. Six shoot through PWM when  $v_a=v_c$ .

The inductor current increases linearly during shoot through state and decreases linearly during non-shoot through state with two different constant rates respectively. For the six shoot through PWM method, the maximum current ripple occurs when the shoot through periods are least distributed, ie, when two of the reference signal equals to each other. Figure 2.32 shows an example when the reference signal  $v_a=v_c$ . Assume that  $1/6$  of third harmonic is injected, and the modulation index is  $M$ , the reference signals can be expressed as:

$$\begin{cases} v_a = M \sin \omega t + \frac{M}{6} \sin(3\omega t) \\ v_b = M \sin(\omega t - \frac{2}{3} \pi) + \frac{M}{6} \sin(3\omega t) \\ v_c = M \sin(\omega t - \frac{4}{3} \pi) + \frac{M}{6} \sin(3\omega t) \end{cases} \quad (2.47)$$

With maximum constant boost control, the shoot through duty ratio is

$$D_0 = 1 - \frac{\sqrt{3}}{2} M \quad (2.48)$$

The total non-shoot through time in a cycle is

$$T_{ns} = \frac{\sqrt{3}}{2} MT_s, \quad (2.49)$$

where  $T_s$  is the switching cycle. Assume that the middle reference signal is not shifted, the traditional zero state  $T_z$  for this instant ( $v_a=v_c$ ) can be calculated by

$$T_z = \left( \left(1 - \frac{1}{2}M - \frac{1}{6}M\right) - \left(1 - \frac{\sqrt{3}}{2}M\right) \right) T_s / 2 = \left( \frac{\sqrt{3}}{4}M - \frac{1}{3}M \right) T_s \quad (2.50)$$

Considering that the total inductor current change in a switching cycle is zero, the current drop in  $T_z$  can be calculated as:

$$\Delta i = \frac{T_z}{T_{ns}} * \frac{V_c}{L} T_0 = \frac{3\sqrt{3} - 4}{6\sqrt{3}} \frac{V_c}{L} T_0 \quad (2.51)$$

The current change in  $T_r$  can be calculated by

$$I_{ripple} = \frac{2}{3} T_0 \frac{V_c}{L} - \Delta i = 0.551 \frac{V_c T_0}{L}. \quad (2.52)$$

Therefore, compared to the modified PWM method, in order to keep the same inductor current ripple, the required inductance with the six shoot through method is about 55%.

### 2.5.3 Capacitor Size

The capacitor size is determined by the capacitor current and the capacitance. The capacitor current rating is the same regardless the modulation method. The capacitance is selected so that the voltage ripple is small and the output THD is low. For a given operating condition (power, load power factor, etc.) the capacitor charge ripple is shown in the following figure for different control methods, different power factors, and modulation indices. So the capacitance requirement is about the same.

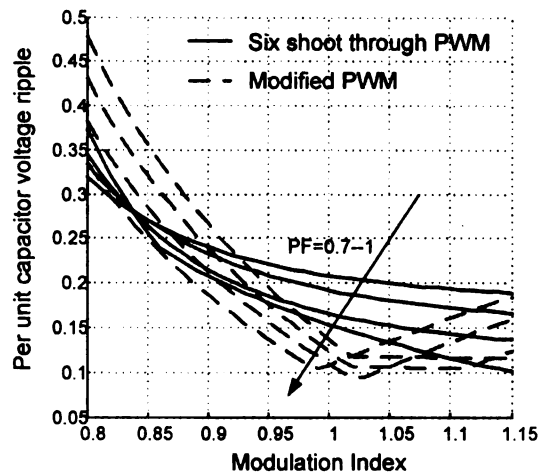


Figure 2.33. Capacitor voltage ripple comparison for different power factor.

## 2.6. Summary

Three control methods: simple control, maximum boost control, and maximum constant boost control have been presented in this chapter. Maximum boost control achieves lowest voltage stress across the devices. However this method will also result in line frequency current through the Z-source inductor, thus increases the requirement for the inductor. The maximum constant boost control minimizes the voltage stress across the device on the basis that there is no line frequency current ripple through the Z-source inductor. A modified PWM method is proposed to minimize the switching loss. A comparison between the modified PWM method and the existing six shoot through PWM method is conducted.



# CHAPTER 3 Modeling and Control of the Z-Source Inverter with RL Load

There are several small signal models proposed [40, 43, 51, 59] for the Z-source inverter. However in all the models, there is only one control parameter, which can not fully represent the inverter characteristics. In this chapter, a complete small signal model for the Z-source inverter will be proposed and a nonlinear controller will be designed. Simulation and experimental results will be provided to confirm the validity of the controller.

## 3.1 Modeling of the Z-source Inverter

### 3.1.1 Model Simplification

For a three phase inverter, the output power is always constant in steady state, thus the ac side can be simplified as a dc load without loss of generality considering the dynamic performance for three phase balance load. Figure 3.1 shows the three phase Z-source inverter with a RL load. When operating at shoot through duty ratio of  $D$  and modulation index of  $M$ , the equivalent circuit is shown in Figure 3.2.

In Figure 3.2, there are two switches, S1 is switching with a duty ratio of  $D$ , the duty ratio of S2 is  $M$ , and  $D + M \leq 1$ . The parameters of the Z-source network are the same as the original circuit. For the Z-source inverter, the output power is

$$P = 3 \left( \frac{M}{1-2D} V_{in} \frac{1}{2Z\sqrt{2}} \right)^2 R_{Load}, \quad (3.1)$$

where  $Z$  is the load impedance per phase.

While the load power of the dc equivalent circuit is

$$P = \left( \frac{M}{1-2D} V_{in} \right)^2 \frac{1}{R} \quad (3.2)$$

By equalizing the power of the two systems, we have

$$R = \frac{8Z}{3 \cos \varphi} \quad (3.3)$$

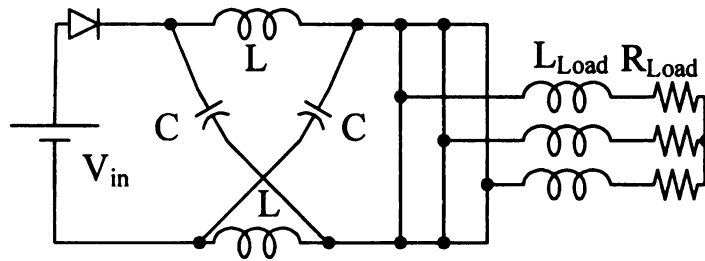


Figure 3.1. Z-source inverter.

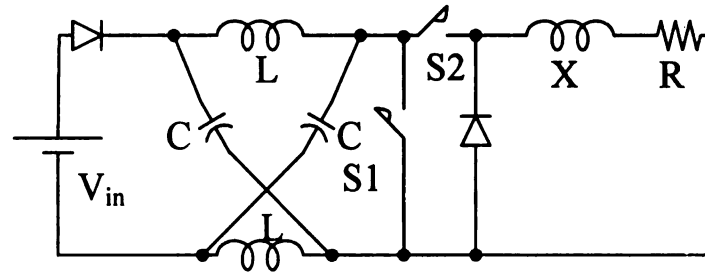


Figure 3.2. dc equivalent circuit.

where  $\cos \varphi$  is the load power factor. Naturally  $X$  is determined so that the time constant of the dc load is the same as the ac load, which means  $L/R$  is kept constant.

### 3.1.2 Modeling by State Space Averaging

To model the equivalent circuit, we have the following assumptions: the Z-source network is symmetrical, so that the currents through the two inductors and the voltages

across the capacitors are the same. With this assumption, there are three state variables: the current through the inductor in Z-source network, the voltage across the capacitor in the Z-source network, and the current through the load inductor.

Before modeling the inverter, the following parameters are defined:

$L$ : inductance of the inductor in Z-source;

$C$ : capacitance of the capacitor in Z-source;

$X$ : dc Load inductor;

$R$ : dc Load resistance;

$D$ : shoot through duty cycle;

$M$ : duty ratio of the other switch (modulation index of the original system);

$i_L$ : current through the inductor in the Z-source;

$i_x$ : load current;

$v_c$ : capacitor voltage;

$V_{dc}$ : input voltage.

There are three states, when S1 is turned on and S2 is turned off, the state equation is

$$\begin{bmatrix} si_L \\ sv_c \\ si_x \end{bmatrix} = \begin{bmatrix} 0 & \frac{1}{L} & 0 \\ -1 & 0 & 0 \\ 0 & 0 & \frac{-R}{x} \end{bmatrix} \begin{bmatrix} i_L \\ v_c \\ i_x \end{bmatrix} \quad (3.4)$$

The duty ratio of this state is  $D$ .

The second state is when both switches are turned off, the state equation is

$$\begin{bmatrix} si_L \\ sv_c \\ si_x \end{bmatrix} = \begin{bmatrix} 0 & \frac{-1}{L} & 0 \\ \frac{1}{C} & 0 & 0 \\ 0 & 0 & \frac{-R}{x} \end{bmatrix} \begin{bmatrix} i_L \\ v_c \\ i_x \end{bmatrix} + \begin{bmatrix} \frac{V_{dc}}{L} \\ 0 \\ 0 \end{bmatrix} \quad (3.5)$$

The duty ratio of this state is  $1-D-M$ .

The third state is when S1 is turned off and S2 is turned on, the state equation is

$$\begin{bmatrix} si_L \\ sv_c \\ si_x \end{bmatrix} = \begin{bmatrix} 0 & \frac{-1}{L} & 0 \\ \frac{1}{C} & 0 & \frac{-1}{C} \\ 0 & \frac{2}{x} & \frac{-R}{x} \end{bmatrix} \begin{bmatrix} i_L \\ v_c \\ i_x \end{bmatrix} + \begin{bmatrix} \frac{V_{dc}}{L} \\ 0 \\ \frac{-V_{dc}}{x} \end{bmatrix} \quad (3.6)$$

The duty ratio of this state is  $M$ .

Using state averaging, the system model can be obtained by

$(3.4)*D+(3.5)*(1-D-M)+(3.6)*M$  as shown in (3.7).

$$\begin{bmatrix} si_L \\ sv_c \\ si_x \end{bmatrix} = \begin{bmatrix} 0 & \frac{2D-1}{L} & 0 \\ \frac{1-2D}{C} & 0 & \frac{-M}{C} \\ 0 & \frac{2M}{x} & \frac{-R}{x} \end{bmatrix} \begin{bmatrix} i_L \\ v_c \\ i_x \end{bmatrix} + \begin{bmatrix} \frac{V_{dc}}{L}(1-D) \\ 0 \\ \frac{-V_{dc}}{x}M \end{bmatrix} \quad (3.7)$$

The output variables to be controlled are

$$\begin{bmatrix} v_c \\ v_x \end{bmatrix} = \begin{bmatrix} 0 & 1 & 0 \\ 0 & 0 & R \end{bmatrix} \begin{bmatrix} i_L \\ v_c \\ i_x \end{bmatrix} - \begin{bmatrix} 0 \\ 0 \end{bmatrix}. \quad (3.8)$$

The small signal model of the circuit becomes

$$\begin{aligned} & \left[ S + \frac{(1-2D)^2}{CSL} + \frac{2M^2}{C(XS+R)} \right] \tilde{v}_c \\ & = \frac{(1-2D)(2V_c - V_{dc}) - 2SLi_L}{CSL} \tilde{D} - \left( \frac{i_x}{C} + \frac{M(2V_c - V_{dc})}{C(XS+R)} \right) \tilde{M} \end{aligned} \quad (3.9)$$

Thus the transfer functions of the capacitor voltage over the shoot through duty ratio and modulation index for a given operating point are respectively:

$$\frac{\tilde{v}_c}{\tilde{D}} = \frac{(XS+R)(V_{dc} - 2SLi_L)}{CLXS^3 + CLRS^2 + (2M^2L + X - 4DX + 4D^2X)S + R - 4DR + 4D^2R} \quad (3.10)$$

$$\frac{\tilde{v}_c}{\tilde{M}} = \frac{-LS(2MV_c - MV_{dc} + i_xR + i_xXS)}{CLXS^3 + CLRS^2 + (2M^2L + X - 4DX + 4D^2X)S + R - 4DR + 4D^2R} \quad (3.11)$$

### 3.1.3 Model Verification

To confirm the small signal model, the bode diagram of the above transfer function is compared with simulation results.

The following figures show the calculated bode diagrams of the inverter at  $M=0.75$ ,  $D=0.2$ ,  $R=3.33\Omega$ ,  $L=1\text{mH}$ ,  $C=1.32\text{mF}$ ,  $X=1\text{mH}$ .

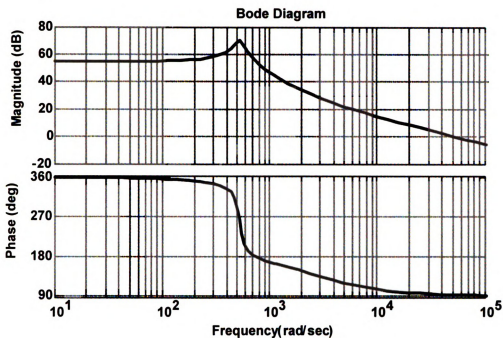


Figure 3.3. Calculated bode diagram of  $V_c/D$ .

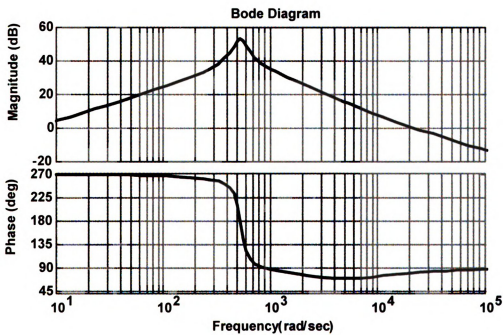


Figure 3.4. Calculated bode diagram of  $V_c/M$ .

Normal simulation software is not able to perform small signal simulation for switching

mode circuits. The PSIM 6.0 [74] provides the ac sweep function for small signal analysis. Figures 3.5-3.6 show the simulated bode diagram of  $V_c/D$  and  $V_c/M$  respectively, which confirms the calculated bode diagrams. The simulation software uses signal injection and calculates the gain and phase point by point on a switching circuit, therefore the results on some points is not very accurate.

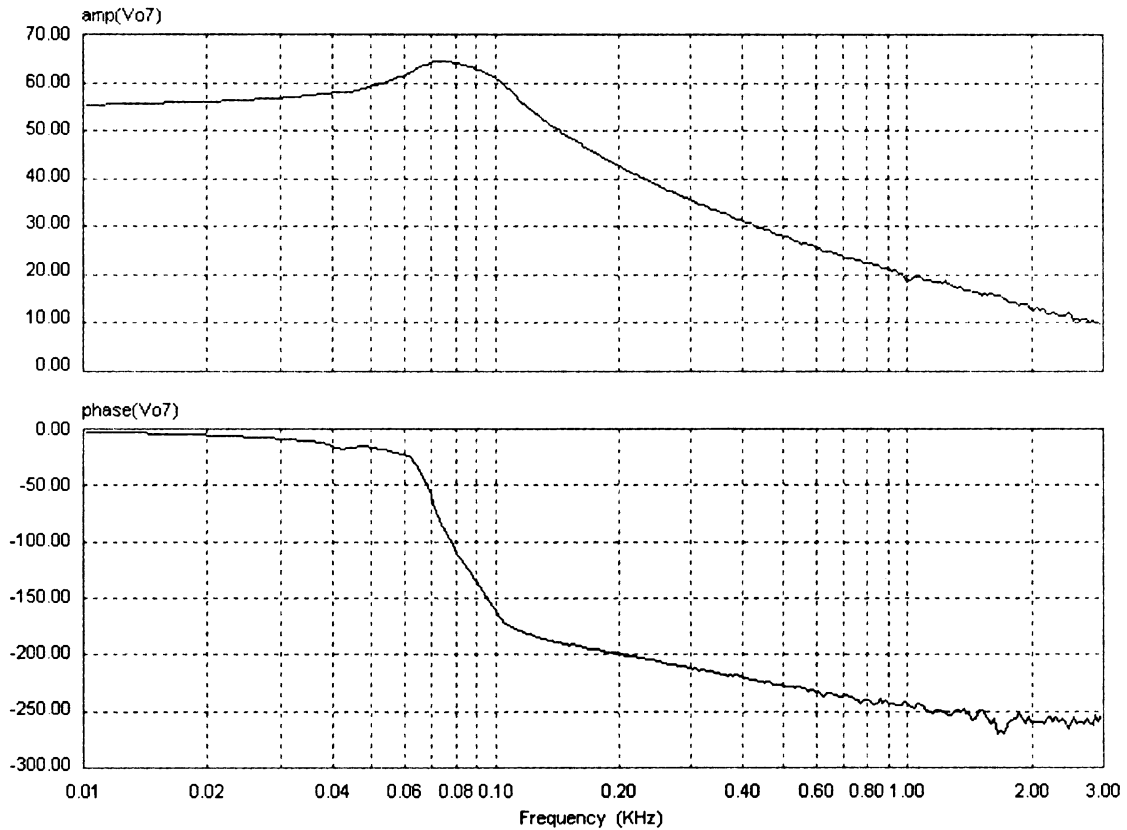


Figure 3.5. Simulated bode diagram of  $V_c/D$ .

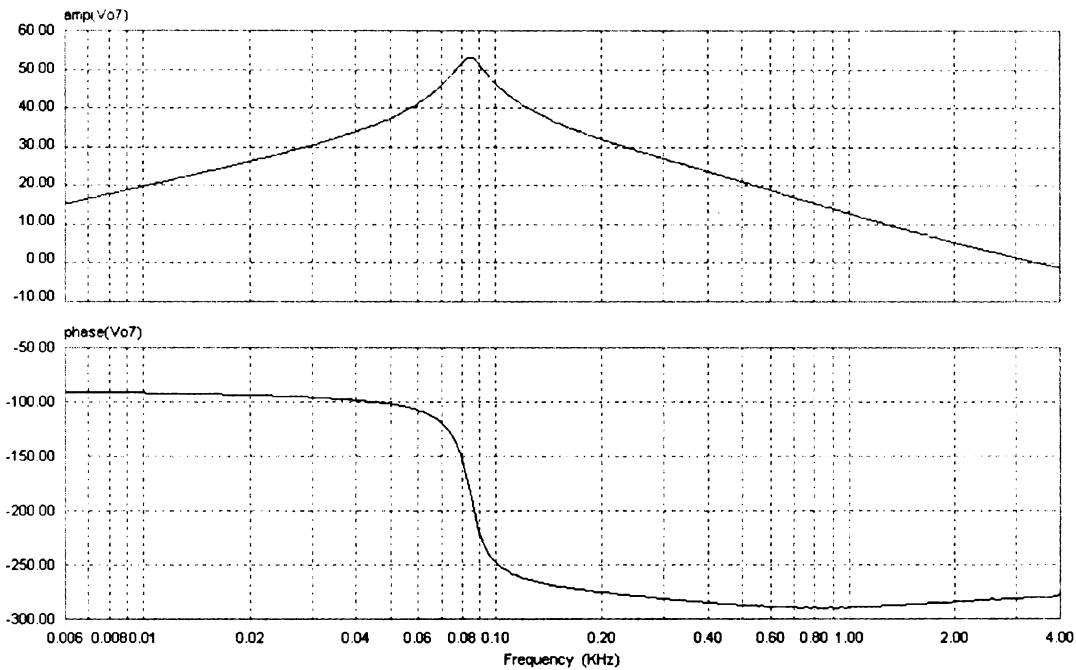


Figure 3.6. Simulated bode diagram of  $V_c/M$ .

From the above results, the bode diagram matches well, the proposed small signal model is verified.

## 3.2 Controller Design

### 3.2.1 Gain Scheduling Controller

As can be seen from (3.7), the system is a nonlinear system. A very common way to design a controller for nonlinear system is to linearize the system around an equilibrium point and design a linear controller for it. However, for tracking purpose, the operating point changes with the reference, the linear controller can not guarantee the stability of the system when the operating point is far from the equilibrium point the controller was designed for.

A natural way to design a nonlinear controller then would be a gain scheduling controller



[75, 76], which changes the controller gain along with the operating point. There is a limit in this control method, the operating point has to change relatively slow so that the system is always at or close to the operating point the controller is designed for, otherwise the system could be unstable.

### 3.2.2 Controller Design

In order to design a gain scheduling controller, one has to design a series of linear controllers for all possible equilibrium points. Also the linear controllers must be parameterized by a certain parameter that is related to the targeted output. The variable parameters at equilibrium points of the system for a targeted output values ( $V_{css}$ ,  $V_{xss}$ ) are:

$$\begin{aligned}
 M_{ss} &= \frac{V_{xss}}{2V_{css} - V_{dc}} \\
 D_{ss} &= \frac{V_{css} - V_{dc}}{2V_{css} - V_{dc}} \\
 i_{lss} &= \frac{V_{xss}^2}{RV_{dc}} \\
 V_{css} &= V_{css} \\
 i_{xss} &= V_{xss}/R
 \end{aligned} \tag{3.12}$$

The system has to be linearized at this equilibrium point. For a general form of system:

$$\dot{x} = f(x, u), \tag{3.13}$$

To linearize the system around an equilibrium point of  $(x_{ss}, u_{ss})$ ,  $f(x, u)$  is expressed in Taylor series for the operating point of  $(x_{ss} + x_{\delta}, u_{ss} + u_{\delta})$ ,

$$\frac{d(x_{ss} + x_{\delta})}{dt} = f(x_{ss}, u_{ss}) + \frac{d}{dx} f(x_{ss}, u_{ss})x_{\delta} + \frac{d}{du} f(x_{ss}, u_{ss})u_{\delta} + 0(x_{\delta}, u_{\delta}). \tag{3.14}$$

As a result, the following equation can be derived:

$$\dot{x}_\delta = \frac{\partial f}{\partial x} f(x_{ss}, u_{ss})x_\delta + \frac{\partial f}{\partial u} f(x_{ss}, u_{ss})u_\delta, \quad (3.15)$$

which is a linear system.

Based on the above method, the model can be linearized at any given equilibrium point, the linearized ABCD parameters are as follows.

$$A = \left. \frac{\partial f}{\partial x} \right|_{x=x_{ss}, u=u_{ss}} = \begin{bmatrix} 0 & \frac{-V_{dc}}{(2v_{css} - V_{dc})L} & 0 \\ \frac{V_{dc}}{(2v_{css} - V_{dc})C} & 0 & \frac{-v_{xss}}{(2v_{css} - V_{dc})C} \\ 0 & \frac{2v_{xss}}{(2v_{css} - V_{dc})x} & \frac{-R}{x} \end{bmatrix} \quad (3.16)$$

$$B = \left. \frac{\partial f}{\partial u} \right|_{x=x_{ss}, u=u_{ss}} = \begin{bmatrix} \frac{2v_{css} - V_{dc}}{L} & 0 \\ -2 \frac{v_{xss}^2}{CRV_{dc}} & -\frac{v_{xss}}{CR} \\ 0 & \frac{2v_{css} - V_{dc}}{x} \end{bmatrix} \quad (3.17)$$

$$C = \left. \frac{\partial g}{\partial x} \right|_{x=x_{ss}, u=u_{ss}} = \begin{bmatrix} 0 & 1 & 0 \\ 0 & 0 & R \end{bmatrix} \quad (3.18)$$

$$D = \left. \frac{\partial g}{\partial u} \right|_{x=x_{ss}, u=u_{ss}} = \begin{bmatrix} 0 & 0 \\ 0 & 0 \end{bmatrix} \quad (3.19)$$

The input voltage is assumed to be varying relatively slowly, so it is not counted in the dynamic response of the system. To simplify the system, the following variable transformation is implemented,

$$\xi = \frac{x}{V_{in}}. \quad (3.20)$$

The ABCD parameters after the transformation become

$$A = \begin{bmatrix} 0 & \frac{-1}{(2\frac{v_{css}}{V_{dc}} - 1)L} & 0 \\ \frac{1}{(2\frac{v_{css}}{V_{dc}} - 1)C} & 0 & \frac{-\frac{v_{xss}}{V_{dc}}}{(2\frac{v_{css}}{V_{dc}} - 1)C} \\ 0 & \frac{2\frac{v_{xss}}{V_{dc}}}{(2\frac{v_{css}}{V_{dc}} - 1)x} & \frac{-R}{x} \end{bmatrix} \quad (3.21)$$

$$B = \begin{bmatrix} \frac{2\frac{v_{css}}{V_{dc}} - 1}{L} & 0 \\ -2(\frac{v_{xss}}{V_{dc}})^2 \frac{1}{CR} & \frac{-\frac{v_{xss}}{V_{dc}}}{CR} \\ 0 & \frac{2\frac{v_{css}}{V_{dc}} - 1}{x} \end{bmatrix} \quad (3.22)$$

$$C = \begin{bmatrix} 0 & 1 & 0 \\ 0 & 0 & R \end{bmatrix} \quad (3.23)$$

$$D = \begin{bmatrix} 0 & 0 \\ 0 & 0 \end{bmatrix} \quad (3.24)$$

The second step in designing a gain scheduling controller is to design the controller for a series of possible equilibrium points. To make sure that the output variables are controlled to the desired values, integral control for the output variables are used. Thus the new state equations are:

$$\begin{aligned}
\dot{\xi} &= A\xi + Bu \\
\dot{\sigma} &= y - r \quad , \\
y &= C\xi + Du
\end{aligned}
\tag{3.25}$$

where  $r$  is the tracking reference signal. Thus the new system becomes

$$\dot{z} = \begin{bmatrix} A & 0 \\ C & 0 \end{bmatrix} z + \begin{bmatrix} B \\ D \end{bmatrix} u .
\tag{3.26}$$

Design a controller  $u = Kz$  so that the closed loop system

$$\dot{z} = \left( \begin{bmatrix} A & 0 \\ C & 0 \end{bmatrix} + \begin{bmatrix} B \\ D \end{bmatrix} K \right) z
\tag{3.27}$$

is stable, which means the poles of the closed loop system locates in the left half plain. MATLAB command *place* can achieve this goal. As a result, we get the controller gain  $K$  for one equilibrium point. There are two output variables, if we parameterize the controller with the two variables with  $n$  possibilities for each, we have to design  $n*n$  controllers. In order to simplify the design process without loss of generality, we can fix the relationship of the targeted values of the two output variables as long as the output voltage is the only variable the system is required to control. From Figure 3.2, when S1 and S2 are turned on and off complementally, the following equation will be reached:

$$V_{css} = V_{xss} .
\tag{3.28}$$

Transfer back to the three phase system, this means the inverter is controlled with simple boost and  $M+D=1$ . However, for the purpose of generality and to improve the transient response, we choose  $M+D<1$ , thus the following equation is derived:

$$V_{css} = k_{ratio} V_{xss} ,
\tag{3.29}$$

where  $k_{ratio} \geq 1$ .

Now we can use only one parameter to parameterize the controller for a given  $k_{ratio}$ , after we design a series of linear controllers and parameterize all the controller gains with  $V_{xss}/V_{dc}$ , the gain scheduling controller design is finished.

It is noteworthy to mention that in all above processes, the input voltage is considered as a given constant value or varying very slowly, this is because that in real system, the input voltage usually changes relatively slow if it is not constant, it will not affect the dynamic performance.

### 3.3 Simulation Results

Simulation of the closed loop system is performed with the following circuit parameters and the configuration shown in Figure 3.2:  $L=1\text{m}$ ,  $C=1.32\text{m}$ ,  $R_d=3.33\text{ohm}$ ,  $X=1\text{mH}$ ,  $V_{in}=200\text{V}$ ,  $k_{ratio}=1.05$  the closed loop system poles are placed to  $[-100+5i -100-5i -200+i -200-i -300]$ . Figure 3.7 shows the simulation results using the model in MATLAB. From the simulation results, the capacitor and output voltage/current follows the reference quite well in a wide range with acceptable amount of overshoot.

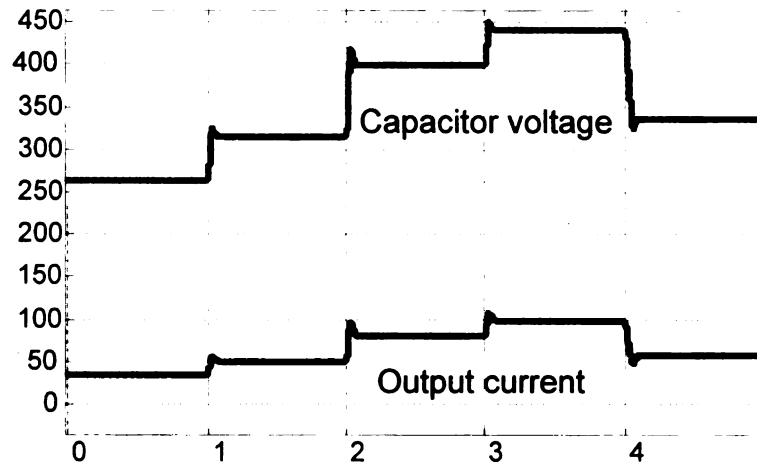


Figure 3.7. Simulation result of closed loop performance.

To examine the robustness of the controller, circuit simulation with mismatched parameters using SABER is performed. The controller is the same one as above, the parameters of the circuit in simulation are  $L=0.85\text{m}$ ,  $C=1.12\text{m}$ ,  $R=3.2\text{ohm}$ ,  $X=1\text{mH}$ ,  $V_{in}=200\text{V}$ ,  $k_{ratio}=1.05$ . The reference output voltage has a slow step change from  $V_{xss}/V_{in}=1.1$  to 1.8 and back to 1.1. The simulation result is shown in Figure 3.8, from which we can see that the output current and the capacitor voltage follows the reference, and the inductor current is off by certain value because of the parameter mismatch and circuitry loss. Therefore, satisfactory performance is obtained even though the circuit parameter is not exactly what the controller is designed for.

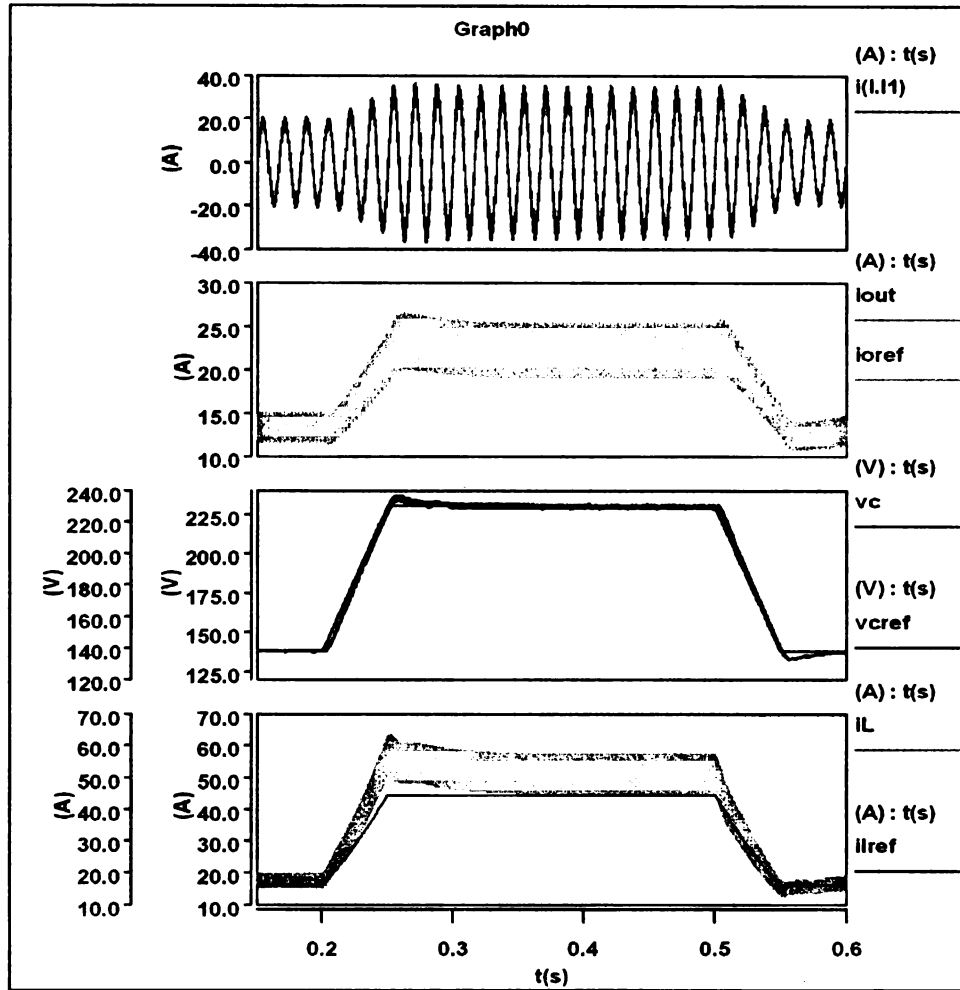
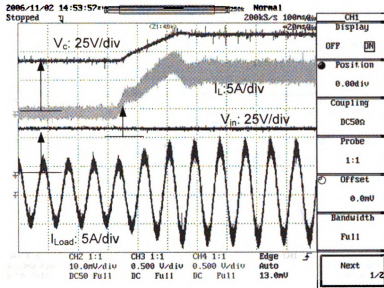


Figure 3.8. Circuit simulation results with parameter mismatch.

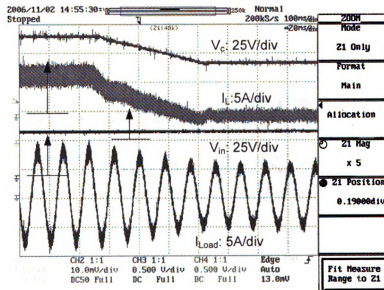
### 3.4 Experimental Verification

To verify the effectiveness of the controller, experiments were conducted. The parameters of the set up are listed as follows:

$L=1\text{mH}$ ,  $C=1.32\text{mF}$ ,  $L_{Load}=1\text{mH}$ ,  $R=3.33\text{ohm}$ ,  $V_{in}=37\text{ V}$ ,  $k_{ratio}=1.15$  (capacitor voltage/output voltage), the reference output voltage has a slow step change from  $V_{xss}/V_{in}=1.1$  to 1.8 and back to 1.1. The experimental results are shown in Figure 3.9.

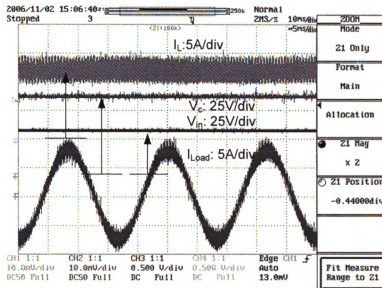


(a) Step up response

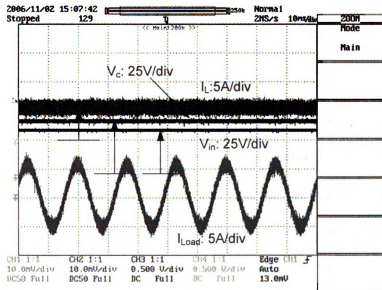


(b) Step down response





(c) Steady state operation when  $V_{xss}/V_{in} = 1.8$



(d) Steady state operation when  $V_{xss}/V_{in} = 1.1$

Figure 3.9. Experimental results.

Figure 3.9 (a) shows the performance of the controller with a step up change. The capacitor voltage,  $V_C$ , and the load current,  $I_{Load}$ , follow the reference very well. Only very small overshoot occurs. The inductor current,  $I_L$ , has to provide extra energy to

charge/discharge capacitor besides the steady state current, thus the it follows the reference less well, however, the overshoot/undershoot is acceptable. Similar results are obtained in Figure 3.9 (b) when a step down change happens. Figure 3.9(c) and (d) show the circuit performance under steady state operation, from where perfect sinusoidal output current can be observed, and the ratio of the capacitor voltage and the input voltage is exactly the value the controller is supposed to regulate. In the experiment, the error in the controller is limited to a certain range in the program to eliminate out of range sensing error, which also results in the transient response being slightly different from the simulation results. In these experiments, the output voltage increase/decrease transition only takes 25-50mS, which is enough for most applications.

### 3.5 Discussion

In the  $Z$ -source inverter, there are two control freedoms: the modulation index,  $M$ , and the shoot through duty ratio,  $D$ . However, the two freedoms are related, which is  $M+D \leq 1$  for simple boost control. In the above controller design, this limit is not considered and the two variables are controlled independently. During the transient, it is possible that the controller outputs a large  $M$  and  $D$ , which can not be implement, this might result in the system becoming unstable. Also, the sensing error might have the same effect. To make the system stable, it is preferred to use a large  $k_{ratio}$ , which results in a small  $M+D$  during steady state. However, this also causes higher voltage stress across the switches. Another way to solve this problem is to limit the variable errors in the program as we did in the experiment. By doing this, the output of the feed back controller is limited during a short period of time, thus the feed forward controller dominates during the step change, and the feed back controller will regulate the output afterwards.

## **3.6 Summary**

In this chapter, a small signal model of the Z-source inverter with a RL load is developed. Based on this model, a nonlinear closed loop controller is also designed using gain scheduling. The detailed modeling process and controller designing process are presented. Simulation results are used to confirm the small signal model. The controller is verified with simulation and experimental results.

# **CHAPTER 4 Z-Source Inverter for Fuel Cell Vehicles—Design and Comparison with Traditional Inverters**

The Z-source inverter is a good candidate for applications like fuel cell vehicles and solar panel systems. In this chapter, comparisons of the Z-source inverter and traditional inverters are provided to show the potential of Z-source inverter for these applications. A detailed design process of the Z-source inverter for fuel cell vehicle is also presented.

## **4.1 Introduction**

Fuel cells are very promising as the emerging energy sources in the near future. They have been used in a variety of areas, such as domestic applications, utility applications, and traction applications [18-21]. Unlike batteries that have a fairly constant output voltage, the fuel cell has a unique V-I characteristic and wide voltage range [77]. Figure 4.1 shows the V-I characteristic of proton exchange membrane (PEM) fuel cell, which is most promising for transportation applications. This unique V-I curve imposes challenges on the conditioning/interface circuits. For example, for fuel cell vehicles, this results in difficulty for high-speed, and high-power operation to achieve a great Constant Power Speed Ratio (CPSR). In addition, because the voltage drops at high power, the inverter has to be oversized.

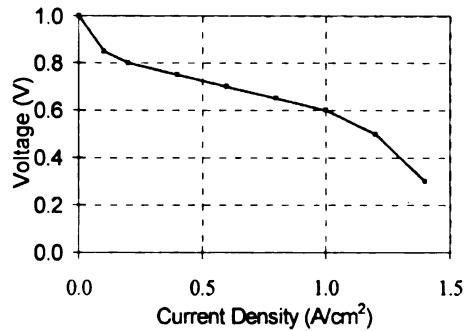
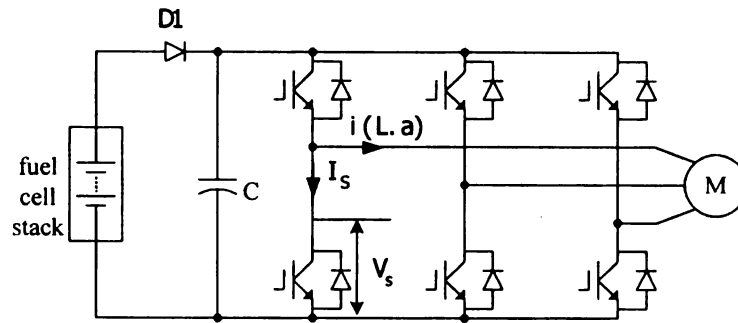


Figure 4.1. Typical PEM fuel cell polarization curve.

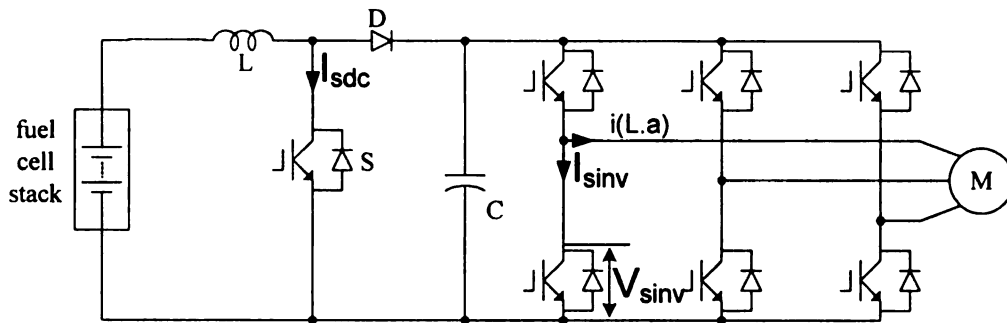
Currently, there are two existing inverter topologies used for hybrid electric and fuel cell vehicles: the conventional 3-phase Pulse Width Modulation (PWM) inverter and a 3-phase PWM inverter with a dc-dc boost converter. Because of the wide voltage range and limited voltage level of the fuel cell stack, the conventional PWM inverter topology imposes high stresses to the switching devices and the motor, and limits the motor's CPSR. The dc/dc boosted PWM inverter topology can alleviate the stresses and limitations, however suffers problems such as high cost and complexity associated with the two-stage power conversion.

## 4.2 System Configurations for Fuel Cell Vehicle

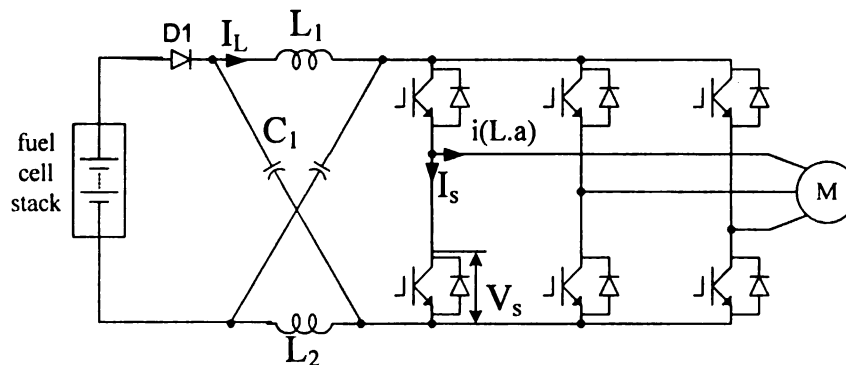
As previously mentioned, three different inverter systems are to be investigated: the conventional PWM inverter, the dc/dc boosted PWM inverter, and the Z-source inverter. Their system configurations for fuel cell vehicles are shown in Figure 4.2 (a), (b), and (c), respectively.



(a) System configuration using conventional PWM inverter



(b) System configuration using dc/dc boosted PWM inverter



(c) System configuration using the Z-source inverter

Figure 4.2. Three inverter system configurations for fuel cell vehicles.

In the traditional PWM inverter, the dc bus voltage, which is also the output voltage of the fuel cell stack, varies with the load. The modulation index has to be controlled to achieve the required output voltage. The boost converter in the dc/dc boosted PWM inverter system boosts the dc voltage only when the required output voltage is higher than

the fuel cell voltage. The Z-source inverter outputs a required voltage by adjusting the shoot through duty ratio with the restriction to keep the voltage across the switches not to exceed their limits.

### 4.3. Comparison Items, Conditions, Equations, and Results

For all comparisons, the conventional PWM inverter and the dc/dc boosted PWM inverter are controlled by SPWM with third harmonic injection to achieve the maximum modulation index possible when necessary. The Z-source inverter is controlled with maximum constant boost control with modified PWM scheme [69]. To compare different inverters, some parameters that are necessary for derivation are listed below.

- $P_o$             The maximum output power;
- $V_{max}$            The maximum output voltage of the fuel cell stack, open circuit voltage;
- $\cos\phi, PF$        The power factor of the motor;
- $V_i$               The fuel cell stack output voltage at maximum power;
- $M$                 The modulation index of inverters, defined by the ratio of the amplitude of the reference waveform and that of the carrier waveform for traditional SPWM;
- $V_{dc}$             The output dc voltage of the boost converter in the dc/dc boosted PWM inverter;
- $k$                 Boost ratio, defined by  $V_{max}/V_i$  for conventional PWM inverter;  $V_{dc}/V_i$ , for dc/dc boosted PWM inverter; and  $k=B$  in (A1.22) for Z-source inverter. Basically, this is the ratio of the maximum dc voltage across the inverter and minimum fuel cell output

voltage;

$D$  Duty ratio of the dc/dc converter in dc/dc boosted PWM inverter;

$I_{crms}$  Capacitor rms current;

$T_s$  Switching cycle;

$I_{peak}$  Peak load current.

### 4.3.1. Total Switching Device Power Comparison

In an inverter system, each switching device has to be selected according to the maximum voltage impressed and the peak and average current going through it. To quantify the voltage and current stress (or requirement) of an inverter system, switching device power is introduced. The SDP of a switching device/cell is expressed as the product of voltage stress and current stress. The total SDP of an inverter system is defined as the aggregate of SDP of all the switching devices used in the circuit. Total SDP is a measure of the total semiconductor device requirement, thus an important cost indicator of an inverter system. The definitions are summarized as follows:

$$\text{Total Average SDP} = (\text{SDP})_{av} = \sum_{m=1}^N V_m I_{m\_average}, \text{ and}$$

$$\text{Total Peak SDP} = (\text{SDP})_{pk} = \sum_{m=1}^N V_m I_{m\_peak}, \text{ where } N \text{ is the number of devices used,}$$

$I_{m\_average}$  and  $I_{m\_peak}$  are the average and peak current through the device respectively, and  $V_m$  is the peak voltage induced on the devices.

In our comparison, the input end diode D1 in the traditional PWM inverter and the Z-source inverter are not considered, because it's difficult to compare the cost of a diode and a switch of the same rating. The average and peak SDPs of conventional PWM



inverter are:

$$(SDP)_{av} = \frac{8V_{\max}P_o}{\cos\phi V_i\pi M}, \quad (4.1)$$

$$(SDP)_{pk} = \frac{8V_{\max}P_o}{\cos\phi V_i M}. \quad (4.2)$$

The average and peak SDPs of dc/dc boosted PWM inverter are:

$$(SDP)_{av} = \frac{8P_o}{\cos\phi\pi M} + \frac{P_o}{V_i} * V_{DC}, \quad (4.3)$$

$$(SDP)_{pk} = \frac{8P_o}{\cos\phi M} + \frac{P_o}{V_i} * V_{DC}. \quad (4.4)$$

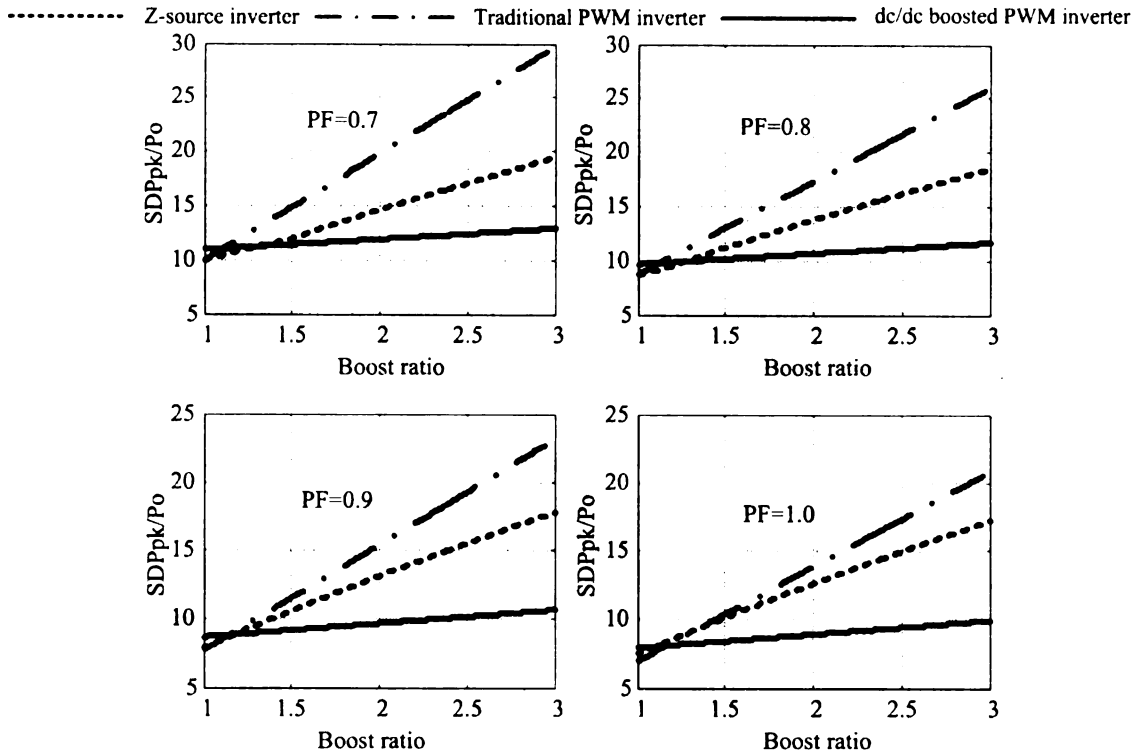
The average and peak SDPs of Z-source inverter are:

$$(SDP)_{av} = \frac{2P_o(2 - \sqrt{3}M)}{(\sqrt{3}M - 1)} + \frac{4\sqrt{3}P_o}{\cos\phi\pi}, \quad (4.5)$$

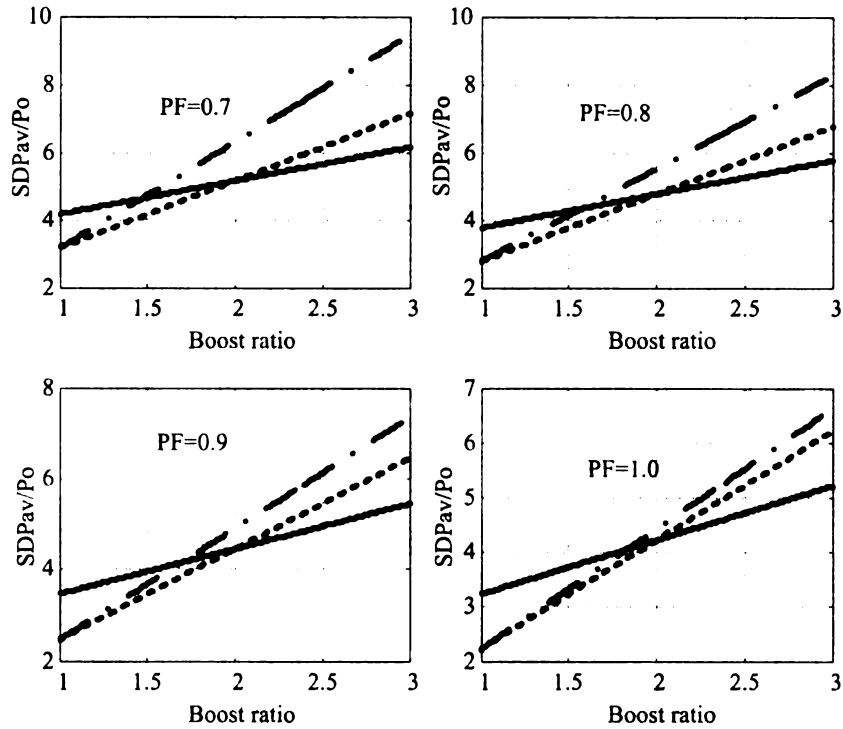
$$(SDP)_{pk} = \max\left(\frac{4P_o}{\sqrt{3}M - 1} + \frac{4P_o}{\cos\phi M}, \frac{8P_o}{\cos\phi M}\right). \quad (4.6)$$

The detailed derivation is in appendix 1.

Assume that the motors for different inverters are all in constant torque region, thus the motor current almost maintains constant for different power. The conventional PWM inverter and the dc/dc boosted PWM inverter are operated with modulation index of 1.15 with third harmonic injection or SVPWM at maximum power condition to minimize the required SDP. Based on the above equations and operation conditions, the required SDP of each inverter can be calculated for different load power factor and boost ratio,  $k$ , the results are shown in Figure 4.3. As mentioned above, the boost ratio is defined by  $V_{\max}/V_i$  for the conventional PWM inverter;  $V_{dc}/V_i$ , for the dc/dc boosted PWM inverter; and  $k=B$  for the Z-source inverter.



(a) Peak SDP for different power factors



(b) Average SDP for different power factors

Figure 4.3. Comparison of SDP of different inverters at different operation conditions.

For the conventional PWM inverter, it is obvious that the required SDP is proportional to the apparent power, therefore the SDP should increase linearly with the decrease of the load power factor. For the dc/dc boosted PWM inverter, the SDP of the inverter increases with the apparent power and the SDP of the dc/dc converter stays constant. It is similar for the Z-source inverter, the SDP contributed by shoot through doesn't change with the apparent power. Therefore, as load power factor reduces, the SDP of conventional PWM inverter increases quicker than the other two inverters, which is verified from Figure 4.3. As can be seen from Figure 4.3, if the same boost ratios are used for the three inverters, the Z-source inverter requires low SDP at low boost ratio region (1-2), especially average SDP, which is also an indicator of thermal requirement and conversion efficiency. When the boost ratio is above 2, the dc/dc boosted PWM inverter is the best in terms of SDP requirement. For very low boost ratio (1-1.25) and high power factor, the SDP of the conventional PWM inverter is very similar or even smaller than the Z-source inverter.

### **4.3.2. Requirement of Passive Components Comparison**

Passive components—inductors and capacitors are also important parts determining the inverter cost and volume. The inductors are designed to limit the current ripple, and the capacitors are designed based on current capacity and capacitance requirement.

#### **4.3.2.1 Inductor Design and Comparison**

For an inductor, the size is determined by the inductance and the current level. The average current,  $I_{av}$ , through the inductor in the dc/dc boosted PWM inverter at maximum power is:

$$I_{av} = \frac{P_o}{V_i}. \quad (4.7)$$

For the Z-source inverter, the average current through the inductor equals to that through the input end diode, based on power balance, the average inductor current can also be calculated by (4.7).

The purpose of the inductors is to limit the current ripple through the semiconductor devices, therefore, the inductance can be determined by a given current ripple level.

The inductor current ripple,  $\Delta I_L$ , in the dc/dc boosted PWM inverter can be calculated by:

$$\Delta I_L = \frac{V_i(V_{DC} - V_i)}{LV_{DC}} T_s, \quad (4.8)$$

where  $L$  is the inductance of the inductor.

The inductor current ripple in the Z-source inverter using maximum constant boost control is:

$$\Delta I_L = \frac{V_i \sqrt{3} M}{2L(\sqrt{3} M - 1)} \left( 1 - \frac{\sqrt{3}}{2} M \right) T_s, \quad (4.9)$$

where  $L$  is the inductance of the inductors.

The detailed derivations of the equations are in appendix 2. In (4.8) and (4.9), all other parameters are known for maximum power operation condition, therefore the inductance requirement can be calculated by limiting the current ripple within a certain range.

For the two inductors in the Z-source inverter, the current through them and the voltage across them are exactly the same, therefore they can be built on the same core, with the same size of one inductor with doubled inductance as shown in Figure 4.4.

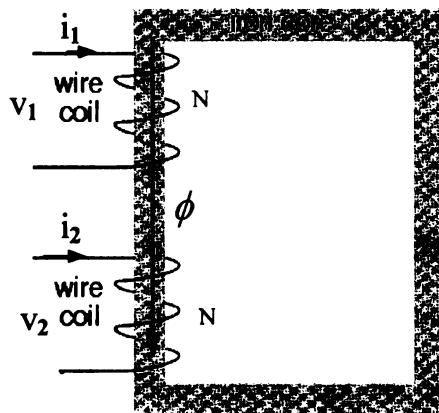


Figure 4.4. Coupled inductors.

For a single coil on one core, the flux through the core is

$$\phi = PNi, \tag{4.10}$$

where  $P$  is a constant related to the core material and dimension,  $N$  is the number of turns of the coil, and  $i$  is the current through the coil. The inductance of the coil is

$$L = \frac{N\phi}{i} = PN^2. \tag{4.11}$$

For the two inductors in the Z-source inverter, because of the symmetry of the circuit, the current through the inductors is always exactly the same. For two coils on one core with exactly the same current,  $i$ , the flux through the core is

$$\phi = 2PNi. \tag{4.12}$$

The resulted inductance of each coil when supplying exactly the same current to the two coils is

$$L = \frac{N\phi}{i} = 2PN^2. \quad (4.13)$$

The inductance of each coil is doubled.

#### 4.3.2.2 Capacitor Requirement Comparison

The current through the capacitor is an important factor determining the capacitor size. It is obvious that the current through the capacitor repeats every 1/3 of the fundamental cycle. From Figure 4.5, the capacitor current can be calculated by the following equation:

$$I_{crms} = \sqrt{\frac{1}{3f} \int_0^{3f} (i_{ic}(t) - i_{oc}(t))^2 dt}, \quad (4.14)$$

where  $f$  is the fundamental frequency.

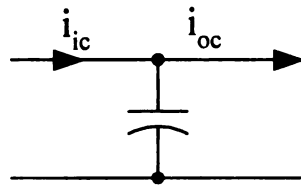


Figure 4.5. Capacitor current ripple calculation.

For the conventional PWM inverter, the input current to the capacitor,  $i_{ic}$ , is assumed to be constant, which equals to the average current,  $\frac{P_o}{V_i}$ . The output current of the capacitor changes with the time, and it can be different for different PWM schemes.

However, the rms current stays the same [78, 79]. For the switching cycle with SPWM scheme shown in Figure 4.6 (a), the instant current can be described as:

$$i_{oc}(t) = \left. \begin{cases} 0 & T0 < t \leq T1, T3 < t \leq T5, T7 < t \leq T8 \\ i_a & T2 < t \leq T3, T5 < t \leq T6 \\ -i_b & T1 < t \leq T2, T6 < t \leq T7 \end{cases} \right\} \quad (4.15)$$

where  $i_a$  and  $i_b$  is the load current of phase  $a$  and  $b$ .

As a result, the following equation can be derived:

$$I_{crms}^2 = \left( -\frac{9}{16} M^2 \cos^2 \varphi + \frac{\sqrt{3}M}{\pi} \cos \varphi + \frac{\sqrt{3}M}{4\pi} \right) I_{peak}^2 \quad (4.16)$$

Based on this equation, the capacitor current for different modulation indices and load

power factors are shown in Figure 6 (a).  $K_i$  is defined by  $K_i = \frac{I_{crms}^2}{I_{peak}^2}$ , where  $I_{peak}$  is

the output peak current.

For the dc/dc boosted PWM, assuming that the control of the dc/dc converter and the inverter share the same carrier, for a certain interval with modulation scheme shown in Figure 5 (b), the input and output current of the capacitor can be described as:

$$i_{ic}(t) = \left. \begin{cases} 0 & T0 < t \leq T2, T8 < t \leq T10 \\ \frac{P_o}{V_i} & T2 < t \leq T8 \end{cases} \right\} \quad (4.17)$$

$$i_{oc}(t) = \left. \begin{cases} 0 & T0 < t \leq T1, T4 < t \leq T6, T9 < t \leq T10 \\ i_a & T3 < t \leq T4, T6 < t \leq T7 \\ -i_b & T1 < t \leq T3, T7 < t \leq T9 \end{cases} \right\} \quad (4.18)$$

The resulted current depends on the relative positions of the reference signals. It is

easier to use numerical calculation than analytical expression. The dc/dc boosted PWM inverter operates as a conventional PWM inverter when the input voltage is higher than the required output voltage with  $D=0$ . When the input voltage is not high enough to output the required voltage, to minimize the switching loss, the inverter is always operated with maximum modulation index possible, 1.15, and the dc/dc converter operates with  $D$  greater than zero to output the required voltage. Figure 4.7 (b) shows the calculated capacitor current for the dc/dc boosted PMW inverter for these two conditions. The solid curves show the capacitor current when the  $D=0$  with different modulation indices, the dotted curves show the capacitor current when  $D>0$  and  $M=1.15$  for different load power factors.

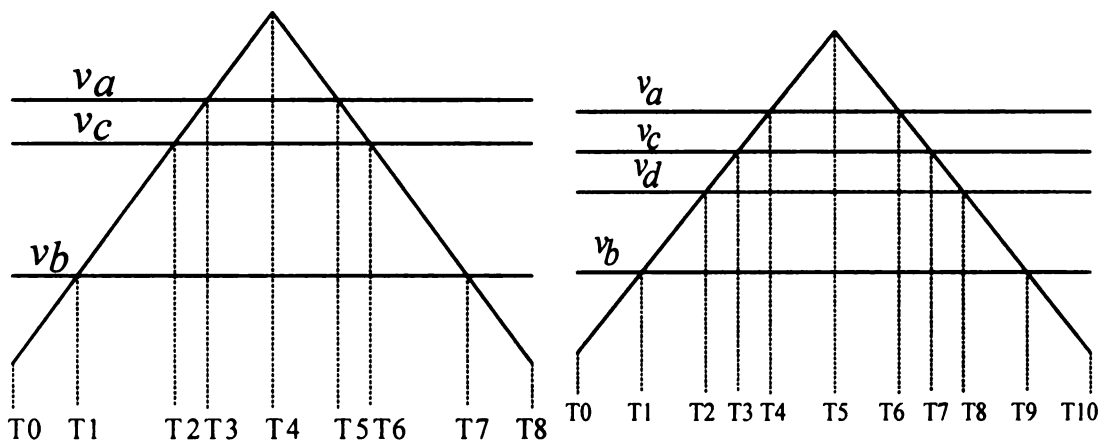
Maximum constant boost control with third harmonic injection shown in Figure 4.6 (c) is used to control the Z-source inverter. As seen from Figure 4.6 (c), when the carrier is higher than  $V_p$  or lower than  $V_n$ , the inverter is in shoot through state, while in between, it operates as traditional SPWM. The input current to the capacitor is the inductor current, which can be considered as constant,  $\frac{P_o}{V_i}$ . During traditional zero states and active states, the output current of the capacitor is the same as the conventional PWM inverter. During shoot through state, the two capacitors are charging the two inductors separately through the inverter bridge, therefore the current through the inverter bridge is twice of the inductor current. More detailed description of the output current of the capacitor at the interval shown in Figure 4.6 (c) as an example is as follows:



$$i_{oc}(t) = \left. \begin{cases} 0 & T1 < t \leq T2, T4 < t \leq T5, \\ & T7 < t \leq T8, T10 < t \leq T11(\text{traditional zero state}) \\ i_a & T3 < t \leq T4, T8 < t \leq T9 \\ -i_b & T2 < t \leq T3, T9 < t \leq T10 \\ 2 \frac{P_o}{V_i} & T0 < t \leq T1, T5 < t \leq T7, T11 < t \leq T12 (\text{shoot through state}) \end{cases} \right\} \quad (4.19)$$

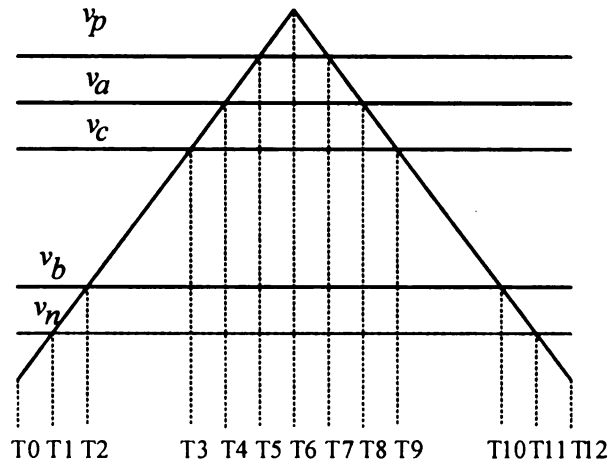
From this equation, we can calculate the current through the capacitors in the Z-source inverter. Similarly, the Z-source inverter can be operated as a conventional PWM inverter when the input voltage is high enough to output the required voltage, and it will be operated with shoot through only when the input voltage is lower than the required output voltage. The resulted capacitor currents for these two different operation conditions are shown in Figure 4.7(c).

It is note worthy to mention that  $I_{peak}$  is different for different inverter systems. For the same fuel cell stack and same power,  $I_{peak}$  of the conventional PWM inverter will be higher than the other two because of lower available voltage.



(a) Conventional PWM inverter

(b) dc/dc boosted PWM inverter



(c) Z-Source inverter

$v_a, v_b, v_c$ : reference signals of inverter PWM;  $v_d$ : reference signal of the dc/dc converter;

$v_p, v_n$ : reference signals controlling the shoot through

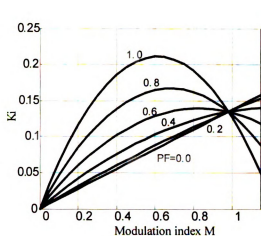
Figure 4.6. PWM scheme of different inverters at a certain interval.

The capacitance can also be an important factor determining its size depending on the type of the capacitor. The capacitance is designed based on limiting the voltage ripple across the capacitor to limit the output current harmonic. From the above analysis of the current through the capacitor, it is easy to numerically calculate the maximum voltage ripple of the capacitors under different conditions. The calculated results are shown in Figure 4.8. The dotted curves in (b) and (c) show the results when boost function is needed.

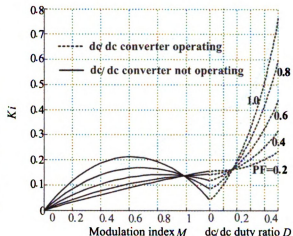
The result is defined by  $K_{vr} = \frac{\Delta Q}{I_{peak} \cdot T_s}$ , where  $\Delta Q$  is the charge causing the

maximum voltage ripple,  $I_{peak}$  is the peak load current,  $T_s$  is the switching cycle. Also,

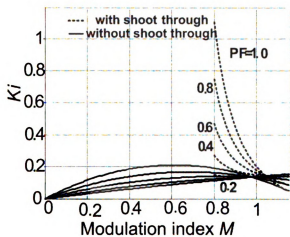
$I_{peak}$  is different for different inverter systems.



(a) Conventional PWM inverter



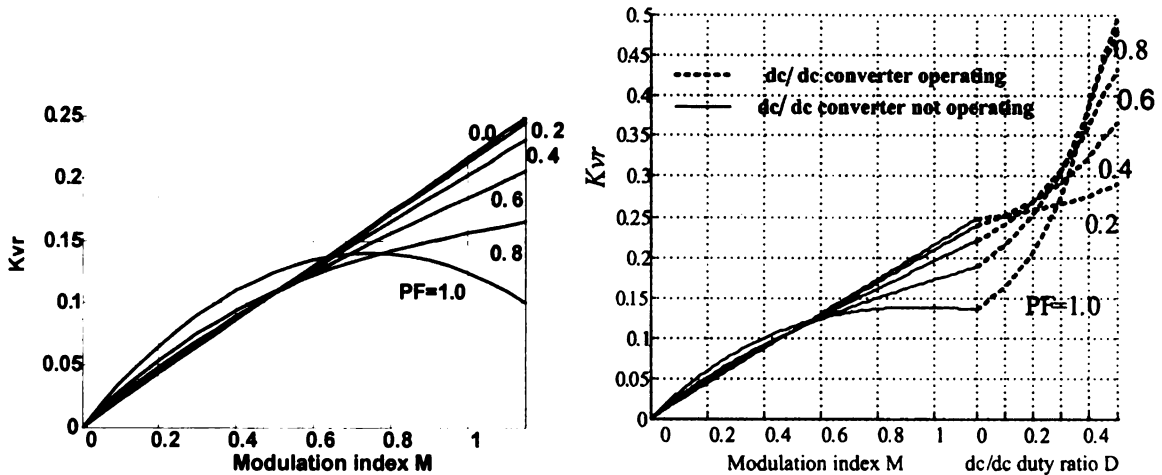
(b) dc/dc boosted PWM inverter



(c) Z-source inverter

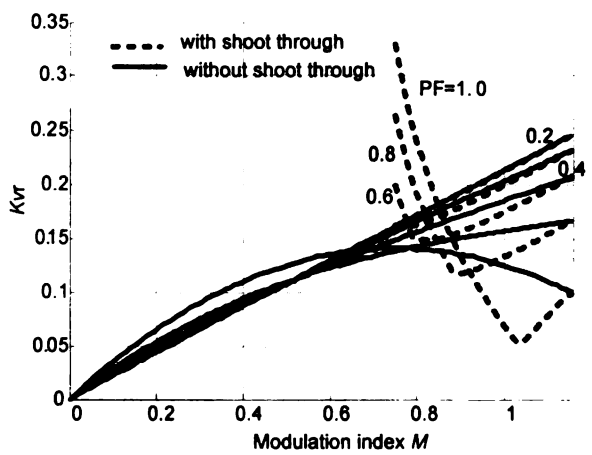
$$K_i = \frac{I_{crms}^2}{I_{peak}^2}, I_{peak} \text{ is the peak load current of the inverter}$$

Figure 4.7. Capacitor current comparison of the inverters.



(a) Conventional PWM inverter

(b) dc/dc boosted PWM inverter



(c) Z-source inverter

Figure 4.8. Capacitor voltage ripple comparison of the inverters.

**4.3.3. CPSR Comparison**

CPSR is limited mainly by available dc voltage of the PWM inverter. The fuel cell voltage decreases as the current drawn increases, which greatly limits the motor’s power output and efficiency at high speed. For the dc/dc boosted PWM inverter and the Z-source inverter, the available output voltage is theoretically infinite. To compare the CPSR limited by the inverter output voltage, certain operating conditions have to be

specified. To make a fair comparison, the same fuel cell stack and the same device voltage ratings are used. This is accomplished by limiting the maximum output voltage of the dc/dc converter,  $V_{dc}$ , the maximum voltage across the device of Z-source inverter,  $\hat{v}_{pn}$ , and the open circuit voltage of the fuel cell,  $V_{max}$ , to the same values. Thus the maximum voltage across the device and the boost ratio are the same for all inverters. The modulation indices of the conventional PWM inverter and the dc/dc boosted PWM inverter are both 1.15, to output the maximum voltage. The maximum obtainable output phase peak voltage of conventional PWM inverter at peak power is

$$\hat{v}_{ac} = V_i \frac{M}{2} = \frac{V_i}{\sqrt{3}} \quad (4.20)$$

The maximum obtainable output voltage of the dc/dc boosted PWM inverter is

$$\hat{v}_{ac} = V_{dc} \frac{M}{2} = \frac{kV_i}{\sqrt{3}} \quad (4.21)$$

For the Z-source inverter, the modulation index used to boost the voltage is determined by [7]:

$$\frac{1}{\sqrt{3}M - 1} = k. \quad (4.22)$$

The resulted obtainable output voltage is:

$$\hat{v}_{ac} = \frac{(k+1)V_i}{2\sqrt{3}}. \quad (4.23)$$

Define the CPSR of conventional PWM inverter to be 1 per unit. The CPSR of dc/dc boosted PWM inverter and the Z-source inverter are  $k$  and  $\frac{k+1}{2}$  respectively.

#### 4.3.4. Reliability Comparison

Compared to traditional PWM inverter and the Z-source inverter, the dc/dc boosted PWM inverter uses one more active device, which inevitably reduces the reliability of the inverter. Also, the Z-source inverter can handle shoot through state, thus momentary shoot through caused by EMI will not affect the inverter operation. While for traditional inverters, this might trigger protection and cause unexpected system shut down.

#### 4.4 Comparison Example

In this section, a comparison example will be conducted based on a given fuel cell and system with the following parameters:

$$V_i=250 \text{ V}; V_{max}=420 \text{ V}; P_o=50 \text{ kW}; \cos\phi=0.9;$$

The conventional PWM inverter and the dc/dc boosted PWM inverter are operated with modulation index of 1.15 with third harmonic injection or SVPWM at maximum power condition. For a fair comparison, the same device voltage ratings are used, which means the boost ratios of the three inverters are kept the same.

With these assumptions, the SDP of different inverters can be calculated and shown in Table.4.1.

Table 4.1 Switching device power comparison example

Inverter Systems	Total Average SDP (kVA)	Total Peak SDP (kVA)
PWM inverter	207	650
dc/dc boosted PWM inverter	207	470
Z source inverter	191	577

Table 4.2. Required passive components

Inverter Systems	Number of inductor	Inductance ( $\mu\text{H}$ )	Average inductor current (A)	Number of capacitor	Capacitance of the capacitor ( $\mu\text{F}$ )	Capacitor rms current (A)	Capacitor voltage rating (V)
Conventional PWM inverter	0	N/A	N/A	1	296	112	420
dc/dc boosted inverter	1	510	200	1	511	105	420
Z-source inverter	2 (1)	339	200	2	428	110	420

Table 4.3. Operation conditions at different power

Power Rating		50 kW	40kW	30 kW	20 kW	10 kW
Fuel cell voltage (V)		250	280	305	325	340
Motor Phase voltage (V)	Conventional PWM inverter	101.7	81.4	61	40.7	20.3
	dc/dc boosted PWM inverter	170.8	136.6	102.4	68.3	34.2
	Z – source inverter	136.8	109.4	82.1	54.7	27.4
Motor current (A)	Conventional PWM inverter	182	182	182	182	182
	dc/dc boosted PWM inverter	108.4	108.4	108.4	108.4	108.4
	Z – source inverter	135	135	135	135	135

The Z-source inverter's average SDP is the lowest among the three while the conventional PWM inverter's SDPs are the highest in both average and peak values.

Usually, the selection of the switching device is based on the rms/average current rating, and also the average SDP is a measurement of thermal requirement.

Table 4.2 shows the passive component comparison with the requirements to limit the inductor current ripple to be less than 10% of its average value, and capacitor voltage ripple less than 3% of the maximum voltage, 420 V @ switching frequency of 10 kHz. The Z-source inverter's two inductors can be built on one core to minimize the size and weight. In general, the required L and C of the Z-source inverter are slightly greater than those of the dc/dc boosted PWM inverter.

For the conventional PWM inverter with the fuel cell model described above, the fuel cell voltage is the dc voltage of the inverter, which drops to 250 V at 200 A. From the 250 V dc, the conventional PWM inverter can only yield 176 V to the motor. This low motor voltage limits CPSR and lowers mechanical output power and efficiency. The PWM inverter with dc-dc boost can keep the dc voltage to 420 V, which in turn increases CPSR by a factor of 1.68. Theoretically the Z-source inverter can output whatever voltage as required. By the restriction of the same switch voltage stress as the traditional PWM inverter and dc/dc boosted PWM inverter, the Z-source inverter can increase the CPSR by 1.34 times over the traditional PWM inverter. In other words, the motor voltage produced by the Z-source inverters is 1.34 times that produced by the conventional PWM inverter, thus the same motor can output 1.34 times the power than when driven by the conventional PWM inverter.

Efficiency is an important criterion for any power converter. High efficiency can reduce thermal requirements and cost.

The inverter system is assumed to be operated in constant torque region and space vector



control is applied to all inverters. Based on this assumption, the output voltage and current of the inverter can be derived in Table.4.3. From the resulted voltage and current, the following devices are chosen for efficiency calculation: the switches for the main inverters of dc/dc boosted inverter and Z-source inverter are Powerex IPM PM300CLA060, the switch for the dc/dc boost converter is Powerex PM300DSA060, the switch for the traditional inverter is Powerex IPM PM450CLA060, the input end diode of the traditional PWM inverter and the Z-source inverter is IXYS MEO 500-06DA.

For the efficiency comparison, only the semiconductor devices losses are considered. For conventional PWM inverter and dc/dc boosted PWM inverter, the IGBT loss consists of switching loss and conduction loss, the diode loss includes conduction loss and reverse recovery loss, the detailed calculation method can be found in [80]. For the Z-source inverter, the loss of the inverter consists of the following parts: conduction loss of the switches during non-shoot through states, switching loss between non-shoot through states, conduction loss of the switches during shoot through state, switching loss of the shoot through state, free wheeling diodes conduction loss and reverse recovery loss during non-shoot through states. The modified PWM sequence of maximum constant boost control is implemented for efficiency comparison, in which one shoot through period is employed in a switching cycle as shown in Figure 4.9. The switching loss for the modified PWM method can be found in chapter 2.

The reverse recovery loss of the free wheeling diodes is reduced because some of the turn off states of the diodes are turn into shoot through turn off, the reverse recovery loss can be calculated accordingly.

Shoot through	Active1	Active2	Zero state	Active2	Active1
---------------	---------	---------	------------	---------	---------

Figure 4.9. Switching states sequence in one cycle.

The conduction losses of the IGBTs and the diodes also change because of the shoot through states. Assuming the shoot through duty ratio is  $D_0$  and the corresponding conduction losses of IGBTs and diodes for traditional PWM inverter under the same load current are  $P_{onIGBT}$  and  $P_{ondiode}$  respectively, which can be calculated based on [80], the conduction losses of the Z-source inverter during traditional states become:

$$P_{onIGBTtraditional} = (1 - D_0)P_{onIGBT} \quad (4.24)$$

$$P_{ondiodetraditional} = (1 - D_0)P_{ondiode} \quad (4.25)$$

Assuming that the inductor current is high enough so that all IGBTs are on during shoot through state, the average current through the IGBTs during shoot through is  $\frac{2I_L}{3}$ , the conduction loss of IGBTs during shoot through is

$$P_{onIGBTshootherough} = D_0 V_{CE(sat)} * \frac{2}{3} I_L, \quad (4.26)$$

where  $V_{CE(sat)}$  is the saturation voltage of the IGBT. From all above discussion, total loss of the inverter bridge can be calculated. Also, the conduction loss and reverse recovery losses of the input end diode of the Z-source inverter and the traditional PWM inverter are considered. The inverter efficiency calculation results are shown in Figure 4.10.

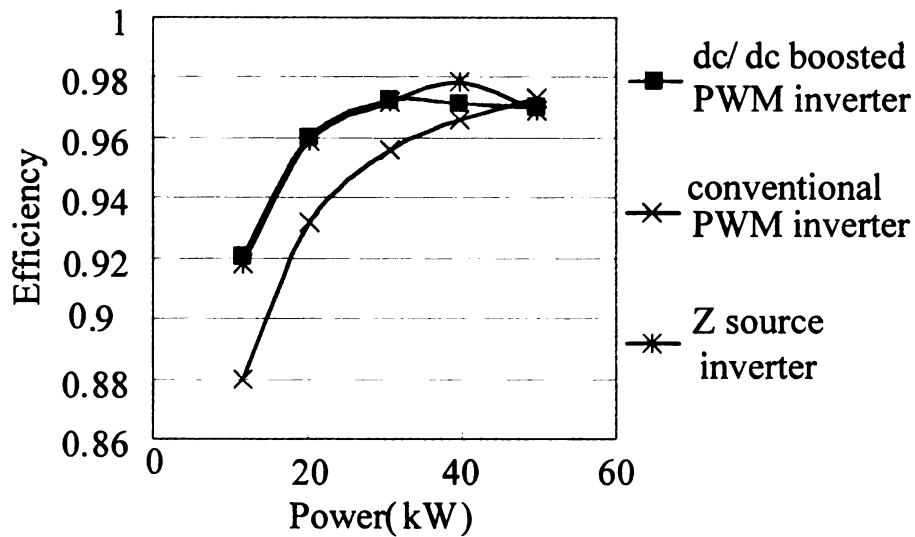


Figure 4.10. Calculated efficiency of inverters.

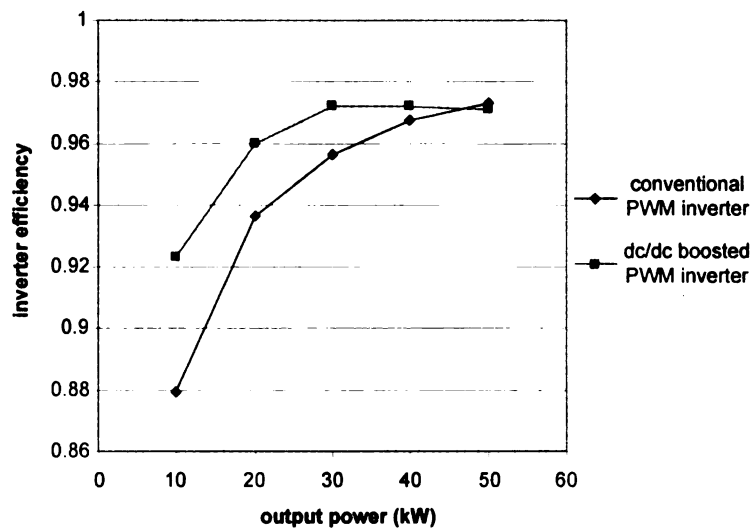
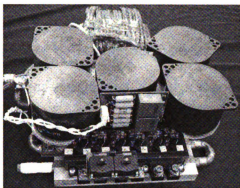


Figure 4.11. Inverter efficiency calculated using software.

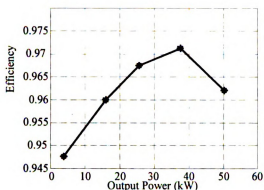
From the above comparison, the Z-source inverter provides the highest efficiency in most regions of the power range of the inverter itself.

To verify the efficiency calculation of the traditional inverters, Mitsubishi average loss simulation software [81] is used. The efficiencies of the conventional PWM inverter and dc/dc boosted PWM inverter calculated from the software under the same operation

conditions are shown in Figure 4.11. As can be seen from Figure 4.10-11, the calculated efficiencies and simulated efficiencies are very close. However, because of the different operating principle, the software can't be used to simulate the efficiency of the Z-source inverter. To verify the efficiency calculation of the Z-source inverter, efficiency measurements on a 50kW Z-source inverter shown in Figure 4.12 (a) are conducted. Developed for a different project, the inverter bridge is Powerex IPM PM600CLA060 to meet high temperature requirement, the inductor is 25  $\mu$  H each and built on one core, which is equivalent to a 50  $\mu$  H inductor, also one film capacitor is connected in parallel with the input voltage source just to minimize the current loop. However, the loss characteristics of the two IPMs are quite similar. The test was carried out on a RL load test and with power factor of 0.8. The resulted efficiency is shown in Figure 4.12 (b). Because of the load, the current at low power becomes smaller than the motor current when operated in constant torque mode. This results in higher efficiencies than the calculated value at low power range. Also, because of the lower power factor, and the losses on the passive components, the efficiency at high power is slightly lower than as expected from the calculated values. Considering all these factors, the calculated efficiencies of the inverters are quite accurate.



(a) 50kW Z-source inverter



(b) Measured efficiencies

Figure 4.12. Efficiency testing and results.

## 4.5. Summary

A comprehensive comparison of the three inverter systems has been performed. General equations and curves of switching device power, passive component requirement, and CPSR have been derived for comparison. A comparison example with detailed specifications has been carried out. For this comparison example, efficiencies of the different systems have also been compared and verified. The comparison results show that the Z-source inverter has lowest average SDP in low boost ratio range (1-2). Also it provides higher efficiencies in most operating ranges. It can increase the CPSR over the conventional PWM inverter significantly. It does slightly increase the passive component requirement.

It is note worthy to mention that this is a purely theoretical comparison. In practical cases for the dc/dc boosted PWM inverter, the associated cost and volume increase of the extra heat sinking effort, and the required gate drive for an extra switch, is also significant. Also, the great reliability enhancement of the Z-source inverter is a very important advantage. In general, the Z-source inverter is very competitive in moderate boost ratio

range (1-2), in which most fuel cells reside. In cases when a low voltage fuel cell is used, and boost ratio much higher than 2 is needed, the dc/dc boosted PWM inverter is the best configuration. In this chapter, the comparison is limited to a fuel cell vehicle without a battery, all configurations can be modified to fuel cell-battery hybrid vehicles by adding a battery [12] to incorporate the regenerative braking function without significant change of the main circuit.

# **CHAPTER 5 Operation Modes and Characteristics of the Z-Source Inverter with Small Inductance or Low Power Factor**

All of the descriptions and analysis done in previous chapters are based on an assumption that the inductance of the inductor in the Z-source network is large, and the load power factor is high so that the inductor current is almost constant. In some applications, the inductance should be minimized in order to reduce cost, volume, and weight. In this chapter, we will analyze the Z-source inverter operation when the inductance is very small and the inductor current has high ripple or is discontinuous. The analysis reveals new operation modes and characteristics. As a result, design guidelines and considerations will be provided.

## **5.1. Introduction**

The traditional voltage source inverter (VSI) is a buck converter which can only produce a voltage lower than the DC bus voltage. A 3-phase VSI has 6 active states and 2 zero states. A zero state is produced when the upper three or lower three switches are turned on at the same time shorting the output terminals. The upper and lower two switches of any phase leg can never be gated on at the same time, otherwise a shoot-through short

circuit would occur and could destroy the inverter. The shoot-through is a forbidden switching state for the traditional VSI. The Z-source inverter shown in Figure 5.1, instead, uses the shoot through state to boost the output voltage. However, under certain load condition and inverter parameters, there could be more operating modes.

In order to make the description of the converter easier, a list of symbols are listed below.

#### Nomenclature

- $V_o$ : Input voltage of the Z-source inverter;
- $v_i$ : Voltage across the inverter bridge;
- $L$ : Inductance of inductors in the Z-source network;
- $C$ : Capacitance of the capacitors in the Z-source network;
- $V_s$ : Voltage stress across the device, equals to maximum value of  $v_i$ ;
- $V_c$ : Voltage across the capacitors in the Z-source network;
- $i_L$ : Current through the inductors in the Z-source network;
- $i_i$ : Current fed to the inverter bridge;
- $i_{in}$ : Input current to the Z-source inverter;
- $T_0, T_7$ : Zero states in SVPWM/SPWM;
- $T_{0-7}$ : Total traditional zero state in one switching cycle;
- $T_1, T_2$ : Active states in SVPWM/SPWM;
- $G$ : Voltage gain, defined by the ratio of output peak phase voltage and half of the input voltage;



$M$ : Modulation index;

$\cos\phi$ : Load power factor;

$T_{st}$ : Shoot through period in one switching cycle;

$T_s$ : Switching cycle;

$Z$ : Load impedance per phase;

$I_{pk}$ : Load peak current;

$V_{out}$ : Output phase rms voltage.

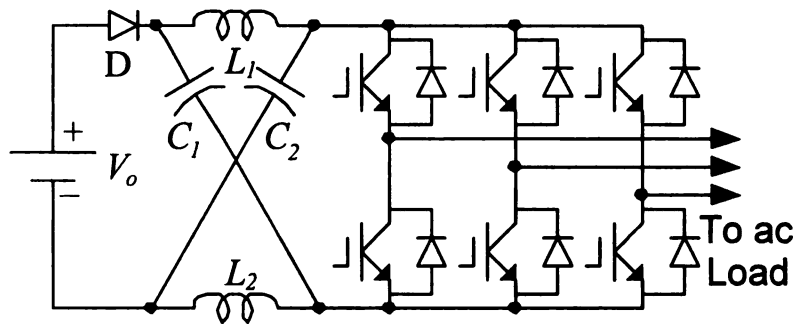


Figure 5.1. The Z-Source inverter.

## 5.2. Operating Principle and Operation Modes Analysis

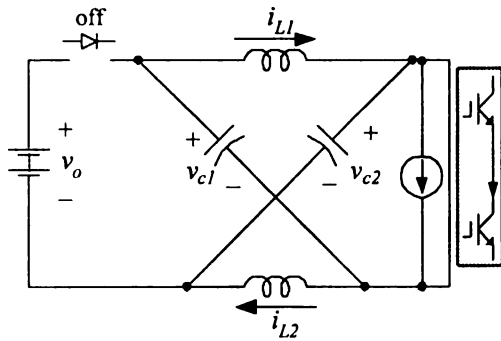
The Z-source inverter utilizes the shoot through zero states to boost voltage in addition to the traditional 6 active states and 2 zero states. The basic operating principle described in [12] assumes that the inductor current is relatively high and almost constant. When the inductance is small or the load power factor is low, the inductor current can have high ripple or even become discontinuous. Instead of having the two operating modes described in [12], the Z-source inverter may have five different operation modes as shown in Figure 5.2 when viewed from the Z-source network. Modes 1 and 2 have been

described in [12], whereas modes 3, 4 and 5 are new modes that may exist for small inductance and low power factor cases.

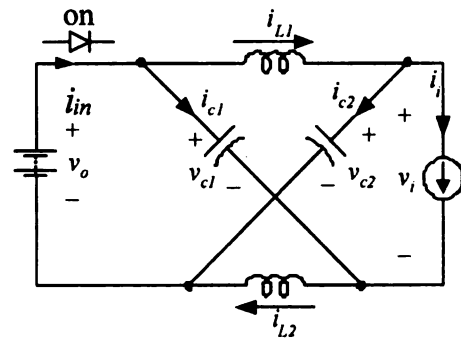
**[Mode 1]:** The circuit is in a switch shoot-through zero state when the two switches in any of the three phase legs are turned on at the same time, the sum of the two capacitors' voltage is greater than the dc source voltage ( $V_{C1} + V_{C2} > V_0$ ), the diode is reverse biased, and the capacitors charge the inductors. The voltages across the inductors are:

$$V_{L1} = V_{C1}, V_{L2} = V_{C2}. \quad (5.1)$$

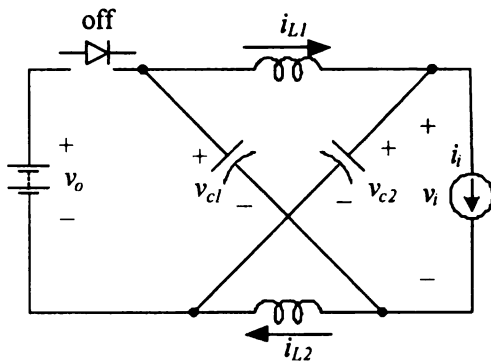
The inductor current increases linearly assuming the capacitor voltage is constant during this period. Because of the symmetry ( $L_1 = L_2 = L$  and  $C_1 = C_2 = C$ ) of the circuit, one has  $v_{L1} = v_{L2} = v_L$ ,  $i_{L1} = i_{L2} = i_L$ , and  $V_{C1} = V_{C2} = V_C$ .



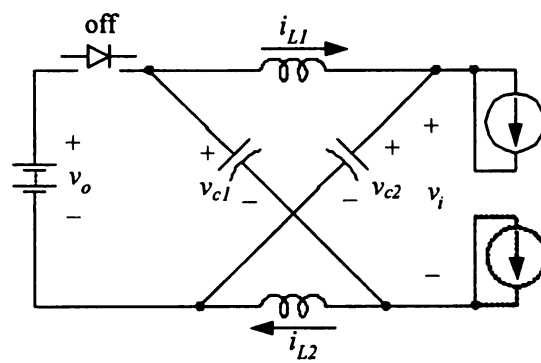
(a) Mode 1



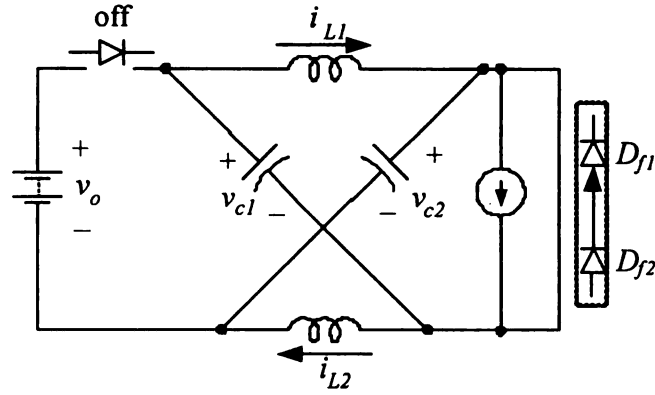
(b) Mode 2



(c) Mode 3



(d) Mode 4



(e) Mode 5

Figure 5.2. Possible operation modes of Z source inverter.

**[Mode 2]:** The inverter is in a non-shoot through state (one of the 6 active states and 2 traditional zero states) and the inductor current meets the following inequation,

$$i_L > \frac{1}{2} i_i. \quad (5.2)$$

Again because of the symmetry of the circuit, the capacitor current  $i_{C1}$  and  $i_{C2}$  and the inductor current  $i_{L1}$  and  $i_{L2}$  should be equal to each other respectively. In this mode, the input current from the dc source becomes:

$$i_{in} = i_{L1} + i_{c1} = i_{L1} + (i_{L2} - i_i) = 2i_L - i_i > 0 \quad (5.3)$$

Therefore, the diode is conducting and the voltage across the inductor is

$$v_L = V_o - V_C, \quad (5.4)$$

which is negative (the capacitor voltage is higher than the input voltage during boost operation when there are shoot through states), thus the inductor current decreases linearly assuming the capacitor voltage is constant. As time goes on, the inductor

current keeps decreasing to a level that no longer the condition of (5.2) can be met and the input current,  $i_{in}$ , or the diode current is decreased to zero, Mode 2 ends and the inverter enters to a new mode.

**[Mode 3]:** The inverter is in one of the 6 active states, and the inductor current equals to half of the inverter dc side current,  $i_i$ . As a result, the input current becomes zero and the diode becomes reverse-biased. Assuming that the inverter load is inductive and has a much larger inductance than that of the inductor  $L_1$  and  $L_2$ , the voltage drop across  $L_1$  and  $L_2$  are negligible and the inductor current and inverter voltage  $v_i$  are respectively

$$i_L = \frac{1}{2} i_i \quad \text{and} \quad (5.5)$$

$$v_i = V_c. \quad (5.6)$$

**[Mode 4]:** The inverter is in one of the 2 traditional zero states ( $i_i=0$ ) and at the end of Mode 2, the inductor current decreases to zero, thus a new operation mode appears. In Mode 4, the diode stops conducting and the inverter is an open circuit to the Z-source network because of  $i_i=0$ . The inductor current becomes zero and maintains zero until the next switching action. Therefore, in this mode, the Z-source circuit is isolated from both the dc source and the load. The load terminals are shorted by the upper three switches or the lower three switches as shown in Figure 5.2 (d).

**[Mode 5]:** Freewheeling diode shoot through state: The inverter is switched to an active state and the inductor current at that instant is less than  $i_i/2$ . After having been switched to an active state, the inverter cannot enter the active state immediately because that the available current from the dc side  $2i_L$  is not enough to supply the load current,  $i_i$ , the inverter enters a free-wheeling state described in Figure 5.2 (e). The two diodes in the

equivalent circuit are the free wheeling diodes of the inverter phase legs. This diode free wheeling state turns the inverter into a shoot through state. During this shoot through state, all the equations of Mode 1 hold true and the inductor current increases linearly. This mode continues until the inductor current reaches  $i/2$  or another switching action happens. The difference between this mode and Mode 1 is that this mode is not intentionally created by the control signal and depends on the load current and the inductor current at the time of switching.

### **5.3. Circuit Analysis and Characteristics**

The Z-source inverter can be operated with both traditional SPWM/SVPWM without any shoot through states and with shoot through to boost the output voltage. Under both cases, the new operation modes may or may not occur depending on the inductance and load conditions. The combination and sequence of the operation modes can be different for different circuit parameters. In this section, the circuit will be analyzed under both traditional SVPWM control and with boost by giving the operation conditions including the combination and sequence of the new modes and the critical conditions for the new modes to happen.

#### **5.3.1. Traditional SVPWM Control**

Under traditional SVPWM control and simple operation, when only the Mode 1 and Mode 2 occurs, the capacitor voltage always equals to the input voltage and the inductor current is a pure dc. However, under certain condition, new operation modes can also occur.

##### **5.3.1.1. Operation Conditions**

For SVPWM control, one switching cycle consists of 4 switching states, two zero states  $T_0$

and  $T_7$  and two of the six active states,  $T_1$  and  $T_2$  for instance. During  $T_0$  and  $T_7$ , the load terminals are shorted by the upper or lower three switches, and there is no current feeding the inverter bridge from the dc side. To simplify the analysis, assume that the current from the dc side to the inverter bridge,  $i_i$ , during the two active states are the same, and the capacitor voltage is always constant. Under these assumptions, there can be two different operation conditions termed as CCM and DCM with the inductor current shown in Figure 5.3 (a) and (b) respectively. In both cases, because of Mode 5, the capacitor voltage is higher than the input voltage. For the CCM condition, the inductor current decreases in the zero state  $T_0$ . When active state  $T_1$  starts, the inductor current is less than  $i_i/2$ , thus freewheeling diode shoot through mode (Mode 5) happens, and the inductor current increases linearly until it reaches  $i_i/2$ . The inductor current then maintains by entering Mode 3 afterwards. The inductor current will decrease again when the inverter enters the second part of the zero states  $T_7$ . In some cases when the inductance is extremely low, the inductor current can reach zero during the zero states and stay at zero in Mode 4 until the next switching action as shown in Figure 5.3 (b), which forms a DCM operation condition.

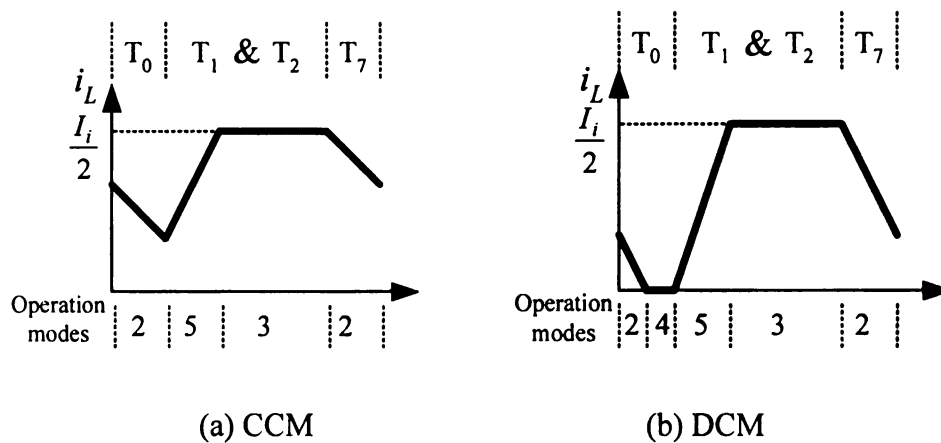


Figure 5.3. Inductor current waveforms for different operation conditions.

It is note worthy to mention that the currents to the inverter bridge at different active states are actually different, which will make the operation condition more complicated and there also could be additional operation conditions, however the basic principle and the possible operation modes are the same. Because of the variation of the line current in a line cycle, more than one operation condition can occur in one line cycle.

Under simple operation condition, when only Mode 1 and 2 occur, the capacitor voltage always equals to the input voltage. With these new operation modes, the capacitor voltage is boosted and the voltage across the device is also increased. Because some parts of the active states becomes a freewheeling diode shoot through state, the output voltage can be higher or lower than the output voltage under simple operation with the same modulation index. Also, the time duration of the freewheeling diode shoot through state depends on the current to the inverter bridge, which changes over a line cycle, this can cause slight harmonics in the output voltage.

#### **5.3.1.2. Critical Condition**

As discussed above, the new modes will bring different characteristics to the inverter, it is important to know under what condition these new modes will happen. The critical condition of the new modes to happen under traditional SVPWM without any controlled shoot through is:

$$M \cos \varphi < \frac{2}{3} \quad (5.7)$$

As from (5.7), when the load power factor is low, there will be new operation modes. The detailed derivation can be found in appendix 3.

### **5.3.2. Maximum Constant Boost Control with Third Harmonic Injection**

When the circuit starts to boost the voltage by introducing shoot through states, the new modes can also happen depending on the load condition and the inductance of the inductors. As stated previously, different control methods might yield different circuit characteristics, therefore a specific control method is required for the analysis. The maximum constant boost control method with third harmonic injection is employed here to analyze the circuit characteristics as an example. Circuit characteristics under other control methods can also be derived by following the provided procedure.

#### **5.3.2.1. Operation Conditions**

The maximum constant boost control with third harmonic injection is quite similar to traditional SVPWM. In each switching cycle, there are two active states,  $T_1$  and  $T_2$  for instance, two zero states,  $T_0$  and  $T_7$ , and one shoot through state,  $T_{st}$ , with the following sequence:  $T_{st}, T_0, T_1, T_2, T_7$ . To simplify the analysis, the currents feeding to the inverter bridge in the two active states are assumed to be the same, and the capacitor voltage is assumed to be constant. Under these assumptions, there are two possible operation conditions as shown in Figure 5.4 (a) and (b) respectively.



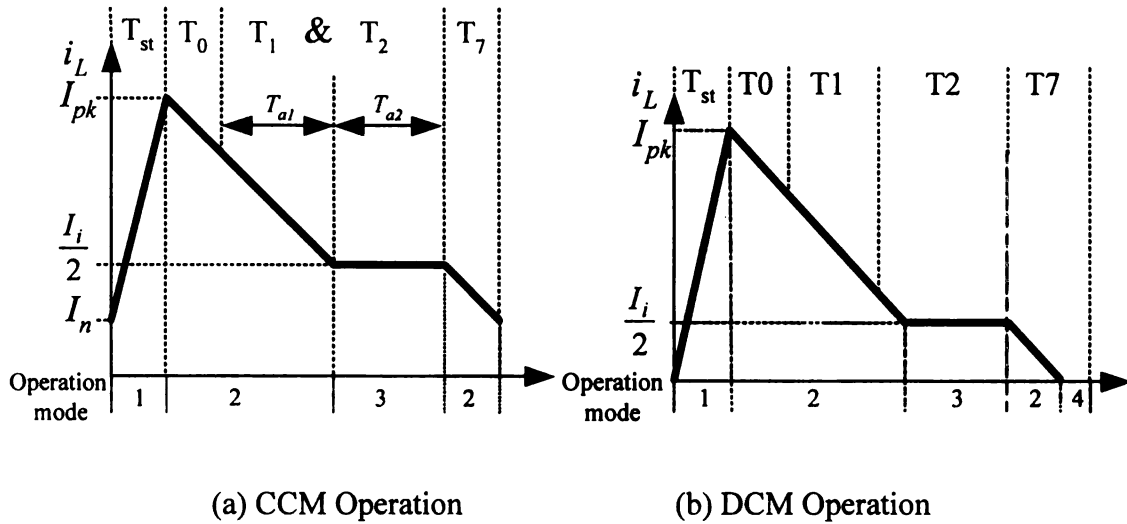


Figure 5.4. Z-source inductor current for different operation conditions.

Figure 5.4 (a) shows the CCM operation condition. In each switching cycle, the circuit starts with a shoot through zero state,  $T_{st}$ , during which the inductor current increases linearly. After  $T_{st}$ , the inverter switches into traditional zero state,  $T_0$ , and then active states with operation Mode 2, during which the inductor current keeps decreasing and is reduced to half of the  $i_i$  in the middle of active states. Then Mode 3 comes into play by keeping the inductor current almost constant and turning off the diode  $D$ . When the active states are over and the circuit is turned into traditional zero state, Mode 2 appears again, and the inductor current decreases linearly until another switching action turning the circuit into switch shoot through state again (Mode 1). During this whole cycle, the inductor current is continuous, therefore this operation condition is termed as CCM condition. In the second half of the traditional zero state, it is also possible that the inductor current decreases to zero before another switch shoot-through state starts, and stays in Mode 4 for the rest of the cycle until the next switching action. Figure 5.4 (b) shows this operation condition, which is termed as DCM condition.

In the practical case, the current fed to the inverter bridge is different for different active states, which will make the operation condition more complicated, however, the basic principles and the possible operation modes are the same, and it will be shown in the following example that the analysis with the simplification still predicts the circuit behavior very well. Also, there can be more than one operation condition during one line cycle because of the variation of  $i_i$  over a line cycle.

### 5.3.2.2. Critical Condition

Using a small inductor can reduce the cost, volume, and weight, but at the same time new operation modes might occur. On the other hand, using a small inductor causes higher current stress to the switches, and more importantly, under the new operation conditions with new operation modes, the voltage to the inverter  $v_i$  is no longer always a constant during active states, which is always  $2V_c - V_o$  in the simple operation condition. This might cause some unexpected output harmonics. Thus in some applications where harmonic regulation is very crucial, one might not want the new operation modes to appear. The critical condition of the new operation modes becomes important to the design of the inductors.

The critical condition of the new operation modes under maximum constant boost control with third harmonic injection can be described by the following inequation,

$$\left. \begin{array}{l} \frac{3M \cos \varphi}{2Z(\sqrt{3}M - 1)} - \frac{\sqrt{3}T_{st}}{L} < \frac{1}{Z} & \cos \varphi \geq \frac{1}{2} \\ \frac{3M \cos \varphi}{2Z(\sqrt{3}M - 1)} - \frac{\sqrt{3}T_{st}}{L} < \frac{1}{Z} \cos(\varphi - \frac{\pi}{3}) & \cos \varphi < \frac{1}{2} \end{array} \right\} \quad (5.8)$$

When this inequation is met, the circuit starts to have new operation modes. The detailed derivation of the critical condition can be found in appendix 4.

## 5.4. Analysis Example

The circuit characteristics will be different when the new operation modes happen. Also it can be different for different operation conditions with different combinations and sequences of the new modes. In this section, we will analyze the circuit characteristics under CCM condition under maximum constant boost control with third harmonic injection as an example. A detailed process will be provided, which can also be used to analyze the circuit under other conditions.

### 5.4.1. Voltage Gain

Assume the circuit is operated under CCM condition throughout the whole line cycle.

The voltage across the capacitors in the Z-source network satisfies equation (5.9)

$$\frac{V_c V_o T_{0+7} T_{st} - T_{st}^2 V_c V_o - T_{0+7} T_{st} V_o^2}{L T_s V_o - 2 T_{0+7} L V_o + 2 T_{0+7} V_c L - V_c L T_s} = \frac{0.455 M \cos \varphi}{Z} \frac{T_s V_c - 2 T_{0+7} V_c + T_{0+7} V_o}{T_s - T_{st} - T_{0+7}} \quad (5.9)$$

With this equation and all known parameters, one can calculate the output voltage and voltage stress across the inverter switches based on the following equations:

$$\text{Output rms phase voltage: } V_{out} = \frac{(2V_c - V_o)T_{a1} + V_c T_{a2}}{2\sqrt{2}(T_{a1} + T_{a2})} M, \quad (5.10)$$

$$\text{Switch voltage stress: } V_s = 2V_c - V_o, \quad (5.11)$$

where  $T_{a1}$  and  $T_{a2}$  are shown in Figure 5.4 (a) and can be calculated by (A5.1) and (A5.2) in appendix 5.

### 5.4.2. Relationship of Voltage Gain Versus Voltage Stress

From the previous discussion in chapter 2, one important criterion to judge the inverter performance is the relationship of voltage gain versus the voltage stress. To evaluate the new operation conditions, a comparison of the voltage stress versus voltage gain relationship of the CCM condition with the simple operation condition under maximum constant boost control with third harmonic injection is provided.

For simple operation condition, the voltage stress,  $V_s$ , versus voltage gain,  $G$ , relationship is provided in chapter 2, which is

$$V_s = (\sqrt{3}G - 1)V_o. \quad (5.12)$$

For the CCM condition under maximum constant boost control, where  $T_{st} = (1 - 0.866M)T_s$ ,  $T_{0+7} = 0.0386MT_s$ , from (5.10), the voltage gain can be calculated by:

$$G = \frac{\sqrt{2}V_{out}}{V_o/2} = \frac{2\pi(V_c(1 - 0.0772M) + 0.0386MV_o)}{3\sqrt{3}V_o}. \quad (5.13)$$

With this voltage gain, the value of  $(\sqrt{3}G - 1)V_o$  is,

$$(\sqrt{3}G - 1)V_o = (2.09 - 0.16M)V_c + (0.08M - 1)V_o. \quad (5.14)$$

The modulation index  $M$  ranges from 0.58 to 1.15, the voltage stress under CCM condition can be approximated as

$$V_s = 2V_c - V_o \approx (\sqrt{3}G - 1)V_o. \quad (5.15)$$

Therefore the voltage stress versus voltage gain relationship of CCM condition under maximum constant boost control with third harmonic injection is about the same as in the

simple operation condition.

### 5.4.3. Design Guidelines

In some applications, one might want to avoid the new modes. When the load power factor and modulation index are not very low, one could design the inductor of the Z-source network according to (5.8) to avoid the unwanted operating modes. However, from (5.8), it is obvious that when the load power factor is very low, say 0, the critical condition is always met and the new operation condition is inevitable. Under these extreme conditions, it is still possible to avoid the DCM by properly choosing the parameters of the Z-source network. The basic design method of the Z-source inverter for simple operation condition is given in chapter 4. Further rules have to be followed to avoid the DCM condition. In all above analysis, the voltage across the capacitor is assumed to be a constant, thus as long as the capacitance is large enough so that the voltage ripple across the capacitor is reasonably low, the capacitor doesn't have any effect on the operation modes. From Figure 5.4, the main difference between CCM and DCM is whether or not the inductor current decreases to zero during  $T_7$ . The inductor current during  $T_{a2}$  when it almost maintains constant in CCM condition can be calculated from (5.16).

$$I_i = \frac{V_c V_o T_{0+7} T_{st} - T_{st}^2 V_c V_o - T_{0+7} T_{st} V_o^2}{2 L T_s V_o - 2 T_{0+7} L V_o + 2 T_{0+7} V_c L - V_c L T_s} \quad (5.16)$$

The detailed derivation can be found in the appendix 6.

Assuming that the inverter is operating under CCM condition, during  $T_7$ , the inverter is under operation mode 2 and the voltage across the inductor is  $V_o - V_c$ . The current drop

during this period is:

$$\Delta I_{T7} = \frac{V_c - V_o}{L} T_7 \leq \frac{V_c - V_o}{L} T_{0+7}. \quad (5.17)$$

$T_7$  changes over the time, however, it never exceeds  $T_{0+7}$ .

The following inequation is a sufficient condition to avoid the DCM condition,

$$\frac{I_i}{2} > \frac{V_c - V_o}{L} T_{0+7}. \quad (5.18)$$

However, this is not very straightforward way to design the inductor, because the capacitor voltage needed in the equation is inductance related too. A simple try and error procedure has to be followed in the design: start from the initial inductance value from design process provided in chapter 4, for a given load and operation condition, calculate the capacitor voltage  $V_c$  according to (5.9). With the resulted  $V_c$ , one can calculate  $\frac{I_i}{2}$  and  $\Delta I_{T7}$  from (5.16) and (5.17), and check whether (5.18) is met. One needs to increase the inductance and go through the process again if (5.18) is not met.

## 5.5. Simulation and Experimental Verifications

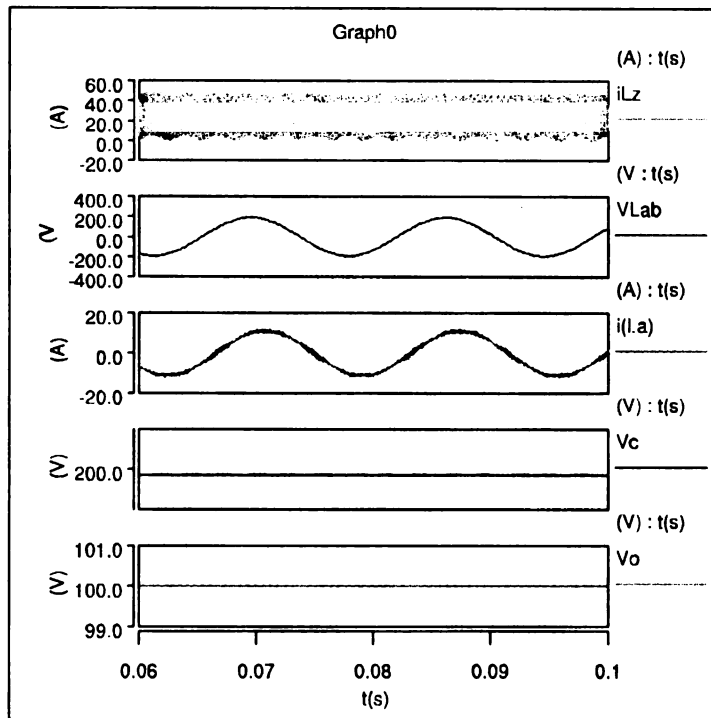
To verify the analysis, simulation of the Z-source inverter with  $L=50\mu\text{H}$ ,  $V_o=100\text{V}$ ,  $f_s=10\text{kHz}$ ,  $f=60\text{Hz}$  (output frequency),  $Z=10\Omega+1\text{mH}$  per phase Y connection under maximum constant boost control with third harmonic injection and modulation index of 0.9 is performed. This circuit operates in CCM condition under these parameters. The simulation results are shown in Figure 5.5 (a) and (b). Experimental results with the same set up are shown in Figure 5.6 (a) and (b). In both cases, the output line to line voltage,  $V_{Lab}$ , is the voltage across the load resistors. Comparison of simulation results

and calculated value of the capacitor voltage at different modulation indices is shown in Figure 5.7. From the simulation and experimental results, we can see that the inductor current stays constant while the dc bus voltage across the inverter bridge decreases to the capacitor voltage in some period, which clearly demonstrates the new operation mode, Mode 3. Also, the analysis results meet the simulation and experimental results very well in terms of voltage boost. The actual operation of the circuit is more complicated than the CCM condition analyzed above because of the inverter current variation over a whole line cycle. However, as from Figure 5.7, the simplified analysis also provides quite accurate estimation of the real performance.

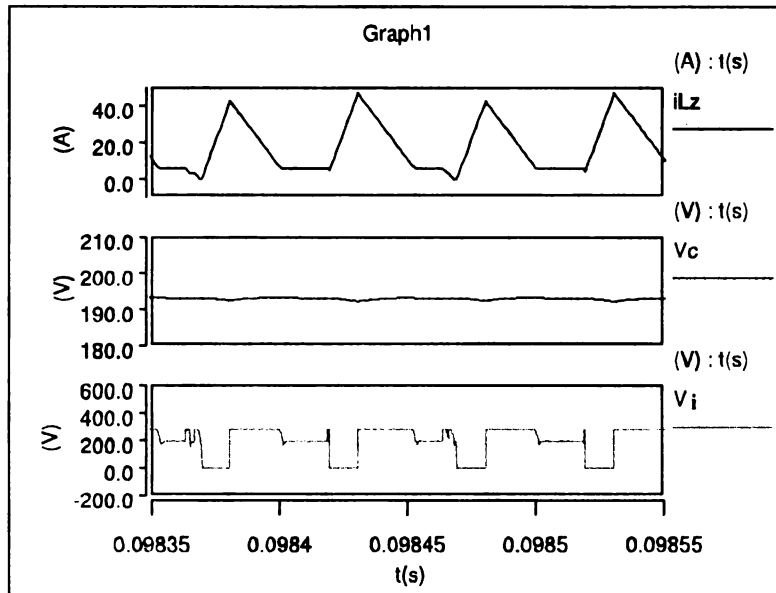
Figure 5.7 also shows that the circuit characteristics of the CCM conditions is quite different from that of simple operation condition, the voltage boost effect of CCM condition is significantly higher than the simple operation condition with the same modulation index and the same control method.

## **5.6. Method to Eliminate the Unwanted Operation Modes**

From the above analysis, by proper design of the Z-source network and proper control, one can avoid the operation Mode 3 to Mode 5 to certain degree in time of unwanted, e.g. avoid the DCM condition. However, it is impossible to completely avoid these modes with the configuration shown in Figure 1. Figure 8 shows a configuration where the input diode is replaced by a switch, by using this configuration, the inverter is able to completely avoid the unwanted operation modes by turning on the switch S during all active states and traditional zero states. Further more, this configuration provides the circuit bi-directional power flow function.



(a)

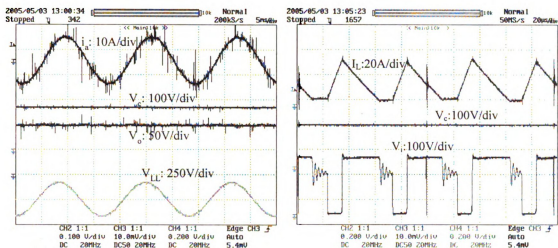


(b)

$V_o$ : input voltage;  $i_{Lz}$ : inductor current;  $V_i$ : dc link voltage across the inverter bridge;  $V_{Lab}$ : output line to line voltage;  $V_c$ : capacitor voltage;  $I(La)$ : Load current

Figure 5.5. Simulation results when operating at CCM condition.





(a)

(b)

$i_a$ : load current;  $V_c$ : capacitor voltage;  $V_o$ : input voltage;  $V_{LL}$ : Load line to line voltage;  $V_i$ :

dc link voltage across the inverter bridge

Figure 5.6. Experimental results of CCM condition.

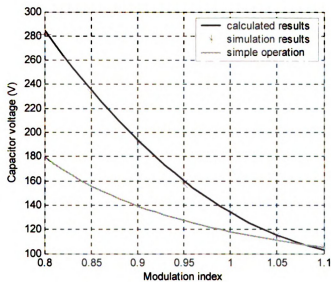


Figure 5.7. Comparison of analyzed results and simulation results of capacitor voltage.

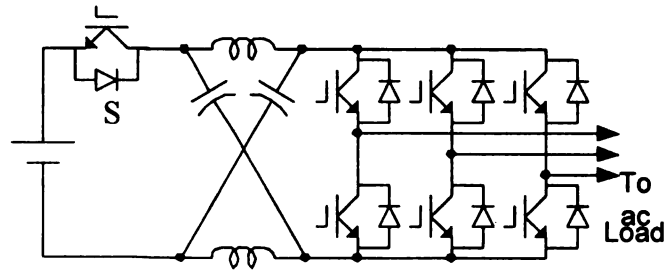


Figure 5.8. Bi-directional Z-source inverter.

## 5.7. Summary

Analysis of the Z-source inverter with small inductance or low power factor is given. Three new operation modes are discussed. It is noted that with a small inductor in the Z-source and low load power factor, there can be very different operation conditions. Circuit operation conditions under traditional SVPWM control and maximum constant boost control with third harmonic injection are both analyzed. The paper also analyzed the Z-source inverter performance with small inductor under maximum constant boost control with third harmonic injection as an example, and provided the capacitor voltage, output voltage and voltage stress –voltage gain relationship. The analysis is verified by simulation and experimental results.

It is note worthy to mention that the circuit can have different combination and sequence of operation modes with different control methods and different circuit parameters, which yields different circuit characteristics. However the analysis method and the detailed derivation method for the equations in the appendices can also be applied to analyze the circuit these conditions. A simple method to totally eliminate the new operation modes by replacing the diode with a switch is proposed as an option. This configuration also provides bi-directional power flow ability.

# **CHAPTER 6 Application and Control of Z-Source Inverter for Traction Drive of Fuel Cell – Battery Hybrid Electric Vehicles**

## **6.1. Introduction**

### **6.1.1 Fuel Cell-Battery Hybrid Vehicles**

Fuel cells (FCs) have achieved global attention as an alternative power source for hybrid electric vehicles (HEVs) [82]. Fuel cell vehicles (FCVs), are being developed by auto manufacturers [83-88], and have generated interest among industry, environmentalists, and consumers. A FCV promises the air quality benefits of a battery-powered electric vehicle, with the driving range and convenience of a conventional internal combustion engine vehicle.

Because of its nature, a fuel cell prefers to be operated under constant power to prolong its lifetime and increase the efficiency. However, the traction power the vehicle demands is ever changing. To balance the difference of these two and also to handle the regenerative energy, a battery is often used as an energy storage device in FCVs, which forms a Fuel Cell-battery Hybrid Electric Vehicle (FCHEV). Therefore, basically the traction drive system of a FCHEV consists of a fuel cell stack, a battery pack, a controller

(power inverter), and a traction motor. The main source of the vehicle's power is the fuel cell. The secondary power source is the battery, which also stores excess energy from the fuel cell, and from regenerative braking. The four utilized operating modes and the power flow diagrams are outlined in the following.

*Mode 1, medium power (Figure 6.1)*

Under medium power, the vehicle traction motor only receives power from the fuel cell. The fuel cell can also provide power to the battery if its state of charge (SOC) is low.

*Mode 2, high power (Figure 6.2)*

During acceleration, or uphill driving, both the fuel cell and the battery provide power to the traction motor. The battery speeds up the vehicle's response time for a request of acceleration, because the fuel cell typically has a slow response time. This also allows the fuel cell to maintain a safe and efficient operating point.

*Mode 3, low power (Figure 6.3)*

Because of the parasitic loads, such as the air compressor, associated with the fuel cell, the fuel cell system efficiency decreases when operated under low power [85]. Thus the vehicle will be operated strictly as a battery powered electric vehicle under low power by turning off the fuel cell stack.

*Mode 4, regenerative braking (Figure 6.4)*

During regenerative braking, the fuel cell produces no power, and the electric motor acts as a generator, using the wheels to apply torque to the motor to generate electrical power, this torque in turn slows the vehicle down. The electrical energy generated during regenerative braking is stored in the battery until needed.

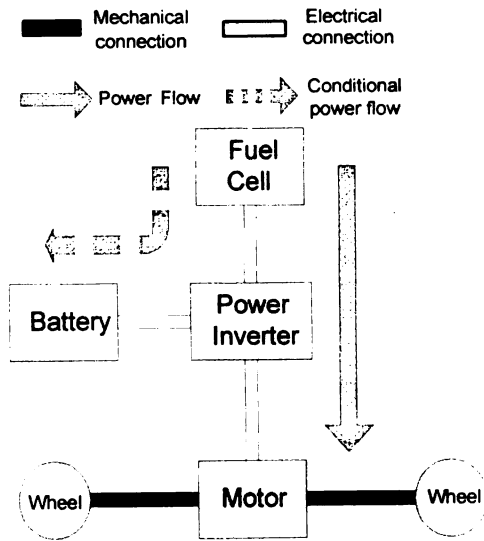


Figure 6.1. Medium power operating mode 1.

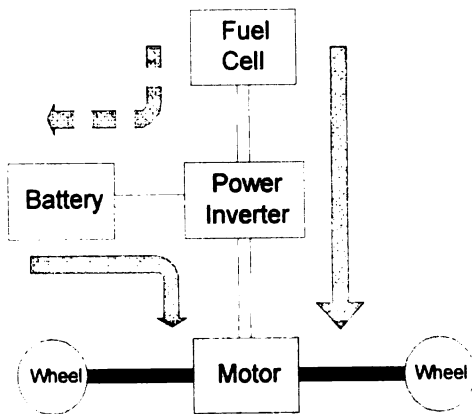


Figure 6.2. High power operating mode 2.

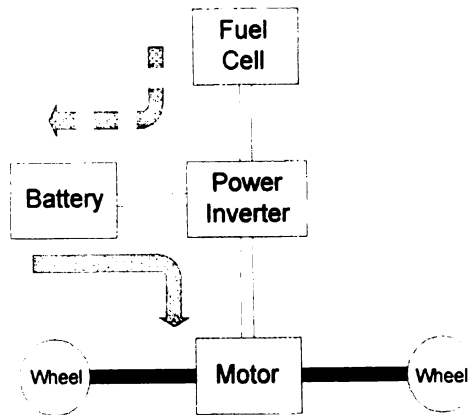


Figure 6.3. Low power operating mode 3.

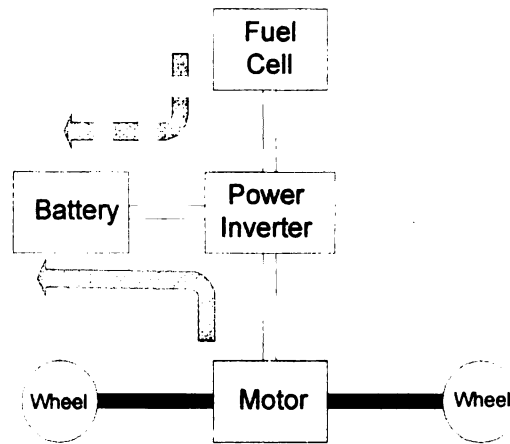


Figure 6.4. Regenerative braking operating mode 4.

It is important to mention that in any of the operating modes, if the SOC of the battery becomes too low, the fuel cell will provide power to charge the battery.

### 6.1.2. Fuel Cell and Battery Characteristics

Although there are many complex subsystems and parasitic loads associated with a fuel cell, we are mainly concerned with the voltage and current. The fuel cell's voltage (and power) is determined by two main factors. First the rate at which hydrogen flows through the fuel cell establishes the level of the V-I polarization curve. Second the amount of current drawn by the inverter determines the point on this curve where the fuel cell will operate. Thus, by controlling the amount of current drawn by the inverter, the fuel cell power can be controlled for given hydrogen flow rate. The typical steady state V-I polarization curve of the fuel cell is shown in Figure 6.5. As can be seen from Figure 6.5, the output voltage of the fuel cell is heavily dependent on the load current as so does the power.

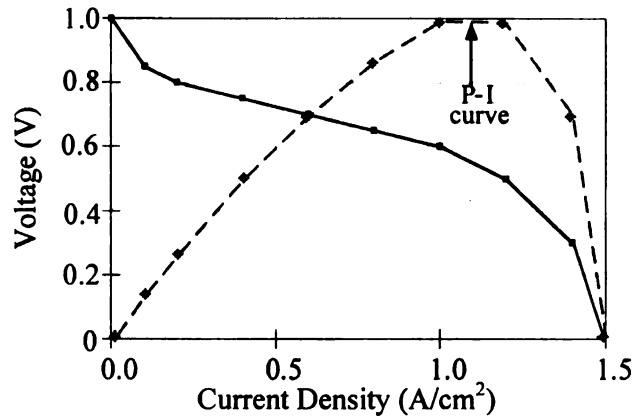


Figure 6.5. Typical fuel cell polarization curve.

On the other hand, the output voltage of a battery is relatively less current dependent because of much smaller internal resistance. The voltage of a battery changes with the SOC of the battery. A typical curve of voltage versus SOC of a 330 V lithium-ion battery is shown in Figure 6.6.

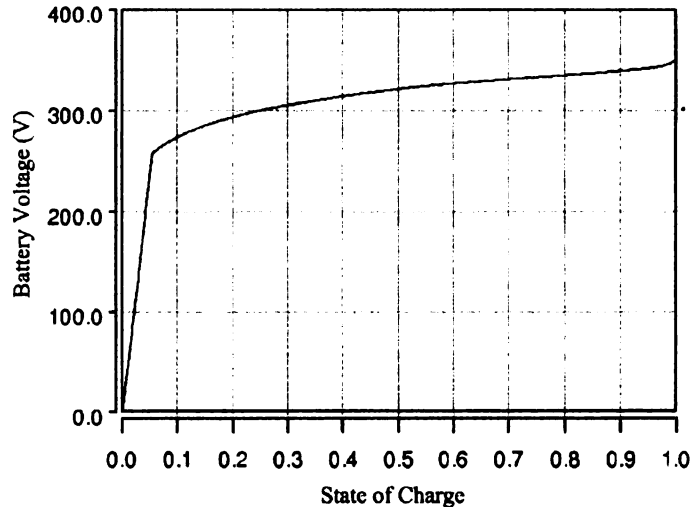
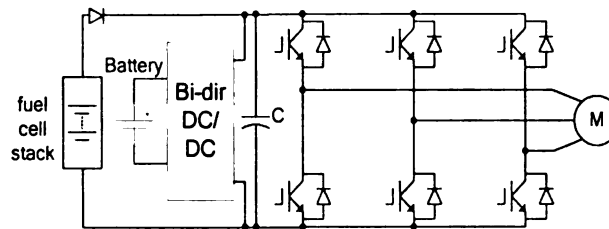


Figure 6.6. Typical lithium-ion battery voltage versus SOC.

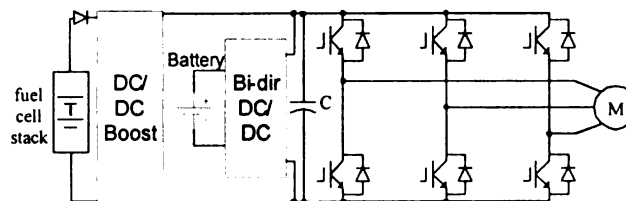
### 6.1.3 Traditional power conditioner configurations

As can be seen from above analysis, the power inverter is the key component in the system to handle all power flow control. The inverter in FCHEV has to output the

requested power to the traction motor, capture excess power from the fuel cell, and to absorb energy from regenerative braking. There are typically two configurations available for this application shown in Figure 6.7. The FCHEV using the conventional inverter (Figure 6.7 (a)) must use a bi-directional dc-dc converter to control the SOC of the battery, because the modulation index is the inverter's only control freedom. Also, the conventional inverter is a buck (step-down) inverter, the output ac voltage is limited below the fuel cell voltage. Because of the wide voltage range of the fuel cell, the conventional inverter imposes high stresses to the switching devices. The dc-dc boosted inverter (Figure 6.7(b)) can reduce these stresses, at the price of higher cost and complexity. The dc-dc boost converter is used to boost (step-up) the voltage from the fuel cell, to a steady dc bus voltage, and the inverter's output ac voltage is controlled by the modulation index. The system configuration using the dc-dc boosted inverter typically uses a bi-directional dc-dc converter to control the SOC of a low voltage battery [83].



(a) System configuration using a conventional inverter



(b) System configuration using a DC-DC boosted inverter

Figure 6.7. Traditional configurations of FCVs.



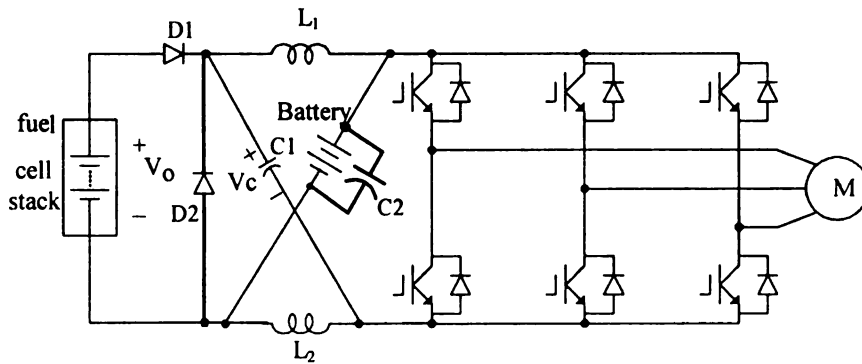
Both configurations use an inverter bridge and at least one dc/dc converter, which increases the cost and system complexity and reduces the system reliability.

In this chapter, several configurations of fuel cell-battery hybrid vehicles using the Z-source inverter will be presented, the control strategy will be discussed. The undesirable operation modes will be eliminated by control. A simple comparison of these configurations will be provided.

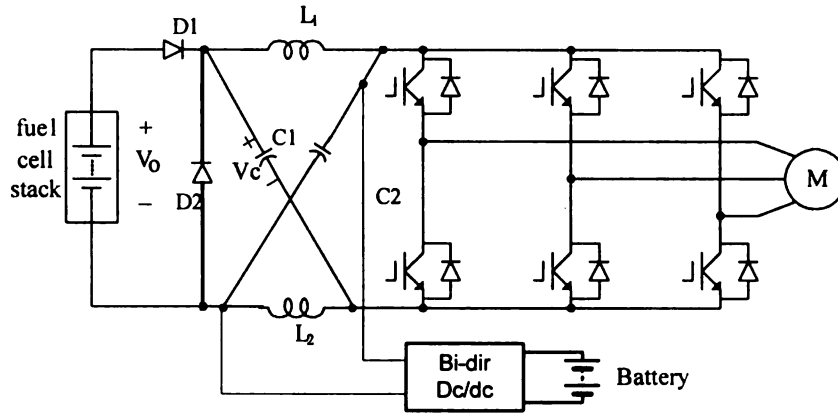
## 6.2. Configurations and Control of Z-source Inverter for FCHEVs

### 6.2.1 Configurations

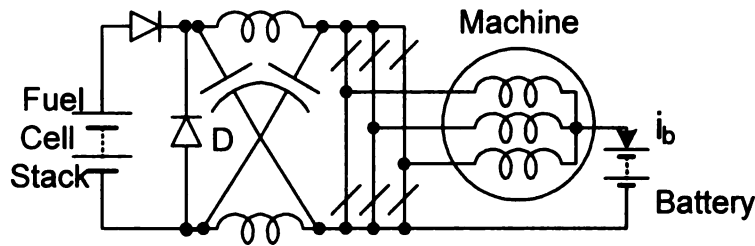
With two control freedoms: shoot-through duty cycle and modulation index, it is possible to use the Z-source inverter in fuel cell-battery hybrid vehicles. Three possible configurations are shown in Figure 6.8.



(a) Configuration with battery connected in parallel with one of the capacitors



(b) Configuration using a dc/dc converter to interface the capacitor and battery



(c) Configuration connecting the battery to the neutral point of the machine

Figure 6.8. Configurations of Z-source inverter for FCHEV.

For the first configuration, the capacitor voltage becomes the battery voltage. In the second configuration, the capacitor voltage is controlled by the dc/dc converter interfacing the battery. For the third configuration, the inverter bridge also serves as a dc/dc converter interfacing the capacitor and the battery. With the PWM scheme shown in Figure 6.9, where  $V_p$  and  $V_n$  control the shoot through duty ratio, and the three reference signals are shifted from the center by  $V_s$ . The voltage relationship between the capacitor and the battery under this PWM method can be derived as:

$$V_c = \frac{2(1-D_0)}{1-D_0-V_s} V_b, \quad (6.1)$$

where  $V_c$  is the capacitor voltage,  $V_b$  is the battery voltage,  $D_0$  is the shoot through duty ratio. Therefore, the capacitor voltage can also be controlled by the battery and shift of the reference signals.

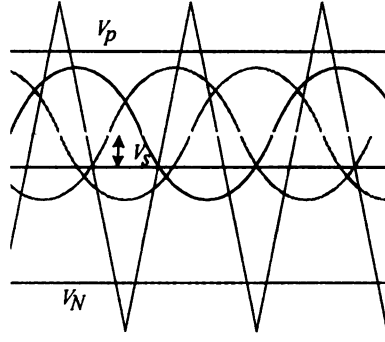


Figure 6.9. PWM scheme for the third configuration.

## 6.2.2 Control of the Inverter

From above discussion, the capacitor voltages of all three configurations are all controlled and we still have two other freedoms: modulation index and shoot through duty ratio, to control output power and battery state of charge.

In this system, there are three power sources/consumers: fuel cell, battery, and the motor, as long as we can control the power flow of two of them, the third element automatically matches the power difference. For Z-source inverter, the relationship of the capacitor voltage and the input voltage is:

$$V_c = \frac{1-D_0}{1-2D_0} V_o, \quad (6.2)$$

where  $D_0$  is the shoot through duty ratio,  $V_o$  is the fuel cell voltage,  $V_c$  is the voltage across the capacitor in Z-source network. From above analysis, the capacitor voltage  $V_c$

is controlled by the battery and/or other circuitry, thus, the fuel cell voltage is controlled to be

$$V_o = \frac{1-2D_0}{1-D_0} V_c . \quad (6.3)$$

For given hydrogen and air flow rates, the V-I characteristic of the fuel cell is determined. As a result, the fuel cell voltage determines the output current and power of the fuel cell. Figure 6.10 shows the V-I curve of a typical 30kW fuel cell, with the controlled fuel cell voltage,  $V_o$ , the shaded area illustrates the output power of the fuel cell.

At the same time, the output power can be controlled by manipulating the modulation index to produce the desired output voltage. The output peak phase voltage of the inverter is

$$\hat{V}_{phase} = (2V_c - V_o) * \frac{M}{2} , \quad (6.4)$$

where  $M$  is the modulation index defined as the ratio of the magnitude of the reference waveform and the triangular waveform in traditional SPWM.

The output power can be expressed as

$$P_{out} = \frac{3pf}{\sqrt{2}} \hat{V}_{phase} I , \quad (6.5)$$

where  $I$  is the rms load current and  $pf$  is the load power factor.

Therefore the system is able to control the fuel cell output power and the output power to the motor at the same time, as a result, the power charging the battery is

$$P_b = V_o I_o - P_{out} . \quad (6.6)$$

Thus we are able to control the *SOC* of the battery and drive the vehicle at the same time.

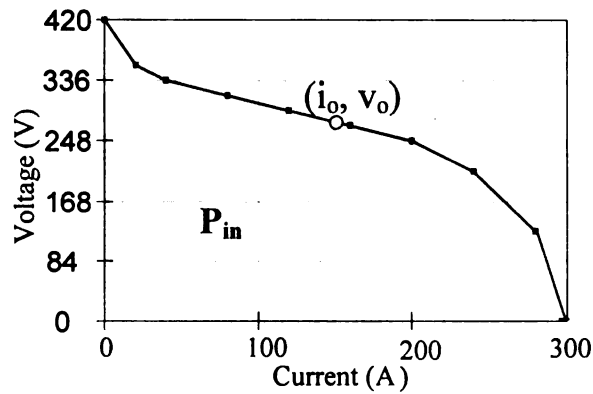


Figure 6.10. Power control of fuel cell by controlling the voltage.

The above method can be used to control the converter when the fuel cell is turned on.

When the vehicle is in low speed cruising mode and not much power is needed, the fuel cell will be turned off and the vehicle becomes a full electrical vehicle. Under this condition, the diode in parallel with the fuel cell bypasses the fuel cell. The equivalent circuit is shown in 6.11.

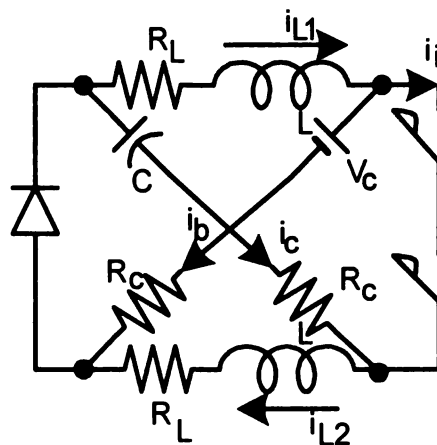


Figure 6.11. Model of the Z-source network considering parasitic parameters when the fuel cell is turned off.

As discussed above, the capacitor voltage is controlled by the battery voltage, therefore, the capacitor voltage is assumed to be  $V_c$ . Assuming the voltage across the diode when conducting is  $V_d$  and the voltage across the inverter bridge when conducting is  $V_s$ , the voltage across the inductor  $L_1$  during shoot through can be calculated by:

$$V_{Lst} = V_c - i_{L1}(R_L + R_C) - V_s. \quad (6.7)$$

With the similar method, we can calculate the inductor voltage during non-shoot through, which is:

$$V_{Lnst} = -(V_b - i_b(R_b - R_C)) - (i_{L1} - i_i)R_c - i_{L1}R_L - V_D. \quad (6.8)$$

Based on the average voltage across the inductor should be zero during steady state, for shoot through duty ratio of  $D_0$ , the following equation should be met:

$$V_{Lst}D_0 + V_{Lnst}(1 - D_0) = 0, \quad (6.9)$$

from which, the average inductor current can be calculated by (6.10).

$$i_{L1} = \frac{1}{R_C + R_L} * ((2D_0 - 1)V_c + i_c(R_b - R_C) + i_iR_C + D_0(i_cR_C - i_iR_C - 2i_cR_b - i_cR_L - V_s + V_D) - V_D) \quad (6.10)$$

From above analysis, the current through L1 and L2 can be controlled by adjusting shoot through duty ratio around 50%. Because  $R_C$  and  $R_L$  are very small, the inductor current will be very sensitive to the shoot through duty ratio. However, this can be easily relieved by employing a simple current feed back control.

Analogous to the four vehicle operation modes shown in Figure 6.1, the inverter has different operation methods too. For mode 1 and 2, the inverter operation is very

similar: the fuel cell power is controlled by shoot through duty ratio, the output power is controlled by the output voltage and current. The only difference is that the output power is higher than the fuel cell power and the battery is being discharged in mode 2, the fuel cell power can be slightly higher/lower than or equal to the output power to charge/discharge or maintain the battery based on the battery SOC in mode 1. For mode 3, the fuel cell is turned off and the diode D2 bypasses the fuel cell. To maintain the inductor current at certain level, the shoot through duty ratio has to be slightly higher than 50%, and the modulation index is still used to control the output voltage/power. For mode 4, to maintain a certain inductor current, the shoot through duty ratio also has to be around 50%, and the power is being charged back to the battery.

### **6.2.3. Simulation and experimental verification**

To verify the above mentioned feature of the Z-source inverter for FCHEVs, three cases are examined and simulated for the first configuration. In these cases the circuit parameters are  $L1=L2=200\mu\text{H}$ ,  $C1=400\mu\text{F}$ , C2 has been replaced (or connected in parallel) with a 6.5Ah lithium-ion battery with a nominal voltage of 330V, switching frequency of 10 kHz, and using constant boost control with third harmonic injection. The characteristics of the battery and fuel cell are shown in Figure 6.6 and Figure 6.10. An RL load is used in the simulation. The legends in the simulation results can be found in Figure 6.15.

#### *Case 1*

The fuel cell voltage is kept constant at 300V ( $P=30\text{kW}$ ), and the load power is varied from 30kW, to 55kW, to 5kW, back to 30kW. As one would expect the battery SOC should remain constant while the load is at 30kW ( $P_{in}=P_{out}$ ). When the load is increased

to 55kW ( $P_{in} < P_{out}$ ) the battery should supply the additional power requested by the load, thus the SOC will decrease. When the load is decreased to 5kW ( $P_{in} > P_{out}$ ) the additional power provided by the fuel cell will charge the battery, increasing the SOC.

These results are verified by simulation, Figure 6.12, starting from the top, the fuel cell voltage is constant, and the fuel cell current is fairly constant. Next are the battery voltage, SOC, load voltage, load current, and load power. Initially the load absorbs 30kW, and the SOC stays constant. The load is then increased to 55kW and the SOC decreases. Next the load is decreased to 5kW, and the SOC increases. Finally the load is returned to 30kW and the SOC remains constant.

This simulation shows that we can operate the fuel cell at an efficient operating point, while the battery handles the load dynamics. This also verifies the Z-source inverter can be used to provide the medium, and high power operating modes.

### *Case 2*

The load power is kept constant at 30kW, and the fuel cell power is varied between 30kW, 50kW, 20kW. Again the battery SOC should remain constant while the fuel cell is producing 30kW. The battery will be charged when the fuel cell power is increased to 50kW ( $P_{in} > P_{out}$ ), increasing the SOC. When the fuel cell power is decreased to 20kW ( $P_{in} < P_{out}$ ), the battery will supply the additional power requested by the load, decreasing the SOC.

This can be verified in Figure 6.13. Starting from the bottom, the load power, current, and voltage are constant, where the power is at approximately 30kW. Next are the battery SOC, battery voltage, fuel cell current, and fuel cell voltage. Initially the fuel cell



produces 30kW, and the SOC stays constant. Then the fuel cell power is increased to 50kW and the SOC increases. Again the fuel cell produces 30kW, and the SOC stays constant. Next the fuel cell power is decreased to 20kW, and the SOC decreases. Finally, the fuel cell again produces 30kW, and the SOC stays constant. Case 2 shows that we can control the fuel cell power, thus controlling the battery SOC.

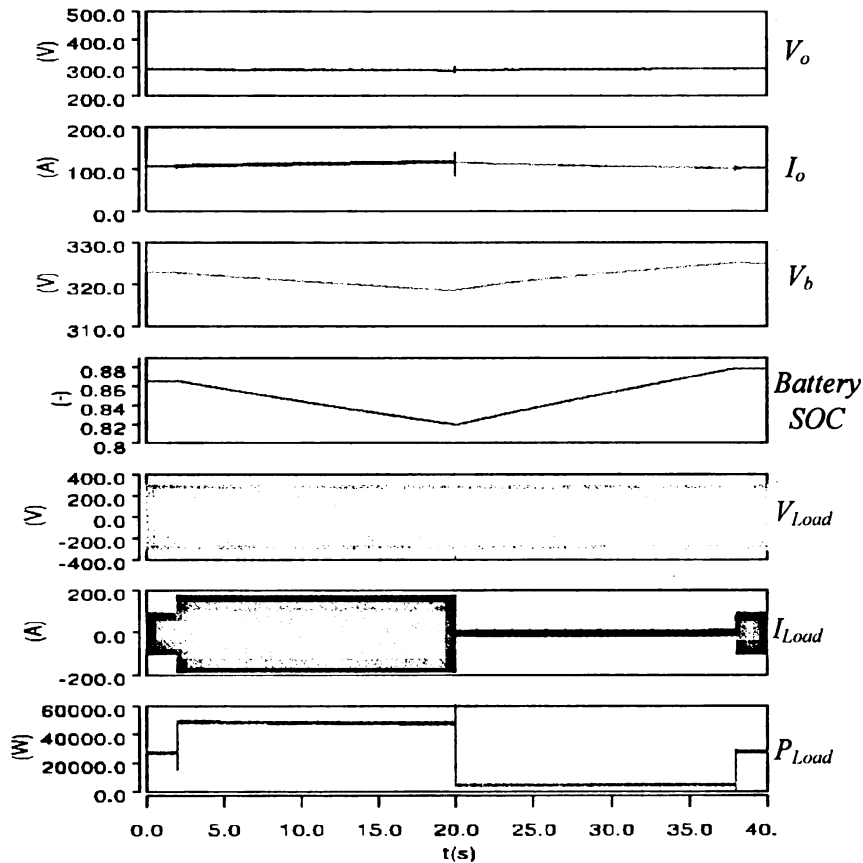


Figure 6.12. Simulation case 1.

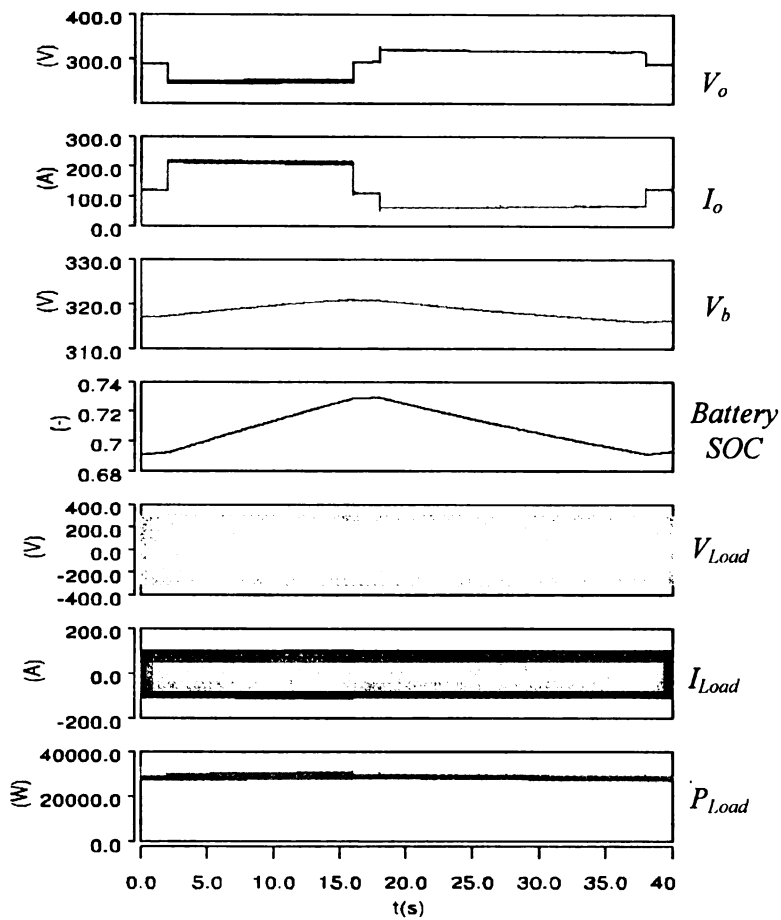


Figure 6.13. Simulation case 2.

### Case 3

The fuel cell operation is stopped, and the load power is varied from 5kW, to 20kW. As one would expect the battery SOC should decrease. When the fuel cell is turned off, D2 provides a current path for any possible current. These results are verified by simulation as seen in Figure 6.14, starting from the top, the fuel cell power is zero. Next are the battery voltage, SOC, load voltage, load current, and load power. Initially the load absorbs 5kW, and the SOC decreases slowly. The load is then increased to 20kW and the SOC decreases more rapidly. Case 3 verifies that the vehicle can be operated without using the fuel cell, strictly as an electric vehicle, as in the low power mode. This also

demonstrates the ability of the inverter to capture power during regenerative braking, when the fuel cell is also turned off and the output voltage and current is out of phase.

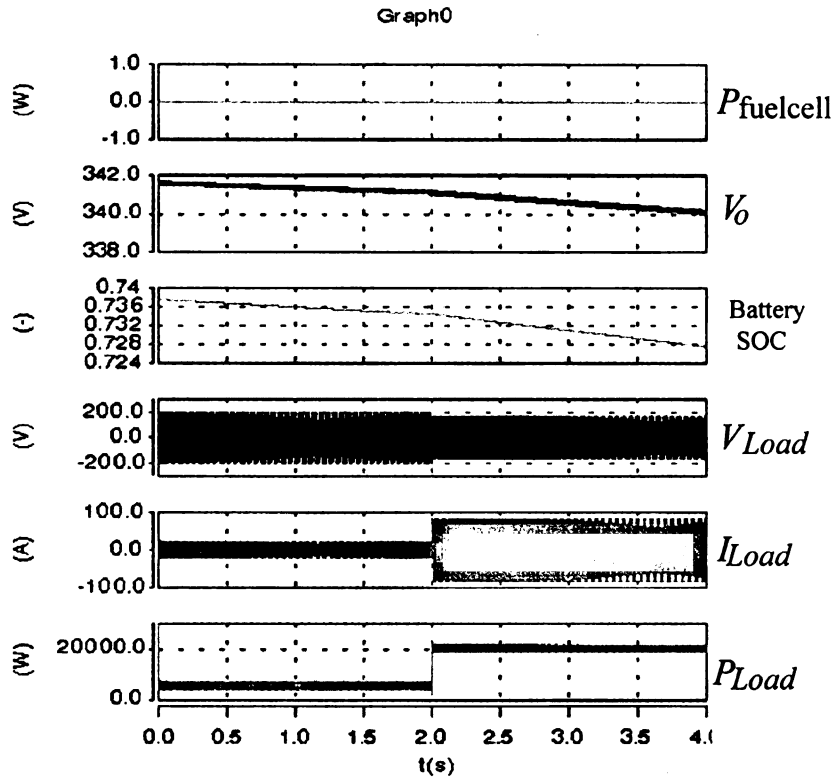


Figure 6.14. Simulation case 3.

A 10kW scaled down prototype has been constructed with the first configuration as shown in Figure 6.15. The battery used in the experiment is a 201V/6.5Ah NiMH battery used in Toyota Prius HEV. The circuit parameters are  $L1=L2=1\text{mH}$ ,  $C1=C2=1.3\text{mF}$ ,  $R_{Load}=5\Omega$ ,  $L_{Load}=1\text{mH}$ , switching frequency of 10 kHz, and using constant boost control with third harmonic injection, a RL load is used. The fuel cell was replicated by a 210V dc voltage source in series with a  $1.35\Omega$  resistor ( $V_{\text{init}}=210\text{V}$ ,  $R=1.35\Omega$ ) to mimic the current dependent output voltage characteristic of the fuel cell, a capacitor of 1mF is connected in parallel with the “fuel cell”.

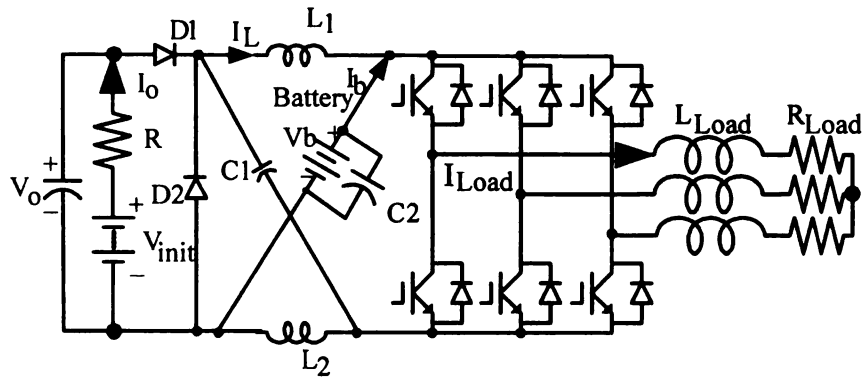


Figure 6.15. Experimental setup.

In the case 1 experiment, the load power is varied from 1.5kW ( $M=0.626$ ,  $D_0=0.065$ ) to 2kW ( $M=0.73$ ,  $D_0=0.061$ ) to 3kW ( $M=0.91$ ,  $D_0=0.054$ ) back to 2kW. The fuel cell power is designed to 2kW constant. The experimental result is shown in Figure 6.16. As from the results, the load current changes as desired, the fuel cell voltage,  $V_o$ , and the fuel cell current,  $I_o$ , are quite constant, and the fuel cell power is about 2kW. The battery voltage is also pretty constant as it supposed to be. The battery current changes to meet the power difference of the load power and the fuel cell power: when the load power is 1.5kW, the battery is charged; when the load power is 2kW, the average battery current is about 0; when the load current is 3kW, the battery is being discharged. Figure 6.16 shows that the battery can be used to handle the load dynamics.

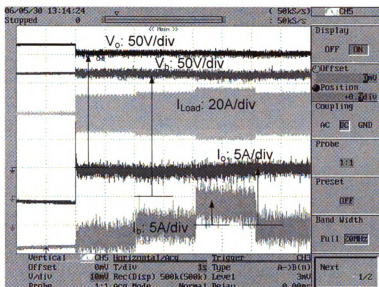


Figure 6.16. Experimental results for case 1.

In the case 2, the load is designed to 2kW constant. The fuel cell power is varied from 1.5kW ( $M=0.756$ ,  $D_0=0.037$ ) to 2kW ( $M=0.73$ ,  $D_0=0.061$ ) to 3kW ( $M=0.694$ ,  $D_0=0.1$ ) back to 2kW. The experimental result is shown in Figure 6.17. As from the results, the load current is constant, the fuel cell voltage and fuel cell current changes, which changes the fuel cell output power as desired. Also the battery current changes to compensate the power difference between the load and the fuel cell power.

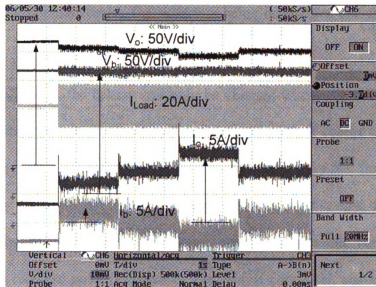


Figure 6.17. Experimental results for case 2.

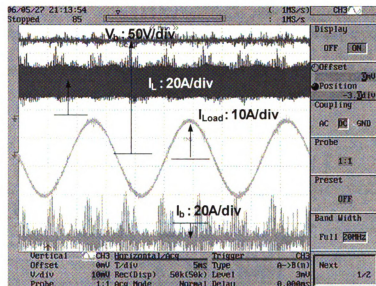


Figure 6.18. Experimental results for case 3.

In case 3, the fuel cell is disconnected, the battery is the only power source powering the load. Shoot through duty ratio of around 50% is used to control the inductor current. The experimental result is shown in Figure 6.18. The load current is pure sinusoidal.

As from the experimental results, the battery is being discharged and the load power is 2.4kW.

In practical application, the battery can only be charged when it is not fully charged, a battery management system is necessary to estimate the state of charge of the battery and feed back to the system to control the fuel cell power. Also, the fuel flow rate should be controlled based on the required system power. There can be several different possible controller configurations. Figure 6.19 shows one of the possible configurations. In this system, the required power is given by the vehicle controller, and battery voltage is measured to estimate the state of charge. With these information, the system coordinator calculates the amount of energy that should be charged/discharged and provide the corresponding shoot through duty ratio to the motor drive controller, also the amount of power that should be supplied by the fuel cell is calculated and sent to the fuel cell controller to regulate the fuel flow rate.

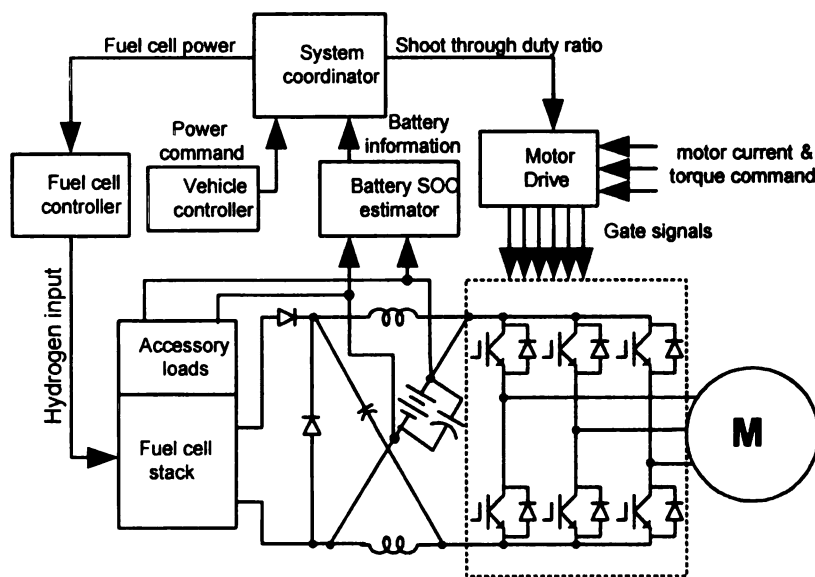


Figure 6.19. Z-source inverter based fuel cell converter control system.

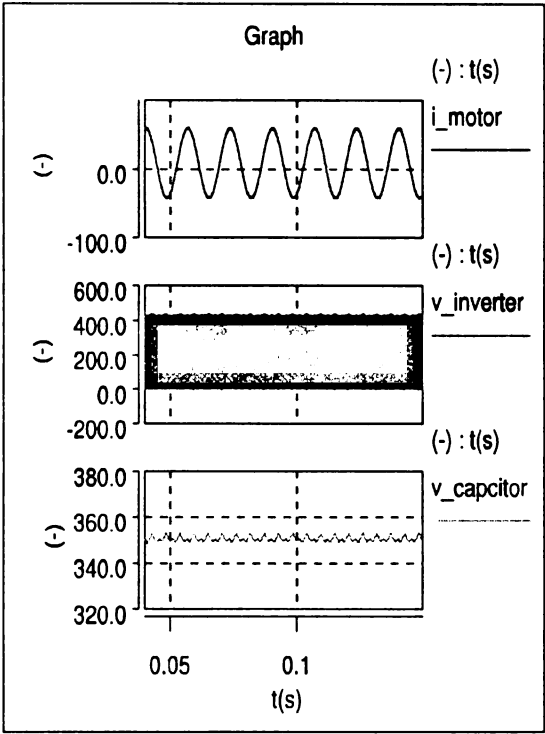
## 6.3. Undesirable Operation Modes and Control to Eliminate Them

### 6.3.1 Undesirable Operation Modes Without Control

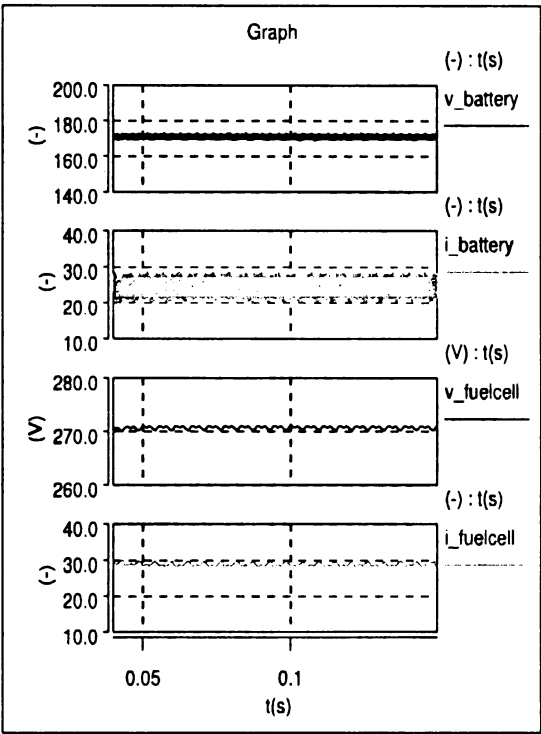
As from the previous chapter, when the load power factor, modulation index, and the inductance of the inductors are low, there could be undesirable operation modes. However, in these systems with batteries, the capacitor voltage is controlled by the battery voltage, therefore the voltage stress is limited. Simulation is performed with configuration 3 to examine the effect of undesirable modes. In this simulation, a RL load is used with  $L_{Load}=3\text{mH}$ ;  $R=0.4936\Omega$  at 60Hz, which yields power factor of 0.4, the parameters of the LC network are  $L=100\mu\text{H}$ ,  $C=1\text{mF}$ , the fuel cell is modeled with a voltage source of 290 V with a  $0.67\Omega$  resistor in series, the battery is at nominal voltage of 160 V and internal resistance of  $0.45\Omega$ , modulation index of 0.3 and shoot through duty ratio of 0.18 are used. Figure 6.20 shows the simulation results.

As from the simulation results, the inverter outputs a perfect sinusoidal current, the voltage across the inverter bridge is well limited. The battery is being charged and there is only very little undesirable operation modes. Therefore, when a battery is used in the system, the undesirable operation modes are not severe problems. However, the undesirable operation modes can also be totally eliminated with a little additional control.

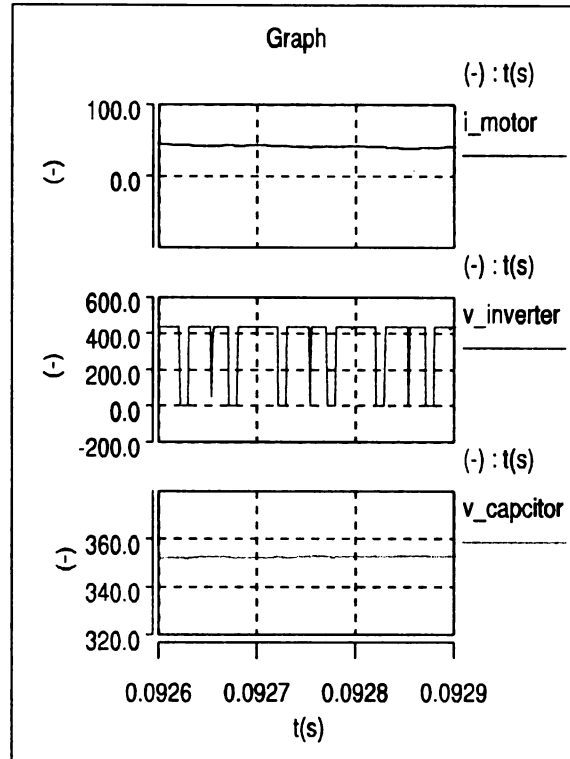




(a)



(b)



(c)

Figure 6.20. Simulation results of configuration 3 with battery connected to the neutral point of the motor.

### 6.3.2 Control Method to Eliminate the Undesirable Operation Modes

Basically, the critical condition for undesirable operation modes to happen is when sum of the two inductor currents is less than the current to the inverter bridge. With a battery, the inductor current can be increased by charging the battery. There are some slight differences for the three configurations. Take configuration 1 for an example, assuming for a given fuel cell load current  $I_f$ , the fuel cell output voltage,  $V_o$ , can be expressed as follows:

$$V_o = f(I_f). \quad (6.11)$$

From eq. (6.3), one can control the fuel cell voltage, so as to control the fuel cell current. The fuel cell voltage is determined by (6.3), therefore, the fuel cell output current,  $I_f$ , and power,  $P_f$ , can be calculated by

$$I_f = f^{-1}(V_o) \quad (6.12)$$

$$P_f = I_f V_f. \quad (6.13)$$

The average current through the inductor L1 equals to the fuel cell output current.

Assuming the output power of the inverter is  $P$ , then the power being charged to the battery is  $P_f - P$ , as a result, the average battery current  $i_b$  is

$$i_b = \frac{P_f - P}{V_b}. \quad (6.14)$$

The average current through L2 is

$$i_{L2} = i_{L1} - i_b = i_f - i_b \quad (6.15)$$

Therefore, by controlling the shoot through duty ratio, one can control  $i_{L1}$  and  $i_{L2}$ , and the battery charging/discharging current. Also, this can also be used to eliminate the unwanted operation modes when the load power factor and/or modulation index is low.

As from (1), the unwanted operation modes will only appear when  $I_{L1} + I_{L2} < I_i$ . One can increase the shoot through duty ratio,  $D_0$ , to reduce the fuel cell output voltage and increase the fuel cell output current, thus increasing  $i_{L1} + i_{L2}$ . At the same time, the inverter output voltage can be controlled by manipulating the modulation index from (6.4). As a result, the fuel cell output power is increased to be higher than the load

power and the battery will be charged during the operation. For example, the initial operating point is  $(I_{f1}, V_{f1})$  in Figure 6.21, by increasing the shoot through duty ratio, the fuel cell operating point moves to  $(I_{f2}, V_{f2})$  assuming the battery voltage is almost constant. Thus the inductor current,  $I_{L1}$ , whose average equals to fuel cell current, increases, and so does  $I_{L1}+I_{L2}$ . At the same time, by controlling the modulation index, the output voltage is maintained and so is the output current. Thus the sum of the two inductor currents can be higher than the load peak current to avoid the unwanted operation modes.

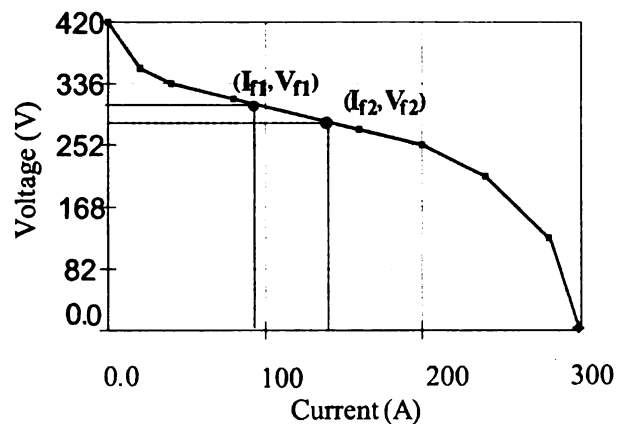


Figure 6.21. Fuel cell V-I characteristics.

In the above discussion, the method to eliminate the undesirable operation modes when the fuel cell is turned on is presented. When the fuel cell is turned off, the inductor current can be controlled from (6.10), therefore the undesirable operation modes can also be eliminated.

### 6.3.3 Experimental Verification of the Control Method

To demonstrate the effectiveness of the proposed control, experiments are carried out based on the setup shown in Figure 6.22. In this setup,  $L1=L2=1\text{mH}$ ,  $C1=C2=1320\mu\text{F}$ ,

a NiMH battery with nominal voltage of  $V_b=201\text{V}$  is connected in parallel with C1. To mimic the characteristic of a fuel cell stack, a voltage source of  $V_{int}=225\text{V}$  connected in series with a resistor of  $0.9\Omega$  is used, a capacitor of  $1\text{mF}$  is connected in parallel with the fuel cell simulator.

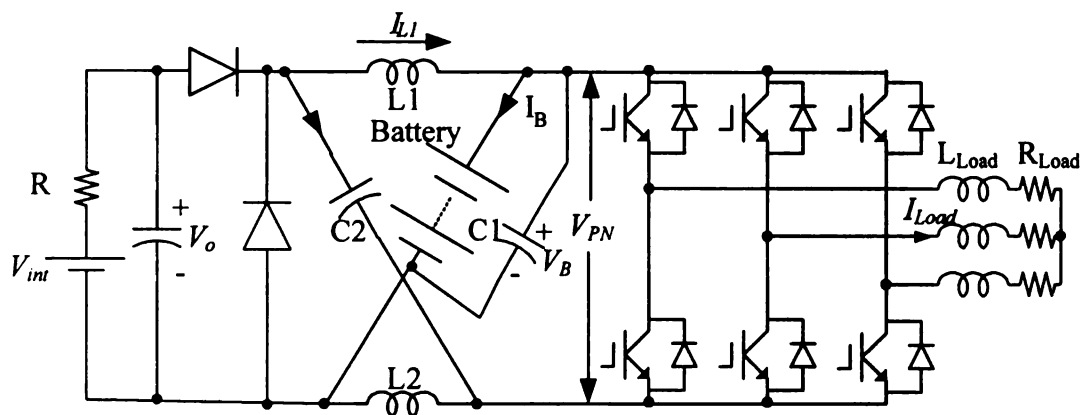


Figure 6.22. Experimental setup.

As analyzed in chapter 5, the unwanted operation modes are most likely to happen under low modulation index and low power factor. Therefore, two sets of experiments were set up to confirm the ability to eliminate the unwanted modes under these conditions:

- 1) Low power factor, and low output current. The fuel cell is on, and the battery is being charged to increase the inductor current to eliminate the undesirable operation modes. This operation condition is similar to low speed cruising for induction machine based vehicles. In the experiment, an extreme case is used: a pure inductive load of  $2\text{mH}$  per phase, and very low modulation index of  $M=0.1$  with the fundamental frequency of  $60\text{Hz}$ . Because the battery is connected in parallel with the fuel cell through a inductor and a diode, the output voltage of the fuel cell can not be higher than the battery, thus the minimum output current of the fuel cell is more than  $20\text{A}$  assuming

the battery is 201V. With this low load current condition, the minimum fuel cell current is enough to prevent the unwanted modes from happening. Therefore, in this case, no shoot through is introduced. The experimental result is shown in Figure 6.23.

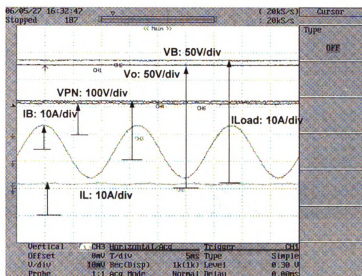
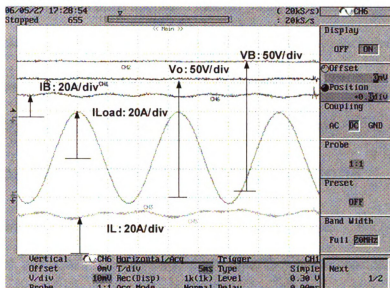


Figure 6.23. Experimental result of case 1.

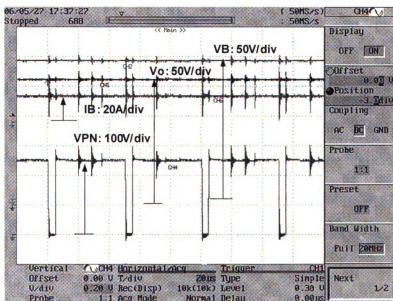
As from the experimental results, the output current is a pure sinusoidal waveform and  $V_{PN}$  is a constant dc voltage that equals to the battery voltage and fuel cell voltage, which clearly shows that only operation modes (a) and (b) appeared. Also, the battery is being charged

2) In the second case, the load power factor is relatively high and the load current is high too, and the load voltage is still low, thus the modulation index is low. This operation is trying to mimic the low speed acceleration mode, where speed is still low and load torque is high so the load voltage is low and load current is high with high power factor. In this experiment, the load is  $2mH+1.2\Omega$  per phase at 60 Hz. The fuel cell is on, to take more current out of the fuel cell, shoot through duty ratio of 0.09 is used, and modulation index of 0.34 is used. The experimental results are shown in Figure

6.24 (a) and (b).



(a) in fundamental cycles



(b) in switching cycles

Figure 6.24. Experimental results for case 2.

From the experimental results, the battery is being charged to produce more inductor current to eliminate the unwanted operation modes. The PN voltage clearly shows that only mode (a) and (b) appeared. Pure sinusoidal output current is achieved.

The experimental result when the fuel cell is turned off is shown in Figure 6.18. As can be seen from the result, there are no undesirable operation modes.

## 6.4. Comparison of the Three Configurations

All of these configurations can be used in fuel cell hybrid vehicles. Each configuration has its own pros. and cons.. In this section, two main factors are considered for purpose of comparison: the cost and output voltage range. In order to make a fair comparison, the maximum allowable voltage stress across the inverter bridge is assumed to be  $V_{inverter}$ .

### 6.4.1 Configuration 1

For this configuration, there are two control freedoms, the shoot through duty ratio and the modulation index. The capacitor voltage equals to the battery voltage,  $V_b$ , the maximum voltage stress across the inverter bridge is  $2V_b$  when the fuel cell is turned off. Therefore, for a given allowable inverter bridge voltage stress, the battery voltage is limited to  $0.5V_{inverter}$ . For a shoot through duty ratio of  $D$ , the fuel cell voltage is:

$$V_o = \frac{(1-2D)V_{inverter}}{2-2D} \quad (6.16)$$

Using maximum constant boost control, the maximum modulation index available for shoot through duty ratio of  $D$  is

$$M = \frac{2(1-D)}{\sqrt{3}} \quad (6.17)$$



The available output phase peak voltage becomes

$$V_{out} = \frac{1}{2} M \left( 2 * \frac{1}{2} V_{inverter} - V_o \right) = \frac{V_{inverter}}{2\sqrt{3}} . \quad (6.18)$$

This is the available output voltage when the fuel cell is turned on. When the fuel cell is turned off, the shoot through duty ratio is 0.5, which is also covered in the above equation.

The cost of this configuration is low because there is no extra component required.

### 6.4.2 Configuration 2

In the second configuration, an extra dc/dc converter is used to interface the battery and the capacitor. Thus the capacitor voltage can be controlled independently without using the two freedoms of the Z-source inverter. Therefore, the voltage across the inverter bridge can always be controlled to its maximum limit by the dc/dc converter. As a result, the obtainable output voltage for a given shoot through duty ratio becomes

$$V_{out} = \frac{1}{2} M V_{inverter} = \frac{(1-D)V_{inverter}}{\sqrt{3}} , \quad (6.19)$$

which is higher than the previous case. This also includes the condition when the fuel cell is turned off and the shoot through duty ratio becomes 0.5, which is the same as the previous case.

With an extra dc/dc converter, the cost of the inverter system is increased.

### 6.4.3 Configuration 3

With the battery connected to the neutral point of the machine, the inverter has an extra control freedom: the shift of the reference signals, however, this freedom is related to the shoot through duty ratio and the modulation index.

To maximize the available output voltage, we choose the pn voltage to be the maximum value that the IGBT module can handle,  $V_{inverter}$ , the fuel cell voltage should be

$$V_o = 2V_c - V_{inverter} = \frac{4(1-D)V_b}{1-D-V_s} - V_{inverter}. \quad (6.20)$$

To get this relationship of the capacitor voltage and fuel cell voltage, the shoot through duty ratio should be

$$D = 1 - \frac{2(1-D)V_b}{(1-D-V_s)V_{inverter}}. \quad (6.21)$$

Therefore the shift of the reference can be expressed as a function of the battery voltage and the shoot through duty ratio in order to keep the inverter bridge voltage to its allowable level:

$$V_s = \frac{-2V_b}{V_{inverter}} + 1 - D \quad (6.22)$$

Assume that the maximum constant boost control is used, the available modulation index under this condition is

$$M = \frac{2(1-D-|V_s|)}{\sqrt{3}} = \frac{2}{\sqrt{3}} \left( 1-D - \left| 1-D - \frac{2V_b}{V_{inverter}} \right| \right). \quad (6.23)$$

Thus the available output voltage is

$$V_{out} = \frac{1}{2} M * V_{inverter} = \frac{1}{\sqrt{3}} (1 - D - \left| 1 - D - \frac{2V_b}{V_{inverter}} \right|) * V_{inverter} \quad (6.24)$$

Therefore, the available output voltage is related to the shoot through duty ratio as well as the battery voltage. In general, the voltage range is between the first two configurations. For this configuration, there is no extra dc/dc converter is needed. However, there might be some dc current flowing through the machine, which increases the motor copper loss, therefore the machine needs to be oversized a little bit.

#### 6.4.4 Comparison Summary

From all above discussion, a summary of the comparison is given in the Table 6.1.

Table.6.1. Comparison of different configurations

Configurations	Battery Voltage	Output voltage range	Cost
1	High	Small	Low
2	Low ~ High	Wide	High
3	Medium	Medium	Medium

The battery voltage is included here because it is also a consideration for safety issues.

### 6.5 Summary

In this chapter, three configurations of fuel cell-battery hybrid vehicles using the Z-source inverter are presented. Basic control methods are described. It is shown that with a battery in the system, the effect of the undesirable operation modes can be

minimized. A control method to totally eliminate the undesirable operation modes is also presented. A simple comparison between the three configurations is provided.

# CHAPTER 7 Conclusions and Recommendations

## 7.1 Contributions

This work has the following contributions:

- Three PWM methods are proposed to achieve simple boost, maximum boost, and maximum constant boost respectively. A modified PWM is also proposed to reduce the switching losses. A comparison with an commonly adopted PWM method shows that the modified PWM method can reduce the switching loss significantly.
- A small signal model for the Z-source inverter is developed, based on this model a closed loop controller is also designed using gain scheduling method. The validity of the model and the controller are verified with simulation/experimental results.
- A comprehensive comparison of the Z-source inverter and traditional inverters for fuel cell vehicle application is conducted. The comparison uses switching device power, passive components requirement, constant power speed ratio, reliability, and inverter efficiency as bench marks. The comparison shows that the Z-source inverter is very promising for applications with low boost ratio.
- Three new operation modes of the Z-source inverter are found and analyzed in detail. The critical condition and consequences when they happen are presented.
- Three configurations of the Z-source inverter for fuel cell-battery hybrid vehicle applications are proposed with the basic control methods. The effect of undesirable

operation modes is minimized in these configurations. Also control methods are proposed to eliminate the undesirable operation modes.

## **7.2 Recommendations for future works**

The modified PWM method proposed in this work reduces the switching loss, but also requires a relatively larger inductor. Further work should be done on the PWM scheme to see if it is possible to double the frequency on the inductor, keeping the switching loss within a reasonable amount, so that the inductor size can be reduced significantly.

The controller designed in this work is for a RL load, further work should be done to design the controller for motor load. The load comes into the picture of the whole system, a comprehensive model of the motor is also needed. Another future job in designing the controller is to consider the limit of the two control freedoms and its effect on the system stability and transient response.

In this work, only the voltage fed Z-source inverter is considered. As a counterpart, the current fed Z-source inverter should also be studied.

# APPENDIX 1 Switching Device Power

## Derivation

### a. Traditional PWM Inverter

For the traditional PWM inverter, the output phase RMS voltage at peak power is

$$V_p = \frac{V_i}{2\sqrt{2}} M. \quad (\text{A1.1})$$

With motor power factor of  $\cos\phi$ , the output line RMS current is

$$I_p = \frac{P_o}{3 \cos\phi V_p}. \quad (\text{A1.2})$$

Because the line current is evenly shared by two switches in a line cycle, the average current through each switch is:

$$I_{av} = \frac{P_o}{3 \cos\phi V_i / (2\sqrt{2}) M} \sqrt{2} * \frac{2}{2\pi} = \frac{4P_o}{3 \cos\phi V_i \pi M}. \quad (\text{A1.3})$$

The maximum voltage stress of the switches occurs when the output power is zero, and the fuel cell voltage reaches its maximum value, which is

$$V_s = V_{\max}. \quad (\text{A1.4})$$

The total average switching device power of the circuit can be derived based on its definition by

$$(\text{SDP})_{av} = 6 * V_s * I_{av} = \frac{8V_{\max} P_o}{\cos\phi V_i \pi M}. \quad (\text{A1.5})$$

The peak current through the switches is the peak line current, from (A1.2),

$$I_{pk} = \sqrt{2}I_p = \frac{4P_o}{3\cos\phi V_i M}. \quad (\text{A1.6})$$

The total peak switching device power of the traditional PWM inverter is

$$(\text{SDP})_{pk} = 6 * V_s * I_{pk} = \frac{8V_{\max}P_o}{\cos\phi V_i M}. \quad (\text{A1.7})$$

### ***b. dc/dc Boosted PWM Inverter***

For the switch in the boost converter, treating the switch and the diode as a switching cell, the maximum voltage it sustains is  $V_{DC}$ , based on power balance, the average current through it during maximum power is

$$I_{avs} = \frac{P_o}{V_i}. \quad (\text{A1.8})$$

The average switching device power of the dc/dc converter is the product of the current and voltage, which is

$$(\text{SDP})_{DCav} = \frac{P_o}{V_i} * V_{DC}. \quad (\text{A1.9})$$

Assume the current through the inductor in the boost converter is constant, the peak current through the switch is the same as the average current. The peak switching device power is

$$(\text{SDP})_{DCpk} = \frac{P_o}{V_i} * V_{DC}. \quad (\text{A1.10})$$

The voltage stress of the inverter switches is  $V_{DC}$ . The RMS phase voltage at



modulation index of  $M$  is

$$V_p = \frac{V_{DC}M}{2\sqrt{2}}. \quad (A1.11)$$

The RMS line current under load power factor of  $\cos \psi$  is:

$$I_p = \frac{P_o}{3V_p \cos \varphi}. \quad (A1.12)$$

The average current through switches under maximum power is

$$I_{avinv} = \frac{I_p \sqrt{2}}{\pi} = \frac{4P_o}{3 \cos \varphi V_{DC} \pi M}. \quad (A1.13)$$

The average switching device power of the system is the sum of SDP of the dc/dc converter and the inverter, which is

$$(SDP)_{av} = 6 * V_{DC} * I_{avinv} + (SDP)_{DCav} = \frac{8P_o}{\cos \varphi \pi M} + \frac{P_o}{V_i} * V_{DC} \quad (A1.14)$$

The peak switch current of the inverter is

$$I_{pkinv} = \sqrt{2} I_p = \frac{4P_o}{3 \cos \varphi V_{DC} M}. \quad (A1.15)$$

The peak switching device power of the system is the sum of the SDP of the dc/dc converter and the inverter

$$(SDP)_{pk} = 6 * V_{DC} * I_{pkinv} + (SDP)_{DCpk} = \frac{8P_o}{\cos \varphi M} + \frac{P_o}{V_i} * V_{DC}. \quad (A1.16)$$

### ***c. Z-Source Inverter***

For the Z source inverter, the current through the inverter switches consists of two

elements, one is the current to the load and the other is the current through them during the shoot through state. Because of the symmetrical structure of the inverter, the current during shoot through in terms of average is evenly distributed in three parallel paths. The current through the inverter during shoot through is twice of the inductor current. Therefore, the average current value in shoot through period through each switch is

$$I_{avss} = \frac{2}{3} I_L, \quad (\text{A1.17})$$

where  $I_L$  is the inductor current. From the input end, the average current through the diode is equal to the sum of the average current through inductor  $L_1$  and capacitor  $C_1$ . In steady state, the average current through the capacitor is zero, the average current through the inductor equals to that of the diode. The output power of the fuel cell stack under maximum power is  $P_o$ , therefore, the average current through the diode as well as the inductor is:

$$\bar{I}_d = I_L = \frac{P_o}{V_i}. \quad (\text{A1.18})$$

While in traditional switching states, the average current is the same as a conventional PWM inverter, therefore the overall average current through inverter switches is the sum of the current in both states, which is

$$I_{avs} = \frac{2}{3} I_L * \frac{T_0}{T_s} + \frac{\sqrt{2}P_o}{3V_o \cos \varphi \pi} (1 - \frac{T_0}{T_s}) = \frac{2}{3} I_L * \frac{T_0}{T_s} + \frac{4(\sqrt{3}M - 1)P_o}{3V_i \cos \varphi \pi M} (1 - \frac{T_0}{T_s}), \quad (\text{A1.19})$$

where  $T_0$  is the shoot through period in a switching cycle  $T_s$ ,  $V_o$  is the RMS output phase voltage. With the maximum constant boost control,  $T_0$  and  $V_o$  can be expressed as

$$T_o = \left(1 - \frac{\sqrt{3}}{2}M\right)T_s. \quad (\text{A1.20})$$

$$V_o = \frac{M}{\sqrt{3M-1}} \frac{V_i}{2\sqrt{2}}. \quad (\text{A1.21})$$

Voltage stress of the inverter switches with constant boost control under modulation index of  $M$  is

$$V_s = BV_i = \frac{V_i}{\sqrt{3M-1}}. \quad (\text{A1.22})$$

The average switching device power of the inverter is

$$(SDP)_{av} = 6I_{avs}V_s = 4I_LV_i \frac{T_0}{T_s(\sqrt{3M-1})} + 8 \frac{P_o}{\cos \varphi \pi M} \left(1 - \frac{T_0}{T_s}\right) = \frac{2P_o(2-\sqrt{3}M)}{(\sqrt{3M-1})} + \frac{4\sqrt{3}P_o}{\cos \varphi \pi} \quad (\text{A1.23})$$

The peak current through the switches occurs during shoot through. To calculate the peak current through the switches, we assume that when the switches are on they are pure resistors with the same resistance, which is shown in Figure A.1.

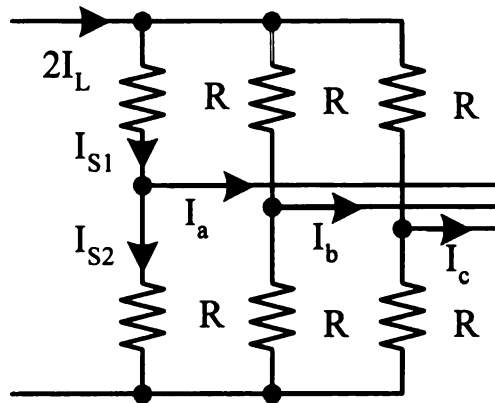


Figure A.1. Inverter model during shoot through

Based on this model and voltage balance of three paths, we can have the following

equations

$$I_{s2} + I_{s1} = \frac{4}{3}I_L, \quad (\text{A1.24})$$

$$I_{s1} - I_{s2} = I_a. \quad (\text{A1.25})$$

where  $I_a$  is the phase a load current. From which we can get

$$I_{s1} = \frac{1}{2}I_a + \frac{2}{3}I_L. \quad (\text{A1.26})$$

The peak current through the switch S1 occurs when the line current of phase A is at its peak, which is

$$I_{lpk} = \frac{\sqrt{2}P_o}{3 \cos \varphi V_o} = \frac{4P_o}{3 \cos \varphi MBV_i}. \quad (\text{A1.27})$$

Thus the peak switch current is

$$I_{pk} = \frac{4P_o}{3 \cos \varphi MBV_i} + \frac{2}{3}I_L = \frac{4P_o}{3 \cos \varphi MBV_i} + \frac{2P_o}{3V_i} \quad (\text{A1.28})$$

The peak switching device power of the inverter is

$$(SDP)_{pk} = 6I_{pk}V_s = 6 \frac{V_i}{\sqrt{3M-1}} \left( \frac{2}{3} \frac{P_o}{V_i} + \frac{1}{2} \frac{4P_o}{3 \cos \varphi MBV_i} \right) = \frac{4P_o}{\sqrt{3M-1}} + \frac{4P_o}{\cos \varphi M}. \quad (\text{A1.29})$$

# APPENDIX 2 Passive Components

## Requirement

### *a. dc/dc Boosted PWM Inverter*

For the inductor in the boost converter, the current ripple can be calculated by the current increase when the switch is on.

$$\Delta I_L = \frac{V_i}{L} DT_s = \frac{V_i(V_{DC} - V_i)}{LV_{DC}} T_s, \quad (\text{A2.1})$$

where  $D$  is the duty cycle.

### *b. Z-Source Inverter*

For the Z-source inverter, when the inverter is in a shoot through state, the voltage across the inductor is the voltage across the capacitor. Therefore the current ripple of the inductor can be calculated as

$$\Delta I = \frac{V_c}{L} T_o, \quad (\text{A2.2})$$

where  $V_c$  is the voltage across the capacitor  $C$ ,

$$V_c = \frac{V_i}{2}(1+B) = \frac{V_i}{2} \frac{\sqrt{3}M}{\sqrt{3}M-1}. \quad (\text{A2.3})$$

and  $T_o$  is the shoot through duty ratio, which is

$$T_o = \left(1 - \frac{\sqrt{3}}{2}M\right)T_s, \quad (\text{A2.4})$$

where  $T_s$  is the switching period.

We have

$$\Delta I = \frac{V_i \sqrt{3} M}{2L(\sqrt{3}M - 1)} \left( 1 - \frac{\sqrt{3}}{2} M \right) T_s. \quad (\text{A2.5})$$

# APPENDIX 3 Critical Condition of New Modes Under SVPWM

In simple operation when only mode 1 and 2 occur, the inductor currents are pure dc. The new modes only happen when the inductor current is less than half of the current to the inverter bridge,  $i_i$ . From the circuit, it is obvious that the average inductor current in the Z-source equals to the average input current. Based on the power balance, the average inductor current can be calculated by

$$\bar{I}_L = \frac{P}{V_o} \quad (\text{A3.1})$$

For modulation index of  $M$ , load peak current of  $I_{pk}$ , and power factor of  $\cos \varphi$ , the inductor current is

$$I_L = \frac{P}{V_o} = \frac{3}{4} M \cos \varphi I_{pk}. \quad (\text{A3.2})$$

The maximum current fed to the inverter bridge is

$$I_{ipk} = \begin{cases} I_{pk} & \cos \varphi \geq \frac{1}{2} \\ I_{pk} \cos(\varphi - \frac{\pi}{3}) & \cos \varphi < \frac{1}{2} \end{cases} \quad (\text{A3.3})$$

The new modes happen when  $I_L < \frac{1}{2} I_{ipk}$ . As a result, the critical condition is

$$\left\{ \begin{array}{ll} M \cos \varphi < \frac{2}{3} & \cos \varphi \geq \frac{1}{2} \\ M \cos \varphi < \frac{2}{3} \cos(\varphi - \frac{\pi}{3}) & \cos \varphi < \frac{1}{2} \end{array} \right\}. \quad (\text{A3.4})$$

However, when  $\cos \varphi < \frac{1}{2}$ , for  $0 \leq \varphi \leq \frac{\pi}{2}$  and  $M < 1.15$ , the inequation is always true,

therefore the critical condition is reduced to  $M \cos \varphi < \frac{2}{3}$ .



# APPENDIX 4 Critical Condition of New Modes Under Maximum Constant Boost Control with Third Harmonic Injection

Under maximum constant boost control with third harmonic injection, the shoot through time,  $T_{st}$ , in one cycle is always constant. For simple operation condition, the inductor current increases linearly during shoot through

and decreases linearly otherwise. The current ripple is

$$\Delta I_L = \frac{T_{st} V_c}{L}. \quad (\text{A4.1})$$

The average inductor current can be calculated by (A3.2), the minimum inductor current with shoot through time of  $T_{st}$  is

$$I_{L \min} = \frac{P}{V_o} - \frac{T_{st} V_c}{2L}, \quad (\text{A4.2})$$

For modulation index of  $M$  in simple operation condition, the output phase rms voltage,  $V_{out}$ , can be calculated by

$$V_{out} = \frac{M V_o}{2\sqrt{2}(\sqrt{3}M - 1)} \quad (\text{A4.3})$$

The output power,  $P$ , can be expressed as

$$P = \frac{3}{\sqrt{2}} V_{out} I_{pk} \cos \varphi = \frac{3 \cos \varphi \left( \frac{MV_o}{2(\sqrt{3}M-1)} \right)^2}{2Z} = \frac{3 \cos \varphi}{8Z} \left( \frac{MV_o}{\sqrt{3}M-1} \right)^2. \quad (\text{A4.4})$$

Under this control method, the relationship of modulation index and shoot through period,  $T_{st}$ , is

$$M = \frac{2}{\sqrt{3}} \left( 1 - \frac{T_{st}}{T_s} \right). \quad (\text{A4.5})$$

The new modes happen when the minimum inductor current is less than half of the maximum current feeding to the inverter bridge expressed in (A3.3).

Put all these equations together, we can get the following critical condition:

$$\left\{ \begin{array}{l} \frac{3M \cos \varphi}{2Z(\sqrt{3}M-1)} - \frac{\sqrt{3}T_{st}}{L} < \frac{1}{Z} \quad \cos \varphi \geq \frac{1}{2} \\ \frac{3M \cos \varphi}{2Z(\sqrt{3}M-1)} - \frac{\sqrt{3}T_{st}}{L} < \frac{1}{Z} \cos\left(\varphi - \frac{\pi}{3}\right) \quad \cos \varphi < \frac{1}{2} \end{array} \right\} \quad (\text{A4.6})$$

# APPENDIX 5 Characteristic Analysis of the Circuit Under CCM Condition

For the operating condition shown in Figure 5.4 (a),  $T_{a1}$  is an active state with operation Mode 2 and  $T_{a2}$  is active state with operation Mode 3. For a given control method and a modulation index,  $T_{st}$ ,  $T_0$ , and  $T_7$  are already determined. To simplify the analysis, assume  $T_{st}$ ,  $T_0$ ,  $T_{a1}$ ,  $T_{a2}$ , and  $T_7$  are constants throughout a whole line cycle, and  $T_0=T_7$ , and the current to the inverter during active states,  $i_i$ , is always a constant. For the CCM operation condition shown in Figure 5.4 (a) and voltage second balance of the inductor, we have following equations

$$T_{a1} = \frac{I_n L + V_c T_{st} - \frac{i_i}{2} L}{V_c - V_o} - T_0, \quad (A5.1)$$

$$T_{a2} = T_s - T_{st} - T_0 - T_{a1} - T_7, \quad (A5.2)$$

$$I_n = \frac{i_i}{2} - \frac{T_0 + T_7}{2} \frac{V_c - V_o}{L}, \quad (A5.3)$$

where  $I_n$  is shown in Figure 5.4 (a).

In shoot-through state, the current to the inverter is

$$i_i = 2i_L. \quad (A5.4)$$

In steady state, the capacitor voltage is constant, and the average current goes through the capacitor is zero, therefore,

$$\begin{aligned}
& I_n(T_{st} + T_0 + T_7 + T_{a1}) + \frac{1}{2} \frac{V_c}{L} T_{st} (T_{st} + T_0 + T_7 + T_{a1}) + \frac{i_i}{2} T_{a2} \\
& = 2I_n T_{st} + \frac{V_c}{L} T_{st}^2 + (T_{a1} + T_{a2}) i_i
\end{aligned} \tag{A5.5}$$

Put all equations together and solve for  $I_i$ , we have

$$i_i = \frac{2(V_c V_o T_{0+7} T_{st} - T_{st}^2 V_c V_o - T_{0+7} T_{st} V_o^2)}{L T_s V_o - 2T_{0+7} L V_o + 2T_{0+7} V_c L - V_c L T_s} \tag{A5.6}$$

The dc link voltage of the inverter during  $T_{a1}$  is  $2V_c - V_i$ , and  $V_c$  during  $T_{a2}$ , therefore, the output phase rms voltage of the inverter can be calculated by:

$$V_{out} = \frac{(2V_c - V_o) T_{a1} + V_c T_{a2}}{2\sqrt{2}(T_{a1} + T_{a2})} M \tag{A5.7}$$

Based on the output voltage, we can calculate the average  $i_i$  in active states from the load side. The average current to the inverter during active state can be calculated as in (A5.8).

$$\begin{aligned}
I_i &= \frac{3}{\pi} \int_{\frac{\pi}{6}}^{\frac{\pi}{2}} \frac{\sqrt{2} V_{out}}{Z} \left( \frac{\sin(\omega t - \varphi) [\sin \omega t - \sin(\omega t - \frac{4}{3} \pi)]}{\sin \omega t - \sin(\omega t - \frac{2}{3} \pi)} \right. \\
& \left. + \frac{\sin(\omega t - \varphi - \frac{2}{3} \pi) [\sin(\omega t - \frac{4}{3} \pi) - \sin(\omega t - \frac{2}{3} \pi)]}{\sin \omega t - \sin(\omega t - \frac{2}{3} \pi)} \right) dt = \frac{1.29 V_{out}}{Z} \cos \varphi
\end{aligned} \tag{A5.8}$$

Putting (A5.7) into (A5.8), and equalizing (A5.6) and (A5.8), one can get (A5.9). One can solve (A5.9) to get capacitor voltage  $V_c$  under this operating condition with maximum constant boost control with third harmonic injection.

$$\frac{V_c V_o T_{0+7} T_{st} - T_{st}^2 V_c V_o - T_{0+7} T_{st} V_o^2}{L T_s V_o - 2T_{0+7} L V_o + 2T_{0+7} V_c L - V_c L T_s} = \frac{0.455 M \cos \varphi}{Z} \frac{T_s V_c - 2T_{0+7} V_c + T_{0+7} V_o}{T_s - T_{st} - T_{0+7}} \tag{A5.9}$$

# References

- [1] Welchko, B.A.; Lipo, T.A.; Jahns, T.M.; Schulz, S.E.; “Fault tolerant three-phase AC motor drive topologies: a comparison of features, cost, and limitations” *IEEE Transactions on Power Electronics*, Volume 19, Issue 4, July 2004, pp.1108–1116.
- [2] Sikorski, A.; Citko, T.; “Current controller reduced switching frequency for VS-PWM inverter used with AC motor drive applications” *IEEE Transactions on Industrial Electronics*, Volume 45, Issue 5, Oct. 1998, pp.792 - 801
- [3] Jun-Keun Ji; Jang-Hwan Kim; Seung-Ki Sui; Hyo-sung Kim; “A novel three-phase line-interactive UPS system with parallel-series active power-line conditioning capabilities using AC line reactor” in *proc. of IEEE Industrial Electronics Society Annual Conference 2004*. Volume 2, 2-6 Nov. 2004, pp.1861 - 1866
- [4] Chuanhong Zhao; Kolar, J.W.;”A novel three-phase three-port UPS employing a single high-frequency isolation transformer” in *Proc. of IEEE Power Electronics Specialists Conference*, 2004 Volume 6, 20-25 June 2004, pp. 4135 – 4141
- [5] Sewell, H.I.; Stone, D.A.; Bingham, C.M.; “Novel, three phase, unity power factor modular induction heater” in *IEE Proceedings Electric Power Applications*, Volume 147, Issue 5, Sept. 2000, pp. 371 – 378
- [6] Hou Zhen Yi; Sun Jin; “Study on control strategy for three-phase four-leg inverter power supply” in *proc. of IEEE Industrial Electronics Society Annual Conference 2004* Volume 1, 2-6 Nov. 2004, pp. 805 - 809.
- [7] Zhang, R.; Lee, F.C.; Boroyevich, D.; Hengchun Mao; “New high power, high performance power converter systems” in *Proc. of IEEE Power Electronics Specialists Conference*, 1998. Volume 1, 17-22 May 1998, pp. 8 – 14.
- [8] Bor-Ren Lin; Yuan-An Ou; Tsung-Yu Yang; “Shunt active power filter with three-phase switch-clamped inverter”, in *Proc. of the IEEE International Conference on Control Applications*, Volume 2, 2-4 Sept. 2004, pp. 1633 - 1638.
- [9] Woo-Cheol Lee; Taek-Kie Lee; Dong-Seok Hyun; “A three-phase parallel active power filter operating with PCC voltage compensation with consideration for an unbalanced load”, *IEEE Transactions on Power Electronics*, Volume 17, Issue 5, Sept. 2002, pp. 807 – 814
- [10] Ekanayake, J.B.; Jenkins, M.; “A three-level advanced static VAR compensator” *IEEE Transactions on Power Delivery*, Volume 11, Issue 1, Jan. 1996, pp. 540 – 545.
- [11] Joos, G.; Espinoza, J.; “Three phase series VAR compensation based on a voltage controlled current source inverter with supplemental modulation index control” in *Proc.*

of *IEEE Power Electronics Specialists Conference*, 20-25 June 1994, pp. 1437 – 1442 vol.2.

[12] Fang Zheng Peng; “Z-source inverter” *IEEE Transactions on Industry Applications* Volume 39, Issue 2, March-April 2003, pp.504 – 510.

[13] T.Sukegawa, K.Kamiyama, K.Matsui, and T.Okuyama, “Fully digital, vector controlled PWM VSI-fed ac drives with an inverter dead-time compensation strategy”, *IEEE transactions on Industry Applications*. Vol. 27, pp.552-559, May/June 1991.

[14] Rizzo, S.C.; Bin Wu; Sotudeh, R.; “Symmetric GTO and snubber component characterization in PWM current-source inverters” *IEEE Transactions on Power Electronics*, Volume 13, Issue 4, July 1998, pp. 617 – 625.

[15] B.K.Bose; “Modern Power Elelctronics and AC Drives” Upper Saddle River, NJ 07458, 2002.

[16] Geza Joos, Gerry Moschopoulos, Phoivos D. Ziogas; “A high performance current source inverter”. *IEEE Transactions on Power Electronics*. Vol. 8, No.4. 1993, pp.571-579.

[17] D.A. Grant and J. A. Houldsworth: “PWM AC Motor Drive Employing Ultrasonic Carrier”. in *Proc. of IEE Conf. PE-VSD*, 1984, London, pp. 234-240.

[18] O'Sullivan, G.A.; “Fuel cell inverters for utility applications” in *Proc. of IEEE Power Electronics Specialist Conference*, 2000, pp. 1191 – 1194.

[19] Tuckey, A.M.; Krase, J.N.; “A low-cost inverter for domestic fuel cell applications” in *Proc. of IEEE Power Electronics Specialist Conference*, 2002, pp. 339 – 346.

[20] Krein, P.T.; Balog, R.; “Low cost inverter suitable for medium-power fuel cell sources” in *Proc. of IEEE Power Electronics Specialist Conference*, 2002. pp. 321 - 326.

[21] Mazumdar, J.; Batarseh, I.; Kutkut, N.; Demirci, O.; “High frequency low cost DC-AC inverter design with fuel cell source for home applications” in *Proc. of IEEE Industry Application Society Annual Meeting*, 2002, pp.789 – 794.

[22] Yi Huang, Miaosen Shen, Fang Z Peng, “A Z-Source Inverter for Residential Photovoltaic Systems” in *Proc. of International Power Electronics Conference 2005*, pp. 1426-1431. April 2005.

[23] Xu-Peng Fang; Zhao ming Qian; Qi Gao; Bin-Gu; Fang-Zheng Peng; Xiao-ming Yuan, “Current mode Z-source inverter-fed ASD system” in *Proc. of Power Electronics Specialists Conference*, 2004. pp. 2805 - 2809 Vol.4.

[24] Takei, M.; Harada, Y.; Ueno, K.; “600 V-IGBT with reverse blocking capability” in *Proc. of International Symposium on Power Semiconductor Devices and ICs*, 2001.

4-7 June 2001, pp. 413 – 416.

[25] F. Z. Peng, X. Yuan, X. Fang, and Z. Qian, “Z-source inverter for adjustable speed drives,” *IEEE Power Electronics Letters*, Volume: 1, Issue: 2, pp. 33-35, June 2003.

[26] F. Z. Peng, “Z-source inverter for adjustable speed drives,” in *Proc of IEEE Power Electronics Specialists Conference*, pp. 249-254, June, 2004.

[27] F. Z. Peng, M. Shen, and Z. Qian, “Maximum Boost Control of the Z-Source Inverter,” *Proc of IEEE Power Electronics Specialists Conference*, pp. 255-260, June, 2004.

[28] Y. H. Kim, H. W. Moon, S. H. Kim, E. J. Cheong, and C. Y. Won, “A fuel cell system with Z-source inverters and ultracapacitors” in *Proc of Power Electronics and Motion Control Conference, 2004*, Volume 3, pp. 1587-1591, 14-16 Aug. 2004

[29] M. Shen, J. Wang, A. Joseph, F. Z. Peng, L. M. Tolbert, and D. J. Adams, “Maximum Constant Boost Control of the Z-Source Inverter,” in *Proc of IEEE Industry Applications Society Annual Meeting, 2004*, pp. 142-147, Oct, 2004.

[30] P. C. Loh, D. M. Vilathgamuwa, Y. S. Lai, G. T. Chua, and Y. Li;” Pulse-width modulation of Z-source inverters” in *Proc of IEEE Industry Applications Society Annual Meeting, 2004*, pp.148-155, Oct. 2004.

[31] M. Shen, A. Joseph, J. Wang, F. Z. Peng, and D. J. Adams, “Comparison of traditional inverter and Z-Source inverter for fuel cell vehicles,” in *Proc of IEEE Workshop on Power Electronics in Transportation, 2004*, pp. 125-132, Oct, 2004.

[32] F. Z. Peng, “Z-source converters and their motor drive applications”, *International Conference on Electric Machines and Systems*, invited paper, paper no. 630-M08-052, Jeju Korea, Nov. 1-3, 2004.

[33] F. Z. Peng, M. Shen, and A. Joseph, “Z-Source Inverters, Controls, and Motor Drive Applications”, *KIEE International Transactions on Electrical Machinery and Energy Conversion Systems*, volume 5-B 2005, pp. 6-12, 2005.

[34] J. W. Jung, M. Dai, and A. Keyhani; “Modeling and control of a fuel cell based Z-source converter” in *Proc. of IEEE Applied Power Electronics Conference and Exposition, 2005*. Volume 2, pp.1112 – 1118, March 2005.

[35] M. Shen, A. Joseph, J. Wang, F. Z. Peng, and D. J. Adams; “Comparison of Traditional Inverters and Z-Source Inverter” in *Proc of IEEE Power Electronics Specialists Conference*, pp. 1692 – 1698, June 12, 2005.

[36] X. Ding, Z. Qian, Y. Xie, and Z. Lu, “Three Phase Z-Source Rectifier”, in *Proc of IEEE Power Electronics Specialists Conference, 2005*, pp. 494 – 500, 2005.

- [37] F. Z. Peng, M. Shen, and Z. Qian; "Maximum boost control of the Z-source inverter", *IEEE Trans. on Power Electron*, Volume 20, Issue 4, pp. 833 – 838, July 2005
- [38] F. Z. Peng, A. Joseph, J. Wang, M. Shen, L. Chen, Z. Pan, R. E. Ortiz, and Y. Huang, "Z-source inverter for motor drives" *IEEE Trans. on Power Electron.*, Volume 20, Issue 4, pp. 857 – 863, July 2005.
- [39] K. Holland and F. Z. Peng; "Control strategy for fuel cell vehicle traction drive systems using the Z-source inverter" in *Proc of IEEE Vehicle Power and Propulsion Conference*, pp. 639-944, 7-9 Sept. 2005.
- [40] J. Liu, J. Hu, and L. Xu;" A Modified Space Vector PWM for Z-Source Inverter - Modeling and Design" in *Proc. of International Conference on Electrical Machines and Systems, 2005*. Volume 2, pp.1242 – 1247, 27-29 Sept. 2005.
- [41] K. You and M. F. Rahman;" A new power converter for ISA 42 V powernet system using matrix converter theory and Z-source inverter concepts" in *Proc of IEEE Vehicle Power and Propulsion Conference*, pp. 461-467, 7-9 Sept. 2005.
- [42] P. C. Loh, D. M. Vilathgamuwa, C. J. Gajanayake, L. T. Wong, and C. P. Ang; "Z-source current-type inverters: digital modulation and logic implementation" in *Proc. of IEEE Industry Applications Society Annual Meeting*, Volume 2, pp. 940-947, 2-6 Oct. 2005
- [43] P. C. Loh, D. M. Vilathgamuwa, C. J. Gajanayake, Y. R. Lim, and C. W. Teo "Transient modeling and analysis of pulse-width modulated Z-source inverter" in *Proc. of IEEE Industry Applications Society Annual Meeting*, Volume 4, pp. 2782-2789, 2-6 Oct. 2005.
- [44] M. Shen and F. Z. Peng, "Operation modes and characteristics of the Z-source inverter with small inductance" in *Proc. of IEEE Industry Applications Society Annual Meeting*, Volume 2, pp. 1253 –1260, 2-6 Oct.2005.
- [45] K. Holland, M. Shen, and F. Z. Peng, "Z-source inverter control for traction drive of fuel cell - battery hybrid vehicles" in *Proc. of IEEE Industry Applications Society Annual Meeting*, Volume 3, pp. 1651 – 1656, 2-6 Oct, 2005.
- [46] K. You and F. M. Rahman, "Modulation and Control Schemes for A New Power Converter Based on Z-source and Matrix Converter for ISA 42 V PowerNet System" in *Proc. of IEEE Power Electronics and Drives Systems Conference, 2005*, Volume 1, pp. 436-441, 28-01 Nov. 2005.
- [47] T. Vinh, T. Chun, J. Ahn, and H. Lee, "Algorithms for controlling both the DC boost and AC output voltage of the Z-source inverter" in *Proc of IEEE Industrial Electronics Society Conference, 2005*, pp. 970-974, Nov. 2005.
- [48] S. Rajakaruna and Y. Jayawickrama, "Designing Impedance Network of Z-Source Inverters" in *Proc. of IEEE Power Engineering Conference, 2005*. pp.1-6, Nov.



2005.

[49] X. Fang, Z. Qian, and F. Z. Peng, "Single-phase Z-source PWM AC-AC converters" *IEEE Power Electronics Letters*, Volume 3, Issue 4, pp. 121 – 124, Dec. 2005.

[50] P. Loh, D. M. Vilathgamuwa, Y. Lai, G. Chua, and Y. Li, "Pulse-width modulation of Z-source inverters" *IEEE Trans. on Power Electron.* Volume 20, Issue 6, pp.1346-1355, Nov. 2005.

[51] C. Gajanayake, D. Vilathgamuwa, and P. Loh, "Small-signal and signal-flow-graph modeling of switched Z-source impedance network" *IEEE Power Electronics Letters*, Volume 3, Issue 3, pp.111-116, Sept. 2005.

[52] P.C. Loh, F. Blaabjerg, S. Feng, and K. Soon, "Pulse-Width Modulated Z-Source Neutral-Point-Clamped Inverter" in *Proc. of IEEE Applied Power Electronics Conference and Exposition, 2006.* pp. 431-437, March 2006.

[53] P. Loh, C. Gajanayake, D. Vilathgamuwa, and F. Blaabjerg;" Evaluation of Resonant Damping Techniques for Z-Source Current-Type Inverter" in *Proc. of IEEE Applied Power Electronics Conference and Exposition, 2006.* pp. 784-790, March 2006.

[54] F. Zhang, X. Fang, F. Z. Peng, and Z. Qian; "A New Three-Phase AC-AC Z-source Converter" in *Proc. of IEEE Applied Power Electronics Conference and Exposition, 2006,* pp. 123 – 126, March, 2006.

[55] X. Ding, Z. Qian, Y. Xie, and F. Z. Peng, "A Novel ZVS Z-Source Rectifier" in *Proc. of IEEE Applied Power Electronics Conference and Exposition, 2006.* pp. 951 – 955, March, 2006.

[56] Y. Huang, F. Z. Peng, J. Wang, and D. W. Yoo, "Survey of the power conditioning system for PV Power generation" In *Proc. IEEE Power Electronics Specialist Conference, 2006,* pp. 3257-3262, June, 2006.

[57] P. C. Loh, F. Blaabjerg, and C. P. Wong, "Comparative Evaluation of Pulse-Width Modulation Strategies for Z-Source Neutral-Point-Clamped Inverter" in *Proc. IEEE Power Electronics Specialist Conference, 2006,* pp.1316-1322, June, 2006.

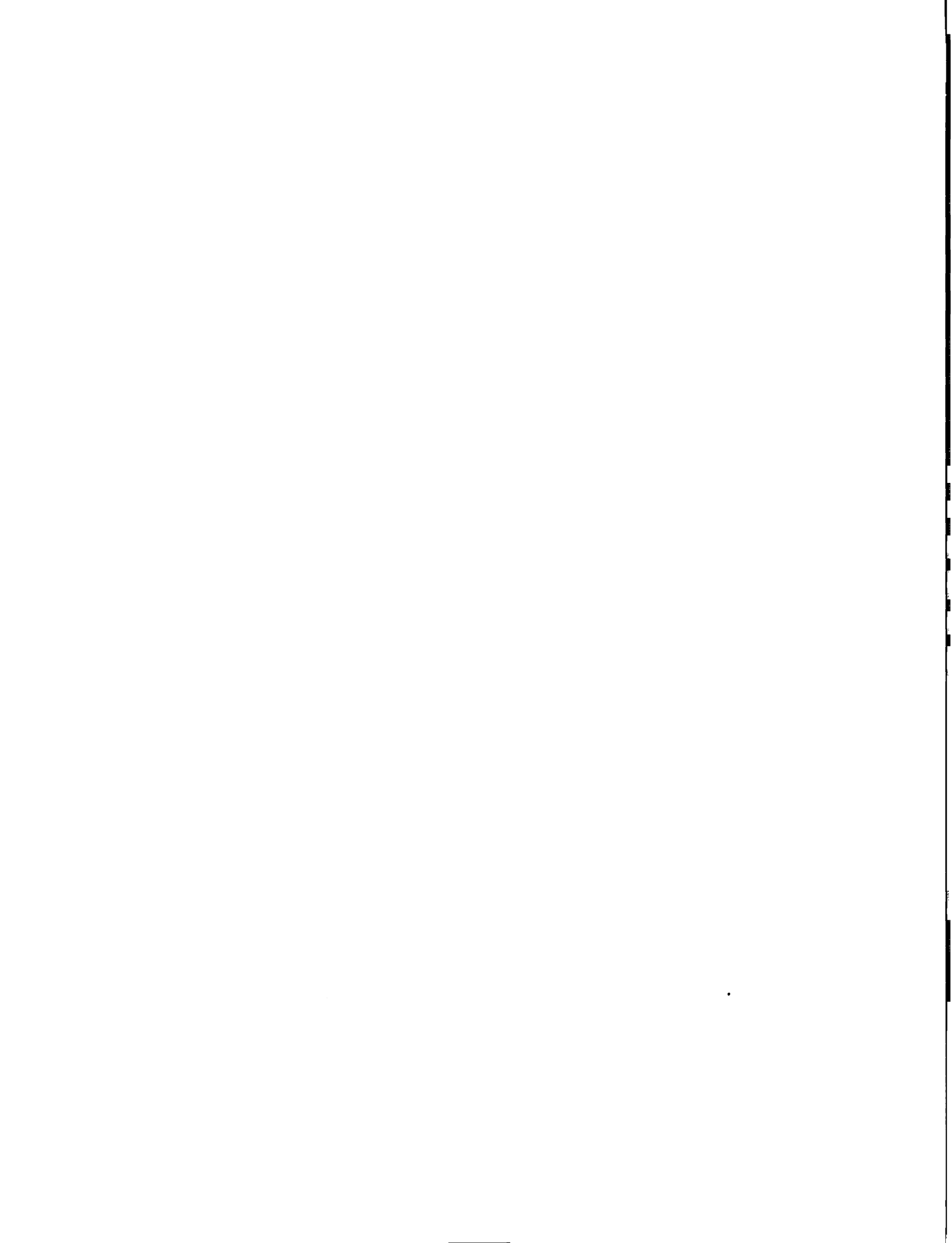
[58] P. Xu, X. Zhang, C. Zhang, R. Cao, and L Chang "Study of Z-Source Inverter for Grid-Connected PV Systems" In *Proc. IEEE Power Electronics Specialist Conference, 2006,* pp. 3252-3256, June, 2006.

[59] C. J. Gajanayake, D. M. Vilathgamuwa, and P. Loh, "Modeling and design of multi-loop closed loop controller for Z-source inverter for Distributed Generation" In *Proc. IEEE Power Electronics Specialist Conference, 2006,* pp. 1353-1359, June, 2006.

- [60] F. Gao, P. C. Loh, D. M. Vilathgamuwa, and F. Blaabjerg, "Performance Analysis of Random Pulse-Width Modulated Z-Source Inverter with Reduced Common Mode Switching" In *Proc. IEEE Power Electronics Specialist Conference*, 2006, pp.1536-1542, June, 2006.
- [61] B. Farhangi and S. Farhangi, "Comparison of z-source and boost-buck inverter topologies as a single phase transformer-less photovoltaic grid-connected power conditioner" In *Proc. IEEE Power Electronics Specialist Conference*, 2006, pp. 74-79, June, 2006.
- [62] Y. Xie, Z. Qian, X. Ding, and F. Z. Peng, "A Novel Buck-Boost Z-Source Rectifier" In *Proc. IEEE Power Electronics Specialist Conference*, 2006, pp. 1225-1229, June, 2006.
- [63] X. Ding, Z. Qian, Y. Xie, and F. Z. Peng, "Transient Modeling and Control of the Novel ZVS Z-Source Rectifier", In *Proc. IEEE Power Electronics Specialist Conference*, 2006, pp. 898-902, June, 2006.
- [64] K. You and M. F. Rahman, "Analytical Comparison of Conduction and Switching Losses of A Novel Matrix-Z-Source Converter and A Conventional VSI Converter for automotive ISA 42 V System" in *Proc. IEEE Power Electronics Specialist Conference*, 2006, pp. 146-152, June, 2006.
- [65] T. Chun, Q. Tran, J. Ahn, and J. Lai , "AC Output Voltage Control with Minimization of Voltage Stress Across Devices in the Z-Source Inverter Using Modified SVPWM" In *Proc. IEEE Power Electronics Specialist Conference*, 2006, pp. 3030-3034, June, 2006.
- [66] M. Shen and F. Z. Peng, "Operation Modes and Characteristics of the Z-Source Inverter with Small Inductance or Low Power Factor" to appear on *IEEE Transactions on Industrial Electronics*.
- [67] Y. Huang, M. Shen, F. Z. Peng, and Jin Wang "A Z-Source Inverter for residential Single-Phase Photovoltaic System" to appear on *IEEE Transactions on Power Electronics*.
- [68] F.Z. Peng, M. Shen, and K. Holland; "Application of Z-source inverter for traction drive of fuel cell - battery hybrid vehicles" to appear on *IEEE Transactions on Power Electronics*.
- [69] M. Shen, A. Joseph, Y. Huang, F. Z. Peng, and Z. Qian, "Design and Development of a 50kW Z-Source Inverter for Fuel Cell Vehicles", *IEEE International Power Electronics and Motion Control Conference 2006* pp.1076-1080, Shanghai, 2006.
- [70] M. Shen and F. Z. Peng, "Control of the Z-Source Inverter for Fuel Cell-Battery Hybrid Vehicles to eliminate unwanted operation modes" in *Proc. of IEEE Industry Application Society Annual Meeting 2006*.

- [71] M. Shen, A. Joseph, J. Wang, F. Z. Peng, and D.J Adams; "Comparison of Traditional Inverters and Z-Source Inverter for Fuel Cell Vehicles" to appear on *IEEE Transactions on Power Electronics*.
- [72] X. Fang, "Three-Phase Z-Source AC-AC Converter for Motor Drives", in *Proc. of IEEE International Power Electronics and Motion Control Conference 2006*.
- [73] P. C. Loh, F. Gao, and F. Blaabjerg, "Topological and Modulation Design of Three-Level Z-Source Inverters" in *Proc. of IEEE International Power Electronics and Motion Control Conference 2006*.
- [74] <http://www.powersimtech.com/>
- [75] H. Khalil, "Nonlinear systems" Third Edition, Prentice Hall, Upper saddle river, New Jersey.
- [76] Wilson J. Rugh, J.S. Shamma, "Research on gain scheduling", *Automatica*, 36, (200), pp.1401-1425.
- [77] C. Wang, M. Nehrir, S. Shaw, "Dynamic models and model validation of PWM fuel cells using electrical circuits." *IEEE Trans. On Power Conversion*, Vol. 20, No.2, pp.442-451, June, 2005.
- [78] J.W.Kolar, H. Ertl, and F.C.Zach, "Calculation of the passive and active component stress of three phase PWM converter systems with high pulse rate," in *proc. of EPE Conf.*, Aachen, Germany, 1989, pp.1303-1311.
- [79] A.M.Hava, R.J.Kerkman, T.A.Lipo, "Simple analytical and graphical methods for carrier based PWM-VSI drives", *IEEE Trans. on Power Electronics*, Vol.14, No.1 1999, pp.49-61.
- [80] "General Considerations: IGBT & IPM modules", Powerex Application notes, A10-A27.
- [81] <http://www.pwr.com/>
- [82] S Pischinger; O Lang; H Kemper; "System Comparison of Hybrid and Fuel Cell Systems to Internal Combustion Engines," *SAE 2002 technical paper series*, October 2002, Ref: 2002-21-0070.
- [83] K. Rajashekara, "Power Conversion and Control Strategies for Fuel Cell Vehicles," in *Proc. Industrial Electronics Society Annual Conference*, 2003, vol. 3, pp. 2865-2870.
- [84] Pukrushpan, Jay T., Stefanopoulou, Anna G., Peng, Huei, "Modeling and Analysis of Fuel Cell Reactant Flow for Automotive Applications," in *Journal of Dynamic Systems, Measurement and Control*, 126 (1), pp. 14-25, March 2004.

- [85] Tadaichi Matsumoto; Nobuo Watanabe; Hiroshi Sugiura; Tetsuhiro Ishikawa; "Development of Fuel-Cell Hybrid Vehicle," *Fuel cell power for transportation 2002 conference, SAE 2002 World congress*, March 2000, Ref: 2002-01-0096
- [86] B. D'Souza, H. Rawlins, J. Machuca, C. Larson, M. Shuck, B. Shaffer, T. Maxwell, M. Parten, D. Vines, and J. Jones, "Texas Tech University Develops Fuel Cell Powered Hybrid Electric Vehicle for FutureCar Challenge 1998," *SAE 1999*, Ref: 1999-01-0612.
- [87] J. Adams, W. Yang, K. Oglesby, and K. Osborne, "The Development of Ford's P2000 Fuel Cell Vehicle," *SAE 2000*, Ref: 2000-01-1061.
- [88] D. Tran, and M. Cummins, "Development of the Jeep Commander 2 Fuel Cell Hybrid Electric Vehicle," *SAE 2001*, Ref: 2001-01-2508.
- [89] E. H. Wakefield; *History of the Electric Automobile*, Warrendale, PA: Society of Automotive Engineers, Inc, 1998.



MICHIGAN STATE UNIV



3 1293 02